Modeling and Fractional-Order Control of Twin Rotor MIMO System

Abebe Alemu Wendimu

Master's thesis
2023

Tomas Bata University in Zlín
Faculty of Applied Informatics

Univerzita Tomáše Bati ve Zlíně
Fakulta aplikované informatiky
Ústav automatizace a řídicí techniky

Akademický rok: 2022/2023

ZADÁNÍ DIPLOMOVÉ PRÁCE

(projektu, uměleckého díla, uměleckého výkonu)

Jméno a příjmení:	**Abebe Alemu Wendimu**
Osobní číslo:	**A21781**
Studijní program:	**N0714A150007 Automatic Control and Informatics in Industry 4.0**
Forma studia:	**Prezenční**
Téma práce:	**Modeling and Fractional-Order Control of Twin Rotor MIMO System**
Téma práce anglicky:	**Modeling and Fractional-Order Control of Twin Rotor MIMO System**

Zásady pro vypracování

1. Review the literature on the fundamentals of fractional-order calculus and its application to control engineering.
2. Familiarize yourself with the real laboratory model of a twin rotor MIMO system and its nonlinear description based on mathematical-physical analysis.
3. Perform the identification experiments and create a linear model of the twin rotor MIMO system. Compare the dynamic properties of the real plant, nonlinear model, and linear model.
4. Design a fractional-order controller, simulate its performance in Matlab/Simulink environment, and apply it to the real laboratory model.
5. Compare the obtained outcomes with an integer-order approach to control design for both real plant and identified model. Discuss and evaluate the results.

Forma zpracování diplomové práce: **tištěná/elektronická**
Jazyk zpracování: **Angličtina**

Seznam doporučené literatury:

1. ABDULWAHHAB, Omar Waleed and Nizar Hadi ABBAS. New Method to Tune a Fractional-Order PID Controller for a Twin Rotor Aerodynamic System. *Arabian Journal for Science and Engineering*, 2017, Vol. 42, pp. 5179–5189. https://doi.org/10.1007/s13369-017-2629-5.
2. AZARMI, Roohallah, Mahsan TAVAKOLI-KAKHKI, Ali Khaki SEDIGH, and Alireza FATEHI. Analytical design of fractional order PID controllers based on the fractional set-point weighted structure: Case study in twin rotor helicopter. *Mechatronics*, Vol. 31, pp. 222-233. https://doi.org/10.1016/j.mechatronics.2015.08.008.
3. COELHO, J., R. NETO, D. AFONSO, C. LEBRES, N. M. FONSECA FERREIRA, and J. A. TENREIRO MACHADO. Application of fractional algorithms in the control of a twin rotor multiple input–multiple output system. In: *6th EUROMECH Conference ENOC 2008*, Saint Petersburg, Russia, 2008.
4. DOĞRUER, Tufan and Nusret TAN. Real time control of twin rotor MIMO system with PID and fractional order PID controller. *Mugla Journal of Science and Technology*, Vol. 6, No. 0, pp. 1-9. https://doi.org/10.22531/muglajsci.669738.
5. CHALUPA, Petr, Jan PŘIKRYL, and Jakub NOVÁK. Modelling of Twin Rotor MIMO System. *Procedia Engineering*, 2015, Vol. 100, pp. 249-258. https://doi.org/10.1016/j.proeng.2015.01.365.
6. IJAZ, Salman, Mirza Tariq HAMAYUN, Lin YAN, and Muhammad Faisal MUMTAZ. Fractional Order Modeling and Control of Twin Rotor Aero Dynamical System Using Nelder Mead Optimization. *Journal of Electrical Engineering and Technology*. 2016, Vol. 11, No. 6, pp. 1863-1871. https://doi.org/10.5370/JEET.2016.11.6.1863.
7. MIHALY, Vlad, Mircea ŞUŞCĂ, and Eva H. DULF. μ-Synthesis FO-PID for Twin Rotor Aerodynamic System. *Mathematics*, 2021, Vol. 9, No. 19. https://doi.org/10.3390/math9192504.
8. RAMALAKSHMI, A. P. S. and P. S. MANOHARAN. Non-linear modeling and PID control of twin rotor MIMO system. In: *2012 IEEE International Conference on Advanced Communication Control and Computing Technologies (ICACCCT)*, Ramanathapuram, India, 2012.
9. XUE, Dingyü. *Fractional-Order Control Systems: Fundamentals and Numerical Implementations*. Berlin: De Gruyter, 2017.

Vedoucí diplomové práce: **doc. Ing. Radek Matušů, Ph.D.**
Ústav automatizace a řídicí techniky

Datum zadání diplomové práce: **16. prosince 2022**
Termín odevzdání diplomové práce: **24. května 2023**

doc. Ing. Jiří Vojtěšek, Ph.D. v.r.
děkan

UNIVERZITA TOMÁŠE BATI VE ZLÍNĚ
Fakulta aplikované informatiky
L.S.

prof. Ing. Vladimír Vašek, CSc. v.r.
ředitel ústavu

Ve Zlíně dne 12. prosince 2022

I hereby declare that:

- I understand that by submitting my Master's thesis, I agree to the publication of my work according to Law No. 111/1998, Coll., On Universities and on changes and amendments to other acts (e.g. the Universities Act), as amended by subsequent legislation, without regard to the results of the defence of the thesis.
- I understand that my Master's Thesis will be stored electronically in the university information system and be made available for on-site inspection, and that a copy of the Master's Thesis will be stored in the Reference Library of the Faculty of Applied Informatics, Tomas Bata University in Zlín.
- I am aware of the fact that my Master's Thesis is fully covered by Act No. 121/2000 Coll. On Copyright, and Rights Related to Copyright, as amended by some other laws (e.g. the Copyright Act), as amended by subsequent legislation; and especially, by §35, Para. 3.
- I understand that, according to §60, Para. 1 of the Copyright Act, Tomas Bata University in Zlín has the right to conclude licensing agreements relating to the use of scholastic work within the full extent of §12, Para. 4, of the Copyright Act.
- I understand that, according to §60, Para. 2, and Para. 3, of the Copyright Act, I may use my work – Master's Thesis, or grant a license for its use, only if permitted by the licensing agreement concluded between myself and Tomas Bata University in Zlín with a view to the fact that Tomas Bata University in Zlín must be compensated for any reasonable contribution to covering such expenses/costs as invested by them in the creation of the thesis (up until the full actual amount) shall also be a subject of this licensing agreement.
- I understand that, should the elaboration of the Master's Thesis include the use of software provided by Tomas Bata University in Zlín or other such entities strictly for study and research purposes (i.e. only for non-commercial use), the results of my Master's Thesis cannot be used for commercial purposes.
- I understand that, if the output of my Master's Thesis is any software product(s), this/these shall equally be considered as part of the thesis, as well as any source codes, or files from which the project is composed. Not submitting any part of this/these component(s) may be a reason for the non-defence of my thesis.

I herewith declare that:

- I have worked on my thesis alone and duly cited any literature I have used. In the case of the publication of the results of my thesis, I shall be listed as co-author.
- The submitted version of the thesis and its electronic version uploaded to IS/STAG are both identical.

In Zlín; dated: 18/08/2023 *Abebe Alemu*, $WENDIMU$, m.p.

Student's Signature

ABSTRAKT

Tato diplomová práce se zaměřuje na modelování laboratorní soustavy Twin Rotor Multiple Input-Multiple Output System (TRMS) a její řízení s využitím regulátorů neceločíselného řádu. Práce začíná důkladným přehledem literatury, který zkoumá modelování a implementaci proporcionálně-integračně-derivačních regulátorů neceločíselného řádu (FOPID) pro systémy TRMS. Tento přehled zahrnuje zkoumání výhod a nevýhod každého navrhovaného přístupu, způsob ověřování pro každou z těchto navržených metod a zkoumání výkonu metody v podmínkách reálného času.

Následně se práce zaměřuje na modelování nelineárního systému TRMS na základě matematicko-fyzikální analýzy. Je vytvořen podrobný nelineární model systému TRMS a porovnán s lineárními a experimentálními daty v reálném čase, a to jak pro elevaci (vertikální pohyb), tak pro azimut (horizontální pohyb).

Statické charakteristiky hlavní rotor-elevace a zadní rotor-azimut jsou poté zkoumány a zobrazeny. Pečlivě jsou zkoumány vlivy hlavního rotoru na azimutální úhel a zadního rotoru na elevační úhel. Faktory ovlivňující měření modelu v reálném čase jsou také zahrnuty do této studie. Práce poté zaměřuje svou pozornost na identifikaci parametrů systému TRMS pomocí různých přístupů, včetně algoritmu "fminsearch" v MATLABu a modelů ARX a ARMAX. Výsledky každého identifikačního postupu jsou porovnány, a následně provedena analýza říditelnosti, pozorovatelnosti a stability na základě lineárních identifikačních modelů "fminsearch" pro elevaci a azimut. Jádrem práce je návrh PID regulátorů jak celočíselného (IOPID), tak také neceločíselného (FOPID) řádu pro soustavu TRMS. Různé optimalizační algoritmy, jako je Particle Swarm Optimization (PSO), Genetic Algorithm (GA) a Nelder-Mead (NM), jsou použity k optimalizaci parametrů regulátorů. Výkon a efektivnost každého optimalizačního postupu jsou vyhodnoceny a porovnány. Dále práce představuje podrobné srovnání navržených regulátorů, zohledňující faktory jako stabilita, doba ustálení, překmit a další parametry. Analýza a srovnání poskytují cenné poznatky o výkonu a vhodnosti různých návrhů regulátorů pro soustavu TRMS.

Závěrem lze říci, že tato diplomová práce přináší významný přínos do oblasti řízení založeného na neceločíselných řádech tím, že se zabývá nelineárním modelováním, identifikací a návrhem řízení soustavy TRMS. Výsledky a závěry prezentované v této práci budou sloužit jako základ pro vývoj pokročilých řídicích strategií pro podobné systémy v budoucnosti, s potenciálním uplatněním v oblastech jako letecký průmysl a robotika.

Klíčová slova: Identifikace, nelineární modelování, regulátory neceločíselného řádu, TRMS

ABSTRACT

This Diploma thesis focuses on the modeling and fractional order control of a Twin Rotor Multiple Input-Multiple Output System (TRMS). The thesis begins with a comprehensive literature review, exploring the modeling and implementation of fractional order Proportional-Integral-Derivative (FOPID) controllers for TRMS systems. This review includes an analysis of the advantages and disadvantages of each proposed system, and along with the testing methodologies for these approaches and their performance evaluation in real-time scenarios

Subsequently, the thesis focuses on the modeling of nonlinear TRMS system based on first princiles. A detailed non-linear model of the TRMS system is developed and compared against both linear and real-time experimental data for both elevation/pitch angle and azimuth/yaw angle.

The static characteristics of both the main-elevation and tail-azimuth are then explored and depicted. The impacts of the main rotor on azimuth angle and the tail rotor on elevation angle are carefully studied. Factors affecting real-time model measurements are also incorporated in this study.

The thesis then shifts its focus to the identification of TRMS system parameters using various approaches, including the "fminsearch" algorithm in MATLAB, as well as the ARX and ARMAX models. The results of each identification method are compared, and further controllability, observability, stability analysis are conducted based on "fminsearch" linear identification models for elevation and azimuth.

The core of the thesis centers around the design of both Integer-Order PID (IOPID) and FOPID controllers for the TRMS system. Various optimization algorithms, such as Particle Swarm Optimization (PSO), Genetic Algorithm (GA), and Nelder-Mead (NM), are employed to optimize the controller parameters. The performance and effectiveness of each optimization technique are evaluated and compared.Furthermore, the thesis presents a comprehensive comparison of the designed controllers, considering factors such as stability, rise time, overshoot, settling time, and other parameters. The analysis and comparison provide valuable insights into the performance and suitability of the different controller designs for the TRMS system. In conclusion, this MSc thesis makes significant contributions to the field of fractional order control by addressing the non-linear modeling, identification, and control design aspects of TRMS systems. The findings and results presented in this thesis serve as a foundation for developing advanced control strategies for similar systems in the future, with potential applications in areas such as aerospace and robotics.

Keywords: Identification, Non-linear Modeling, Fractional Order Control, TRMS

ACKNOWLEDGEMENTS

I would like to express my heartfelt appreciation to all those who have supported and contributed to my journey. Firstly, I am deeply grateful to my supervisor, Doc. Ing. Radek Matušů, for his invaluable guidance, mentorship, and an endless support throughout my studies. His expertise, dedication, and encouragement have been instrumental in shaping my academic and personal growth. His belief in my abilities and constant words of encouragement have inspired me to persevere and achieve my goals.

Additionally, I extend my sincere thanks to Ing. Petr Chalupa for his exceptional guidance, encouragement to explore new ideas, and insightful feedback, which have significantly shaped this thesis and enriched my understanding of the subject. I am also grateful to Professors: Doc. Ing. Marek Kubalčík, Doc. Ing. František Gazdoš, Ing. Milan Navrátil, Ing. Juan Carlos Beltrán Prieto, Doc. Ing. Zuzana Komínková Oplatková, and all the other academic and administrative staff of TBU, as well as the Ministry of Education, Youth, and Sports - Government of the Czech Republic, for their collaboration, and guidance and financial support throughout my MSc. journey. Their contributions have been instrumental in my academic growth and the successful completion of this thesis.

Furthermore, I am grateful to my beloved wife, my daughter, my family, and friends for their love, support, understanding, and encouragement during challenging times. Their presence and encouragement have been my guiding light throughout this journey. I am also thankful to my fellow classmates and colleagues for their collaboration and the shared experiences that have enriched my academic and personal growth.

Lastly, I would like to acknowledge the contributions of all the researchers, authors, and professionals whose work has influenced and enriched my academic pursuits. I dedicate this thesis to all the individuals who believe in the power of knowledge and education to make a positive impact in the world.

Thank you all for being an integral part of this meaningful journey.

DEDICATION

Dedicated to

The Grand Weaver of My Life:

JESUS CHRIST

TABLE OF CONTENTS

INTRODUCTION

The motivation behind this thesis stems from the complexity of the TRMS, which poses significant challenges in control engineering due to its cross-coupling, nonlinearity, and MIMO nature. Accurate modeling of the TRMS is essential for effective control design and implementation, as it accurately represents the actual plant. Despite being a nonlinear MIMO system, the control of TRMS is still in a relatively immature stage, highlighting the need for advanced and innovative control techniques. In this context, fractional-order calculus-based controllers offer greater flexibility in adjusting options compared to conventional integer-order techniques, making them promising candidates for controlling TRMS. However, fractional-order control is an active area of research that still requires further development and robustness.

A Comprehensive Overview of Twin Rotor MIMO Systems

In recent years, the field of control engineering has experienced remarkable growth, with researchers actively working to create and test various control algorithms for complex systems. One such intricate system that presents significant challenges in terms of control is the Twin Rotor Multiple-Input-Multiple-Output (TRMS) system, a helicopter model crafted by Feedback Instruments Ltd®.

The TRMS serves as a valuable tool for researchers and students, providing hands-on experience in control system design and analysis. It is frequently used to develop and test advanced control algorithms, while also serving as a platform to evaluate the performance of various control strategies. As a result of its wide adoption in research and education, the TRMS has become a well-established benchmark system in the field of control engineering. It offers a reliable platform to study the complexities of multivariable, nonlinear systems, thereby fostering a deeper understanding of control theory and its practical applications in real-world scenarios.

The two-button TRMS has the following functions:

I. **Emergency Disconnect (Red Button):** The red button serves as an emergency disconnect for communication between the TRMS real model and the computer. In case of fault detection or any unforeseen issues that require an immediate halt in communication, pressing the red button will instantly sever the connection, ensuring safety and preventing further operation.

Figure 0.1 Twin Rotor MIMO System.

I. **Start Communication (Green Button):** On the other hand, the green button is used to initiate communication between the TRMS real model and the computer. When the system is ready for operation and all safety checks have been completed, pressing the green button establishes the connection. This enables data exchange and facilitates the transmission of control signals between the TRMS and the computer, allowing the system to function as intended.

The term "Twin" in the TRMS refers to the system's distinctive feature of having twin propellers that are capable of independent rotation both vertically and horizontally. The TRMS incorporates separate DC motors to drive both the main and tail rotors, enabling them to rotate freely and perform their respective functions. Unlike traditional helicopters, which rely on blade angle attack alterations to affect movement, the TRMS adjusts aerodynamic forces through changes in motor input voltage. Controlling the TRMS requires advanced techniques due to its non-linear nature, coupled with instability similar to that of an actual helicopter's two-input two-output system design.

Input:

- Control voltage of the main rotor
- Control voltage of the tail rotor

Output:

- Elevation / Pitch angle: The elevation/pitch angle in a TRMS represents the rotation of the twin rotors around the vertical plane (i.e., around the horizontal axis), which corresponds to the motion of the system in the up and down direction.
- Azimuth / Yaw angle: The azimuth/yaw angle in a TRMS represents the rotation of the twin rotors around the horizontal plane (i.e., around the vertical axis), which corresponds to the motion of the system in the left and right direction.

In this paper, the terms *elevation* and *pitch angle* as well as the term "*azimuth* and *yaw angle* have been used interchangeably.

The terms "screw" and "unscrew" used in this thesis have the following definitions.

TRMS with Screws: In this context, "screw" refers to the process of tightening or fixing the twin rotors in a specific configuration. For example, when we adjust the screws in the vertical plane, the rotation of the TRMS becomes primarily influenced by the horizontal plane. Conversely, if we adjust the screws in the horizontal plane, the TRMS becomes primarily influenced by the vertical plane. By strategically adjusting these screws, precise control over the system's motion in different planes can be achieved.

TRMS with Unscrew: Conversely, if "unscrew" refers to loosening or adjusting the twin rotors' position, it means that the rotation of one rotor can affect the motion of the other rotor. The degree of screwing or unscrewing is carefully investigated during laboratory measurements.

Objective

General Objective

The primary aim of this diploma thesis is to model and apply Fractional-Order Control to a Twin Rotor MIMO System.

Specific Objectives

To achieve the main goal, this thesis will focus on the following specific objectives:

I. Conduct a comprehensive literature review on the fundamentals of fractional-order calculus and its application to control engineering.

II. Gain familiarity with the real laboratory model of a twin rotor MIMO system and analyze its nonlinear behavior through mathematical and physical analysis.

III. Perform identification experiments to create a linear model of the twin rotor MIMO system. Subsequently, compare the dynamic properties of the real plant, nonlinear model, and linear model.

IV. Design a fractional-order controller, simulate its performance using the Matlab/Simulink environment, and then apply it to the real laboratory model.

V. Compare the outcomes obtained from the fractional-order control approach with those from an integer-order control design for both the real plant and the identified model. Additionally, discuss and evaluate the results of the comparison.

By accomplishing these specific objectives, the thesis will contribute to a better understanding of fractional-order control and its application to the Twin Rotor MIMO System.

Thesis Organization

The thesis consists of two main parts: the Theory part (which includes the Literature Review section) and the Analysis part (from the Implementation of Nonlinear Model TRMS on MATLAB Simulink to the Conclusions and Recommendations section). Findings and analysis of each result are explained clearly in the analysis sections. To clarify further, the thesis work is organized into four main works, as the following block diagram.

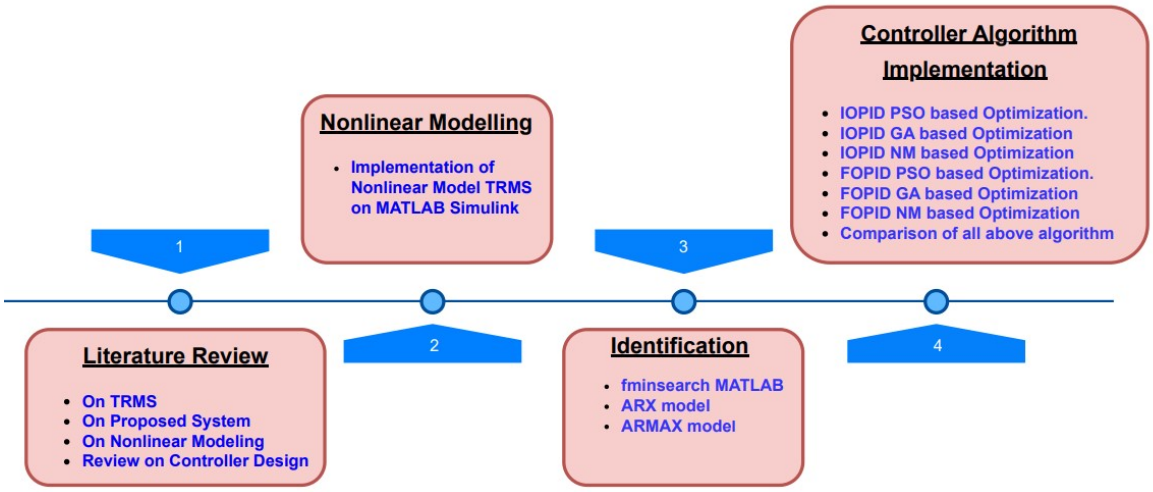

Figure 0.2 Thesis organization

I. THEORY

1 LITERATURE REVIEW

1.1 Review on Modeling and Control of Twin Rotor MIMO System

Numerous studies have highlighted the challenging nature of the Twin Rotor MIMO System (TRMS), as discussed in [1], [2], and [3]. The TRMS is characterized by high coupling, instability, nonlinearities, coupling between inputs and outputs, and susceptibility to disturbances. Effective control system design for the TRMS requires the application of advanced control techniques. Its behavior closely resembles that of a helicopter, exhibiting significant cross-coupling between its channels.

Control strategies for the TRMS encompass a range of linear and non-linear techniques, including PID control, adaptive control, fuzzy control, and neural networks. To evaluate the performance of these algorithms, various metrics such as overshoot, settling time, and control effort are considered [4], [5].

In the field of control systems, [6] provides a comprehensive review of recent developments in fractional-order modeling, which has garnered more attention than classical integer-order model transfer functions. Their research indicates that fractional-order models have gained prominence in system identification compared to classical integer-order model transfer functions. The authors discuss how fractional calculus and models have made significant contributions to real-world processes, achieving superior results compared to conventional science. Additionally, their survey of available literature on the topic serves as a valuable resource for facilitating future investigations.

The article by [7] presents the implementation of a novel method to tune a fractional-order PID controller for a Twin Rotor Aerodynamic System (TRMS). The TRMS model was derived based on Lagrange's equations, and the resulting nonlinear equations were linearized around a specific operating point to develop a controller for the system.

The paper focuses on comparing the performance of an IOPID controller, represented by PID, with a FOPID controller, represented by $PI^{\lambda}D^{\mu}$. To optimize the FOPID controller, the authors tuned its five parameters to minimize a performance index. This index was a weighted sum of four frequency domain specifications: gain crossover frequency, phase margin, ISO damping property (to ensure robustness against process gain variation), and magnitude peak value at the resonant frequency.

Simulation results indicated that the FOPID controller outperformed the PID controller in terms of performance and robustness, as it accurately fulfilled the design

specifications. However, it's important to note that the authors did not test the controller on a nonlinear model or a real-time plant. This limitation could affect the generalizability of the results since a linear model may not accurately represent the dynamics of a nonlinear or real-time plant. Additionally, a linear model not identified from the real plant may not accurately reflect its actual dynamics. Further experimentation on nonlinear or real-time systems would be beneficial for a more comprehensive evaluation of the FOPID controller's performance.

In their research, the authors in [8] introduced an analytical approach for tuning the parameters of the set-point weighted fractional order PID (SWFOPID) controller using the filtered fractional set-point weighted (FFSW) structure. The main objective was to achieve the desired closed-loop performance by incorporating a fractional order prefilter. This method is specifically designed for stable plants described by a simple three-parameter fractional order model, which can be considered as the fractional order counterpart of a first-order transfer function without time delay.

To validate their approach, the authors implemented the proposed method on a laboratory scale CE 150 helicopter platform. The obtained results were then compared with those achieved by applying a filtered fractional order PI (FFOPI) controller with a similar structure. Based on their findings, the practical results demonstrated the effectiveness of the proposed method in achieving the desired closed-loop performance for the system.

In their research, [9] proposed the application of fractional algorithms in the control of a TRMS system. They derived a nonlinear mathematical equation based on Newton's second law of motion to model the system and provided an overview of the system model.

The authors utilized the PSO algorithm to tune the controllers. They compared the performance of fractional and integer-order PID controllers and employed the PSO algorithm to optimize the controller for minimum error. Testing with a real helicopter demonstrated that the fractional order PID or PID$^{\mu}$ controller outperformed the integer-order PID in terms of speed and error reduction.

Furthermore, the time response of the PID$^{\mu}$ controller was smoother, exhibiting less overshoot and reduced input/output cross-coupling. While both controllers yielded satisfactory output responses, the IOPID required more energy to perform the same task, as suggested by the authors.

In their work, [10] introduced a real-time control approach for the TRMS using both PID and fractional-order PID controllers. They utilized the 'System Identification Toolbox' to determine the mathematical models of the TRMS and then derived the parameters of the fractional-order PID controller based on the identified plant model. The optimization algorithm employed for tuning the controller parameters was the Genetic Algorithm, implemented in the Matlab program, to achieve different integral performance criteria.

The study focused on real-time control of both pitch and yaw positions of the TRMS, comparing the performance of the PID controller and the fractional-order PID ($PI^{\lambda}D^{\mu}$) controller. The authors evaluated four different integral performance criteria: ISE (Integral of Squared Error), IAE (Integral of Absolute Error) , ITAE (Integral of Time-weighted Absolute Error), and ITSE (Integral of Time-weighted Squared Error). Their findings showed that the ITSE-based controller design was the most successful in terms of response performance.

Overall, they successfully demonstrated the real-time control of a nonlinear Twin Rotor MIMO System with two inputs and two outputs using a fractional order PID controller, offering a promising approach for controlling complex systems.

In [11], the author conducted experimental studies to model TRMS. They derived a nonlinear mathematical model based on first principles modeling and also identified a linear model from step responses using the fminsearch MATLAB function. To validate their models, they compared the step responses of the nonlinear model based on first principles, the linear model based on identification by fminsearch, and real-time experiments of TRMS.

The results of their study indicated that the enhanced nonlinear model performed significantly better than the other models. The courses of the other models deviated more from the courses of the real-time plant. This observation highlighted the accuracy and reliability of the enhanced nonlinear model in capturing the TRMS behavior.

The study's conclusion emphasized the successful design of a valid model for the Twin Rotor MIMO System, which could serve as a solid foundation for further research in the field. However, the scope of their work did not include implementing a controller algorithm for this valid model. Nevertheless, their work contributed valuable insights into the modeling aspect of TRMS, which is crucial for designing effective control strategies for such complex systems.

In [12], the author introduced the Fractional Order Modeling and Control of Twin Rotor Aero Dynamical System using Nelder Mead Optimization. The technique involves identifying a fractional order model of the system using input-output data from a nonlinear system. The Grünwald-Letnikov method of approximation is utilized for model identification.

Based on the identified model, the study proceeds to design two separate FOPID controllers to control the pitch and yaw axes of the TRMS. The controller parameters are tuned using Nelder-Mead optimization, and their performance is compared with PSO techniques. The evaluation of the system's performance is done using the integrated absolute error (IAE) metric, which tends to produce a response with less sinusoidal oscillation.

The transient analysis of the controller is based on specifications such as settling time, rise time, overshoot, and steady-state error. For frequency domain analysis, the study employs gain margin, phase margin, and operating bandwidth as tools.

The results indicate that the fractional order model of the TRMS provides a better representation of the system dynamics compared to the integer order model. Additionally, the Nelder-Mead optimization technique applied to the nonlinear TRMS leads to more optimally tuned controller parameters compared to PSO.

Overall, the study demonstrates that the FOPID tuned using Nelder-Mead optimization exhibits improved performance in terms of transient response and ensures reaching the steady-state condition earlier than the FOPID tuned using PSO and conventional PID controller. Furthermore, the FOPID controller shows less overshoot compared to the PID controller.

However, it's important to note that the authors did not test the controller on a real-time plant, which could limit the generalizability of the results. Linear models may not accurately represent the dynamics of real-time plants, and a linear model not identified from the plant may not accurately reflect its dynamics. Therefore, further testing and validation on a real-time plant would be necessary to confirm the practical effectiveness of the proposed controller.

In [13], the authors proposed a non-linear modeling and PID control approach for the TRMS. The TRMS mathematical model is derived based on the electrical-mechanical diagram of the TRMS, and the control is implemented in MATLAB/Simulink using two degrees of freedom (2-DOF) PID controllers for both horizontal and vertical directions.

Two types of controllers are presented: the first one is a 2-DOF controller using a simple PID, and the second one is a 2-DOF controller using cross-coupled PID. The performance of these controllers is evaluated using three different reference inputs: step response, sine wave response, and square wave response. The evaluation involves comparing the error between the plant output and the control output of the PID controller.

According to their observations, the total error of the sine wave response is reduced. However, the authors could not draw clear conclusions about the performance comparison between the simple PID controller and the cross-coupled PID controller based on their proposal results.

It is essential to note that the authors did not test the controllers on a real-time plant, which might limit the generalizability of the results. Linear models may not accurately represent the dynamics of real-time plants, and a linear model not identified from the plant may not accurately reflect its dynamics. Therefore, further testing and validation on a real-time plant would be necessary to assess the practical effectiveness of these controllers.

Moreover, a limitation of this paper is that only the simple PID controller is implemented without further comparison with other advanced controllers, such as fractional order PID. The comparison with other advanced controllers could provide additional insights into the performance and robustness of the proposed controllers.

Overall, while the paper presents valuable contributions to the field of control systems for the TRMS, further research and testing on real-time plants and comparison with other advanced controllers would be beneficial to enhance the credibility and applicability of the proposed control approach.

In [14], the authors introduced a parameter estimation technique for a fractional-order with delay model of a Twin Rotor MIMO System (TRMS). Their main objective was to model the TRMS using a fractional-order transfer function with time-delay. To achieve this, they formulated an optimization problem and utilized the Nelder-Mead algorithm, a popular optimization technique, to solve it. The "fminsearch" function from the MATLAB® software package was employed to implement the Nelder-Mead algorithm effectively.

Additionally, the authors leveraged the FOMCON toolbox in MATLAB® to demonstrate the effectiveness of fractional-order derivative operators in accurately character-

izing the behavior of the TRMS system.

The findings of the study indicated that the proposed fractional-order model with time delay for the TRMS offered a significant improvement in system representation compared to the conventional integer-order model, especially when the integer-order model required a higher number of model parameters. This improvement was evidenced by the reduced error obtained through experimental simulations.

The research presented in this paper highlights the benefits of incorporating fractional-order modeling techniques in capturing the dynamics of complex systems like the TRMS more accurately. By using fractional-order transfer functions with time-delay, the authors were able to obtain a better fit to the actual system behavior, leading to improved modeling accuracy and reduced errors.

Overall, this study contributes to the growing body of research that explores the advantages of fractional-order modeling in various control systems, showcasing the potential of fractional calculus in enhancing system representation and performance analysis.

In [15], the authors proposed a Fractional Order Sliding Mode Controller (FOSMC) for the TRMS. The FOSMC was designed by formulating a sliding surface in fractional order specifically for the TRMS. By decoupling the system, the interdependency between the horizontal and vertical planes was neglected, and the control input for the TRMS was derived based on this sliding surface.

To validate the stability and convergence of the decoupled control input in finite time, the authors utilized Lyapunov's criteria for stability. Separate matching of parameters, such as angle error, sliding surface, and control law, was performed for the horizontal and vertical planes using Sliding Mode Control (SMC) in MATLAB/Simulation. The overall controlled trajectory was then obtained by combining the trajectories of the vertical and horizontal planes. This approach effectively reduced the chattering effect typically associated with traditional SMC.

The results of the study demonstrated that the designed FOSMC for the TRMS successfully controlled the system's trajectory while significantly reducing the chattering effect. By leveraging fractional order sliding mode techniques, the authors achieved improved performance and smoother control of the TRMS, which is particularly beneficial in practical applications where chattering can cause undesirable effects.

The research presented in this paper contributes to the advancement of control strategies for complex systems like the TRMS, showcasing the advantages of incorporating

fractional order techniques to enhance control performance and mitigate undesired phenomena like chattering. The successful application of the FOSMC in this study opens up avenues for further exploration of fractional order control methods in various control engineering applications.

In [16], the author emphasized that fractional-order calculus has a long history in mathematics and engineering. Despite this historical background, the adoption of relevant fractional-order concepts in control systems research has been relatively slow. The author observed that there is still comparatively low interest in the topic, as evidenced by the literature review conducted in the MSc thesis.

The statement highlights the current state of fractional-order control systems research, indicating that while fractional-order calculus has been known for a long time, its practical application and integration into control engineering have not yet gained widespread attention and popularity. The literature review performed in the thesis likely provides an overview of the existing research landscape, revealing the need for further exploration and investigation to promote the understanding and utilization of fractional-order concepts in control systems.

According to [17], the research in the field of controlling and modeling Twin Rotor MIMO systems has been centered around addressing various challenges such as highly-coupled dynamics, nonlinear behavior, uncertainties, and gyroscopic torque. To tackle these complexities, efficient robust dynamic controllers have been the focus of investigation.

The authors conducted a comprehensive review of previous research work and highlighted a wide range of control strategies employed in the context of Twin Rotor MIMO systems. These strategies encompass both linear and nonlinear control approaches, showcasing the diverse techniques used to enhance the control performance of the system.

Some of the control strategies discussed in the literature include:

- Proportional Integral Derivative (PID) control
- Particle Swarm Optimization (PSO) based PID control
- Linear Quadratic Regulator (LQR) with output feedback control
- Backstepping control strategy

- Sliding Mode Control (SMC)
- Integral Sliding Mode Control
- Second-order Sliding Mode Control (SOSMC) combined with LQR
- Model Predictive Control (MPC) evaluation applied to MIMO systems

By exploring and analyzing these various control strategies, the authors aimed to provide valuable insights and a comprehensive overview of the state-of-the-art in controlling Twin Rotor MIMO systems. Understanding the strengths and limitations of these approaches can aid in the development of improved control techniques and foster further advancements in the field.

1.2 Exploring Nonlinear Mathematical Modeling: An Overview

The proposed nonlinear mathematical modeling is based on first-principles-based modeling, which refers to an approach utilized in scientific and engineering disciplines to construct mathematical models of systems. This method involves deriving the model from fundamental physical principles and known governing equations, thereby capturing the underlying physics of the system. It relies on basic laws, theories, and empirical relationships that govern the system's behavior, providing a solid foundation for understanding and predicting its dynamics accurately.

The first-principles-based modeling approach involves the following steps:

I. Identify the system: The first step is to identify the system of interest and the system's inputs and outputs.

II. Develop the governing equations: The next step is to develop the equations that govern the behavior of the system. This involves applying fundamental physical principles that describe the dynamics of the system.

III. Simplify the model: The equations derived in step II are often complex and may involve many variables and parameters.

IV. Simulate and validate the model: The final step is to simulate the model and compare its predictions to experimental data from the real laboratory model and data from the identified linear plant. In the analysis part, a comprehensive comparison of the step responses between the nonlinear plant model, the linear

plant obtained through identification, and the real laboratory model is conducted and thoroughly discussed.

By comparing the responses of the nonlinear plant model, the linear plant derived from system identification, and the real laboratory model, valuable conclusions can be drawn regarding the fidelity of the identified model. Also comparison of the step responses among the nonlinear plant model, the linear plant obtained through identification, and the real laboratory model forms a crucial step in validating the accuracy and performance of the constructed model.

It also provides a more accurate representation of the system, which can lead to better predictions and improved control systems. However, first-principles-based modeling is often complex and time-consuming, and requires a deep understanding of the underlying physics of the system being modeled.

1.3 Modelling of Twin Rotor MIMO System-Part -1

As previously mentioned, the TRMS is a highly nonlinear, multivariable, and coupled dynamic system widely used in control system analysis and design. The TRMS comprises two rotors mounted on a platform, each having two DOF for horizontal and vertical motion. The motion of the rotors is independently driven by motors.

It's important to emphasize that the TRMS model includes specific parameters and constants related to its physical properties, such as masses, lengths, and motor characteristics. These parameters are vital for accurately representing the system's behavior and should be obtained through measurements or experiments.

In this subsection, the methodology of this mathematical model is briefly explained, and the initial models of the TRMS are described. Both the 1-DOF model (without considering coupling effects) and the 2-DOF model (with coupling effects considered) are presented. The mathematical representation of the nonlinear plant is derived from Newton's 2nd law of motion, which serves as the foundation for constructing the mathematical model.

A mathematical model of the TRMS can be derived based on research conducted by [18] and [19]. The equations of motion for each rotor are coupled through the flexible beam, and they can be expressed in terms of the rotor angles, angular velocities, and the beam deflection angle. To simplify the TRMS model, a four-point mass system

is used, comprising the main rotor, tail rotor, balance-weight, and counter-weight, as depicted in Figure 1.1.

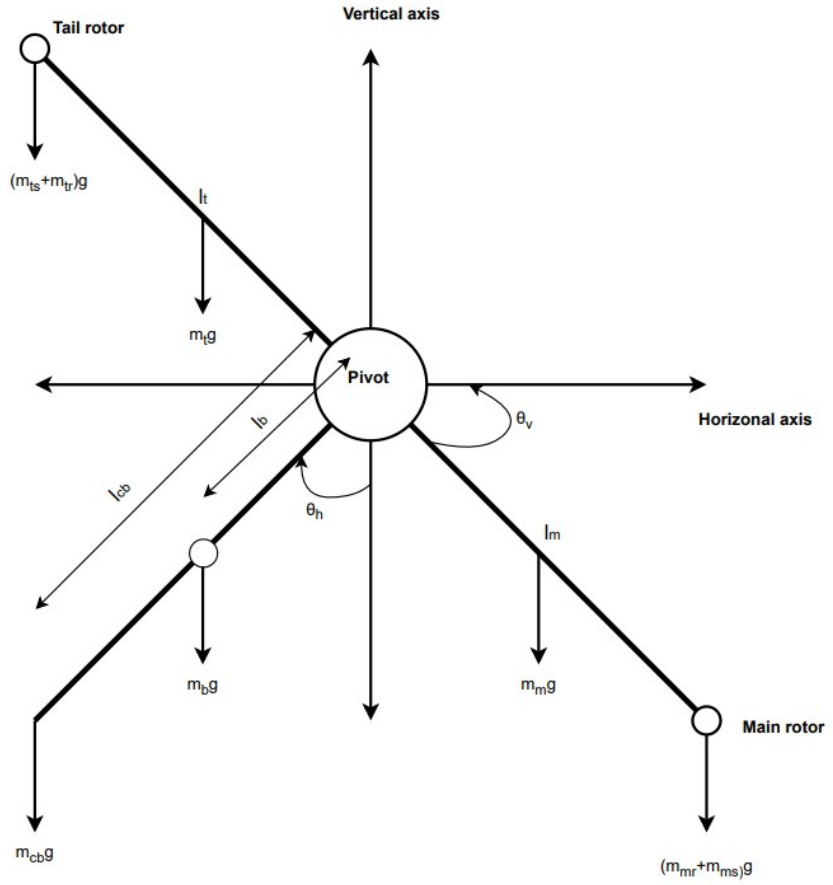

Figure 1.1 Free body diagram of a Twin Rotor MIMO System.

As shown in Figure 1.1, the propellers produce driving torque, and the mathematical model considers Newton's second law of rotation to derive the vertical and horizontal components of the system. Gravitational forces are also taken into account. The modeling process first considers the main rotor in the vertical plane, followed by the tail rotor in the horizontal plane.

The TRMS outputs are the elevation/ pitch angle (θ_v) with respect to the vertical axis and the azimuth / yaw angle (θ_h) with respect to the horizontal axis. The mathematical model developed through this approach serves as a fundamental basis for understanding and controlling the dynamics of the TRMS [20], [11], [21].

The mathematical model of TRMS is developed under the following assumptions:

1. The dynamics of the propeller subsystem can be expressed by first-order differential equations.
2. The friction in the system is of the viscous type, meaning it follows viscous damping characteristics.
3. The propeller air subsystem can be described by the flow theory of aerodynamics, which considers the aerodynamic forces and effects on the propellers.

These assumptions provide a basis for developing the mathematical representation of the TRMS.

Vertical Plane - Elevation/ Pitch Angle The total torque on vertical plane is

$$\sum_{k=1}^{4} M_v = J_v \frac{dS_v}{dt} = M_{v1} + M_{v2} + M_{v3} + M_{v4} \tag{1.1}$$

Where, the following definitions and equations hold: Moments of gravity forces (M_{v1}) applied to the beam and making it rotate around the horizontal:

$$M_{v1} = g[((\frac{m_t}{2} + m_{tr} + m_{ts})l_t - (\frac{m_m}{2} + m_{mr} + m_{ms})l_m)\cos\theta_v - (\frac{m_b}{2} i_b + m_{tb} l_{cb})\sin\theta_v] \tag{1.2}$$

The above equation can be written in compact form as:

$$M_{v1} = g[(A - B)\cos\theta_v - C\sin\theta_v] \tag{1.3}$$

Where:

$$A = (\frac{m_t}{2} + m_{tr} + m_{ts})l_t$$
$$B = (\frac{m_m}{2} + m_{mr} + m_{ms})l_m$$
$$C = (\frac{m_b}{2} l_b + m_{tb} l_{cb})$$

Moments of propulsive forces (M_{v2}) applied to the beam:

$$M_{v2} = i_m F_v(w_m) \tag{1.4}$$

The angular velocity w_m of main propeller is a nonlinear function of a rotation angle of the DC motor describing by the following equation without deep analysis of [22] and also given in [11] and [23].

$$w_m(u_{vv}) = 90.90u_{vv}^6 + 599.73u_{vv}^5 - 129.26u_{vv}^4 - 1238.64u_{vv}^3 + 63.45u_{vv}^2 + 1238.41u_{vv} \tag{1.5}$$

Additionally, the propulsive force F_v moving the joined beam in the vertical direction

is describing by a nonlinear function of the angular velocity w_m.

$$F_v(w_m) = -3.48x10^{-12}w_m^5 + 1.09x10^{-9}w_m^4 + 4.123x10^{-6}w_m^3 - 1.632x10^{-4}w_m^2 + 9.544x10^{-2}w_m \tag{1.6}$$

The relationship between the input voltage and the propulsive force for the main rotor: The model of the motor-propeller dynamics is obtained by substituting the nonlinear system by a serial connection of a linear dynamics system. This can be expressed as:

$$\begin{aligned} \frac{du_{vv}}{dt} &= \frac{1}{T_{mr}}(-u_{vv} + u_v) \\ \frac{du_{vv}}{dt}T_{mr} + u_{vv} &= u_v \\ (T_{mr}s + 1)u_{vv} &= u_v \\ \frac{u_{vv}}{u_v} &= \frac{K_{mr}}{(T_{mr}s + 1)} \end{aligned} \tag{1.7}$$

DC motor input voltage is u_v, and motor time constant of the main rotor is T_{mr} static gain of the DC motor is K_{mr}.

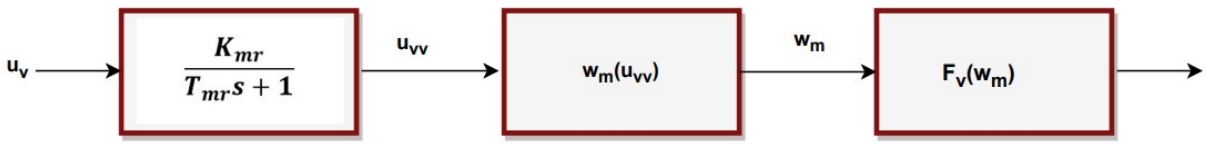

Figure 1.2 The relationship between the input voltage and the propulsive force for the main rotor.

Moment of Centrifugal forces corresponding to motion of beam around vertical axis:

$$M_{v3} = -\frac{1}{2}\omega_h^2(H)sin2\theta_v \tag{1.8}$$

$With : H = A + B + C)$

Remember trigonometric properties of: $sin2\theta_v$=$2sin\theta_v cos\theta_v$

Moment of friction (M_{v4}) depends on the angular velocity of the beam around the horizontal axis.

$$M_{v4} = -\omega_v k_v \tag{1.9}$$

$$Where : \omega_v = \frac{d\theta_v}{dt}$$

The total Torque for Vertical plane is therefore,

$$
\begin{aligned}
& J_v \frac{dS_v}{dt} = M_{v1} + M_{v2} + M_{v3} + M_{v4} \\
& \frac{dS_v}{dt} = \frac{g[(A-B)cos\theta_v - Csin\theta_v] + i_m F_v(w_m) - \frac{1}{2}\omega_h^2(H)sin2\theta_v - \omega_v k_v}{J_v} \\
Where: \; & A = (\frac{m_t}{2} + m_{tr} + m_{ts})l_t \\
& B = (\frac{m_m}{2} + m_{mr} + m_{ms})l_m \\
& C = (\frac{m_b}{2} i_b + m_{tb} l_{cb}) \\
& H = Al_t + Bl_m - (\frac{m_b}{2} l_b^2 + m_{cb} l_{cb}^2) \\
& \omega_h = \frac{d\theta_h}{dt} \\
& \omega_v = \frac{d\theta_v}{dt}
\end{aligned}
\tag{1.10}
$$

The total inertia for vertical plane as follows:

$$J_v = \sum_{k=1}^{8} J_{vi} = J_{v1} + J_{v2} + J_{v3} + J_{v4} + J_{v5} + J_{v6} + J_{v7} + J_{v8} \tag{1.11}$$

Moment of Inertia for main rotor with motor

$$J_{v1} = m_{mr} l_m^2 \tag{1.12}$$

Moment of Inertia for main rotor beam

$$J_{v2} = m_m \frac{l_m^2}{3} \tag{1.13}$$

Moment of Inertia for solid cylinder shaped counter weight

$$J_{v3} = m_{cb} l_{cb}^2 \tag{1.14}$$

Moment of Inertia for rod of counter weight

$$J_{v4} = m_b \frac{l_b^2}{3} \tag{1.15}$$

Moment of Inertia for tail rotor with motor

$$J_{v5} = m_{tr} l_t^2 \tag{1.16}$$

Moment of Inertia for tail beam

$$J_{v6} = m_t \frac{l_t^2}{3} \tag{1.17}$$

Moment of Inertia for shield of main rotor

$$J_{v7} = \frac{m_{ms}}{2} r_{ms}^2 + m_{ms} l_m^2 \tag{1.18}$$

Moment of Inertia for shield of tail rotor

$$J_{v8} = m_{ts} r_{ts}^2 + m_{ts} l_t^2 \tag{1.19}$$

The total Inertia for Vertical plane is therefore,

$$J_v = \sum_{k=1}^{8} J_{vi} = J_{v1} + J_{v2} + J_{v3} + J_{v4} + J_{v5} + J_{v6} + J_{v7} + J_{v8}$$
$$= (m_{mr} + \frac{m_m}{3} + m_{ms})l_m^2 + (m_{tr} + \frac{m_t}{3} + m_{ts})l_t^2 + m_{cb}l_{cb}^2 + m_b\frac{l_b^2}{3} + m_{ts}r_{ts}^2 + m_{ts}r_{ts}^2 + \frac{m_{ms}}{2}r_{ms}^2 \tag{1.20}$$

Horizontal Plane - Yaw Angle Similarly, the motion of the beam in the horizontal plane (around the vertical axis) is described by the following figure. The tail rotor model is produced from the driving torques's as the following

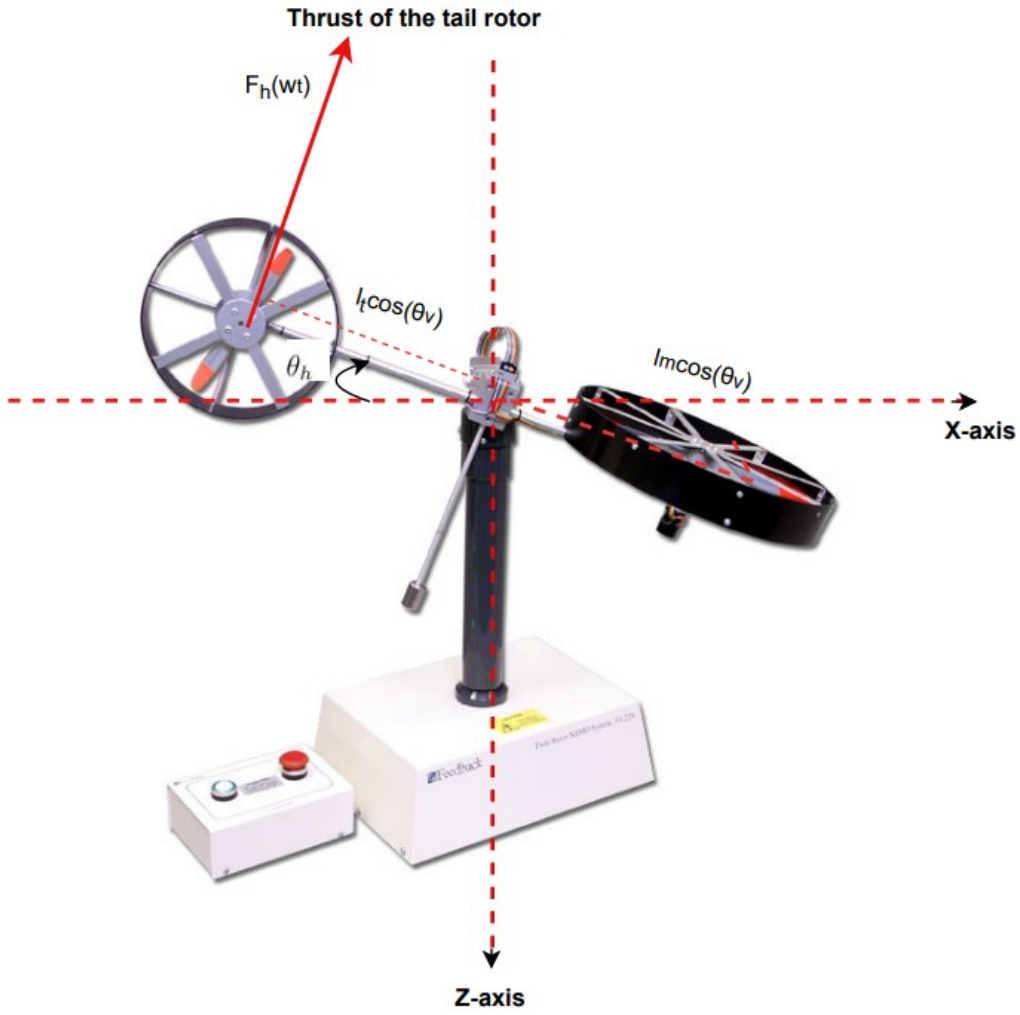

Figure 1.3 The motion of TRMS on the vertical axis.

The total torque on horizontal plane is

$$\sum_{k=1}^{2} M_h = J_h \frac{dS_h}{dt} = M_{h1} - M_{h2} \tag{1.21}$$

M_{h1} Moment of Propulsive forces (Thrust) applied to beam

$$M_{h1} = F_h(w_t) l_t cos\theta_v \tag{1.22}$$

Similarly, the angular velocity w_t of tail is described by a nonlinear function as the following equations as stated in [11], [22] and [23].

:

$$w_t(u_{hh}) = 2020u_{hh}^5 + 194.69u_{hh}^4 - 4283.15u_{hh}^3 - 262.87u_{hh}^2 + 3796.83u_{hh} \tag{1.23}$$

Furthermore, the propulsive force F_h moving the joined beam in the Horizontal direction is describing by thev following as stated in the same references.

$$F_h(w_t) = -3x10^{-14}w_t^5 + 1.595x10^{-11}w_t^4 + 2.511x10^{-7}w_t^3 - 1.808x10^{-4}w_t^2 + 0.8080w_t \tag{1.24}$$

An equation of motion for motor-propeller dynamics can be derived by connecting a nonlinear system to a system of linear dynamics. The following can be expressed as follows:

$$\frac{du_{hh}}{dt} = \frac{1}{T_{tr}}(-u_{hh} + u_h) \tag{1.25}$$

DC motor input voltage is u_h, and motor time constant of the tail rotor is T_{tr} static gain of the DC motor is K_{tr}.

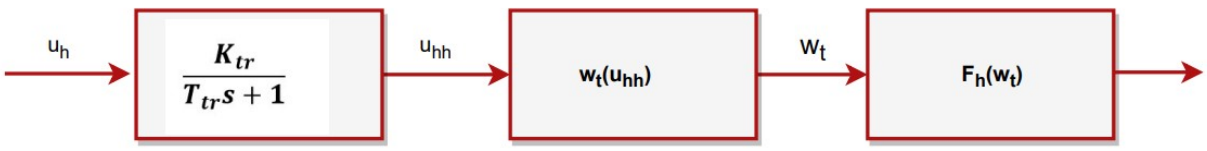

Figure 1.4 The relationship between the input voltage and the propulsive force for the tail rotor.

M_{h2} Moment of Friction depending on the angular velocity of beam around the vertical axis

$$M_{h2} = -\omega_h k_h \tag{1.26}$$

$$\sum_{k=1}^{2} M_h = J_h \frac{dS_h}{dt} = F_h(w_t) l_t cos\theta_v - \omega_h k_h \tag{1.27}$$

The inertia for horizontal plane :

$$J_h = \sum_{k=1}^{8} J_{hi} = J_{h1} + J_{h2} + J_{h3} + J_{h4} + J_{h5} + J_{h6} + J_{h7} + J_{h8}$$

$$\begin{aligned}
J_{h1} &= \frac{m_m}{3}(l_m cos\theta_v)^2 \\
J_{h2} &= \frac{m_t}{3}(l_t cos\theta_v)^2 \\
J_{h3} &= \frac{m_b}{3}(l_b sin\theta_v)^2 \\
J_{h4} &= m_{tr}(l_t cos\theta_v)^2 \\
J_{h5} &= m_{mr}(l_m cos\theta_v)^2 \\
J_{h6} &= m_{cb}(l_{cb} sin\theta_v)^2 \\
J_{h7} &= \frac{m_t s}{2} r_{ts}^2 (l_t cos\theta_v)^2 \\
J_{h8} &= m_{ms} r_{ms}^2 + m_{tm}(l_m cos\theta_v)^2
\end{aligned} \tag{1.28}$$

In compact form:

$$J_h = Dsin^2\theta_v + Ecos^2\theta_v + F$$

$$\begin{aligned}
Where: D &= \frac{m_b}{3} l_b^2 + m_{cb} l_{cb}^2 \\
E &= (\frac{m_m}{3} + m_{mr} + m_{ms}) l_m^2 + (\frac{m_t}{3} + m_{tr} + m_{ts}) l_t^2 \\
F &= m_{ms} r_{ms}^2 + \frac{m_{ts}}{2} r_{ts}^2
\end{aligned} \tag{1.29}$$

Summary of Both Vertical and Horizontal equations:

$$\begin{aligned}
\frac{dS_v}{dt} &= \frac{g[(A-B)cos\theta_v - Csin\theta_v] + l_m F_v(w_m) - \frac{1}{2}\omega_h^2(H) sin2\theta_v - \omega_v k_v}{J_v} \\
\frac{d\theta_v}{dt} &= \omega_v \\
\frac{d\theta_v}{dt} &= \omega_v = S_v + \frac{J_{tr}\omega_t}{J_v}
\end{aligned} \tag{1.30}$$

Where:

S_v: The angular momentum of the beam in the vertical plane.

ω_t: The angular velocity of the tail rotor.

$$\begin{aligned}
\frac{dS_h}{dt} = \frac{d\theta_h^2}{dt^2} &= \frac{F_h(w_t) l_t cos\theta_v - \omega_h k_h}{J_h} \\
\frac{d\theta_h}{dt} &= \omega_h \\
\omega_h &= S_h + \frac{J_{mr}\omega_m cos\theta_v}{J_h} = S_h + \frac{J_{mr} w_m cos\theta_v}{Dsin^2\theta_v + Ecos^2\theta_v + F}
\end{aligned} \tag{1.31}$$

Where:
S_h: The angular momentum of the beam in the horizontal plane.

ω_m: The angular velocity of the main rotor

The Aero Force Balance (AFB) scale is indeed a crucial calibration factor used in wind tunnel testing of aircraft models. It represents the force measured by the AFB, which is mounted on the aircraft model, per unit of force generated by the model's propulsion system.

In the specific case of a Twin Rotor MIMO (Multiple-Input, Multiple-Output) system, the AFB scale is typically given by the expression: AFB scale = 5 / (2.895 * 2048)

The dimensions and masses of the components of the TRMS can be determined through physical measurements, and these values are usually provided in the TRMS manual [24]. The constants' measurements are summarized in the table below:

Symbol	Definition	Value
m_m	The mass of the beam part holding the main rotor	0.0145 kg
m_{mr}	The mass of the main rotor	0.228 kg
m_{ms}	The mass of the main shield	0.225 kg
m_t	The mass of the beam part holding the tail rotor	0.0155 kg
m_{tr}	The mass of the tail rotor	0.206 kg
m_{ts}	The mass of the tail shield	0.162 kg
m_{cb}	The mass of the counterweight	0.068 kg
m_b	The mass of the counterweight beam	0.022 kg
l_m	The length of the main part of the beam	0.24 m
l_t	The length of the tail part of the beam	0.25 m
l_{cb}	The distance between the counterweight and the pivot	0.13 m
l_b	The length of the counterweight beam	0.13 m
r_{ms}	Radius of the main shield	0.155 m
r_{ts}	Radius of the tail shield	0.10 m
k_h	Constant	$0.1099\,\mathrm{N\,s\,rad^{-1}}$
m_b	Mass of the counterbalance beam	0.022 kg
g	Gravitational acceleration of the earth	$9.81\,\mathrm{m\,s^{-2}}$

Table 1.1 Parameters of TRMS - Part 1 [24]

1.4 Modelling of Twin Rotor MIMO System-Part -2

According to Diagram 1.5, the derivation of the non-linear model equations is possible. Specifically, the momentum equations can be derived to describe the vertical movement

[25].

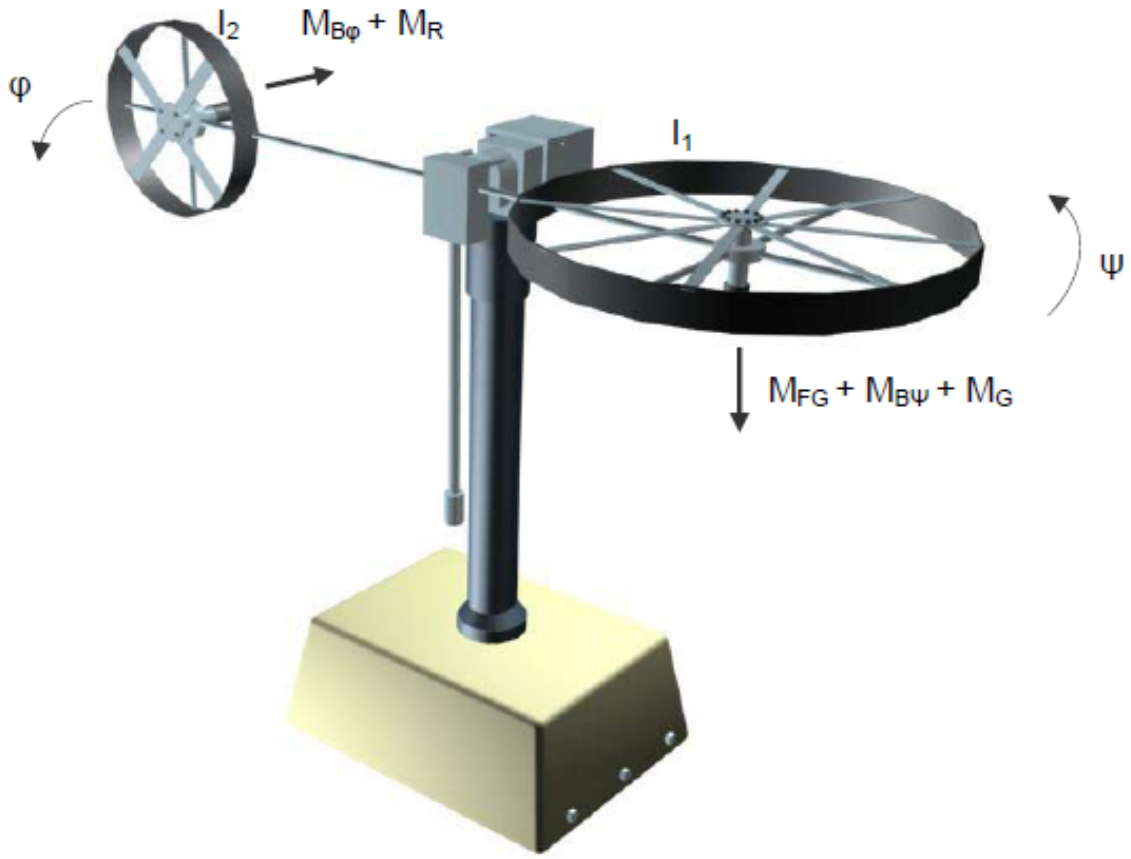

Figure 1.5 The TRMS Model [25]

.

$$I_1.\ddot{\psi} = M_1 - M_{FG} - M_{B\psi} - M_G \tag{1.32}$$

Where the following equation is valid:

$$\begin{aligned} M_1 &= a_1\tau_1^2 + b_1\tau_1 \quad \text{(Nonlinear static characteristics)} \\ M_{FG} &= M_g \sin\psi \quad \text{(Gravity momentum)} \\ M_{B\psi} &= B_{1\psi}\dot{\psi} + B_{2\psi}\text{sign}(\dot{\psi}) \quad \text{(Friction forces momentum)} \\ M_G &= K_{gy}M_1\dot{\phi}\cos\psi \quad \text{(Gyroscopic momentum)} \end{aligned} \tag{1.33}$$

The motor momentum is described by:

$$\tau_1 = \frac{k_1}{T_{11}s + T_{10}}.u_1 \tag{1.34}$$

For horizontal plane motion, the similar equations valid:

$$I_2.\ddot{\phi} = M_2 - M_{B\phi} - M_R \tag{1.35}$$

Where the following equation is valid:

$$\begin{aligned} M_2 &= a_2\tau_2^2 + b_2\tau_2 \quad \text{(Nonlinear static characteristics)} \\ M_{B\psi} &= B_{1\phi}\dot{\psi} + B_{2\phi}\text{sign}(\dot{\phi}) \quad \text{(Friction forces momentum)} \end{aligned} \tag{1.36}$$

The cross reaction momentum, M_R is approximated by:

$$M_R = \frac{k_c(T_o s + 1)}{T_p s + 1}.\tau_1 \tag{1.37}$$

The DC motor with electrical circuit is described by:

$$\tau_2 = \frac{k_2}{T_{21}s + T_{20}}.u_2 \tag{1.38}$$

The measurements of the constants are provided in the TRMS manual [25] and summarized in the table below:

Symbol	Definition	Value
I_1	Moment of inertia of vertical plane	$6.8 \times 10^{-2}\,\mathrm{kg\,m^2}$
I_2	Moment of inertia of horizontal plane	$2 \times 10^{-2}\,\mathrm{kg\,m^2}$
a_1	Static characteristic of parameter	0.0135
b_1	Static characteristic of parameter	0.0924
a_2	Static characteristic of parameter	0.02
b_2	Static characteristic of parameter	0.09
M_g	Gravity momentum	$0.32\,\mathrm{N\,m}$
$B_{1\psi}$	Friction momentum	$6 \times 10^{-3}\,\mathrm{N\,m\,s\,rad^{-1}}$
$B_{2\psi}$	Friction momentum	$1 \times 10^{-3}\,\mathrm{N\,m\,s^2\,rad^{-1}}$
$B_{1\phi}$	Friction momentum	$1 \times 10^{-1}\,\mathrm{N\,m\,s\,rad^{-1}}$
$B_{2\phi}$	Friction momentum	$1 \times 10^{-2}\,\mathrm{N\,m\,s^2\,rad^{-1}}$
K_{gy}	Gyroscopic momentum of parameter	$0.05\,\mathrm{s\,rad^{-1}}$
k_1	Gain of main rotor	1.1
k_2	Gain of tail rotor	0.8
T_{11}	Main rotor denominator	1.1
T_{10}	Main rotor denominator	1
T_{21}	Tail rotor denominator	1
T_{20}	Main rotor denominator	1
T_p	Cross reaction momentum of the parameter	2
T_o	Cross reaction momentum of the parameter	3.5
k_c	Tail rotor denominator	-0.2

Table 1.2 Parameters of TRMS - Part 2 [25]

1.5 An Overview on Controller Design

1.5.1 Integer Order PID Controller - IOPID

IOPID controllers are widely popular control algorithms that compute a control command equal to the sum of three components. These controllers calculate the error as the difference between the desired output of the system and the actual output and apply a correction based on proportional (denoted P), integral (denoted I), and derivative (denoted D) terms. The IOPID controller dynamically adjusts the control signal by considering the present error, the accumulated error over time, and the rate of change of the error, leading to effective and precise control in a wide range of applications.

- **Proportional component**: This component applies the proportional gain to the control error, which is the difference between the desired output of the system and the actual output. It generates an output value that is proportional with the current error value, thus determining the proportion of the output response to the error [26].

- **Integral component**: The integral gain is applied to the integral of the error. It ensures that the system will only stabilize when the error reaches zero, preventing any steady-state errors. It generates an output value that is directly proportional with the accumulated error over time and is used to drive the error towards zero [26].
- **Derivative component**: This component applies the derivative gain to derivative of error. It generates an output value that is directly proportional with rate at which the error has been changing and is used to anticipate the future error and reduce the overshoot [26].

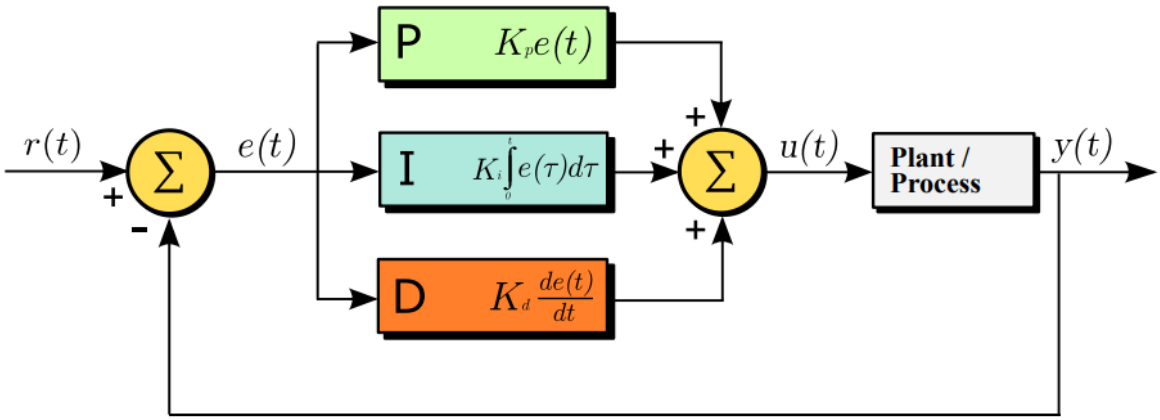

Figure 1.6 A block diagram of a IOPID controller in a feedback loop [26].

Where: - $r(t)$: The desired setpoint at time t.
- $e(t)$: The error at time t, which is the difference between the desired setpoint and the current process variable.
- $u(t)$: The control signal (output) at time t sent to the actuator.
- $y(t)$: The measured process variable at time t.
- K_p: The proportional gain.
- K_i: The integral gain.
- K_d: The derivative gain.

Mathematical form:

The overall control function

$$u(t) = K_p \cdot e(t) + K_d \frac{de(t)}{dt} + K_d \frac{de(t)}{dt} \tag{1.39}$$

The ratio between the controller output, U(s), and the error, E(s), is termed the controller transfer function, yielding the following outcomes:

$$C(s) = \frac{U(s)}{E(s)} = K_p + \frac{K_i}{s} + K_d s \tag{1.40}$$

Tuning an IOPID controller is indeed an iterative process. Several methods can be employed for tuning an IOPID controller, with one of the popular techniques being the Ziegler-Nichols method. However, this paper introduces an alternative approach for IOPID controller tuning using optimization methods, specifically the Particle Swarm Optimization (PSO), Genetic Algorithm (GA), and Nelder-Mead (NM) methods.

In the subsequent sections, the paper provides a comprehensive explanation of the tuning methods for PSO, GA, and NM algorithms. These optimization techniques aim to find the best set of controller parameters that optimize the system's performance and meet the desired control objectives for the IOPID control scheme.

1.5.2 An Overview of the Dynamic Behavior of a System

In control theory and system analysis, a step response is a common method for characterizing the dynamic behavior of a system. It represents how a system reacts to an abrupt change, known as a step input, where the input variable abruptly transitions from one value to another.

To analyze the step response, the system's output variable is plotted against time, starting from the moment the input change occurs. Several key parameters can be used to characterize the step response, including:
Rise time: the time it required or takes for the output to rise from 10% to 90% of of its final steady-state value after a step input is applied. A fast rise time indicates good performance, but may lead to overshoot or oscillations [27].

Settling time: time takes or required to achieve the settling of the output within tolerance error band (usually 5%) of its final steady-state value after a step input is applied and a shorter settling time indicates better performance [27] [28] [29].

Overshoot: the maximum percentage by which the output exceeds its final value before settling. A smaller overshoot indicates better performance [27] [28] [29].

Steady-state error: is the difference between the desired input and the actual output when the system has reached steady-state. A smaller steady-state error indicates better performance [27] [28] [29].

These parameters are important for understanding the behavior of a system and for

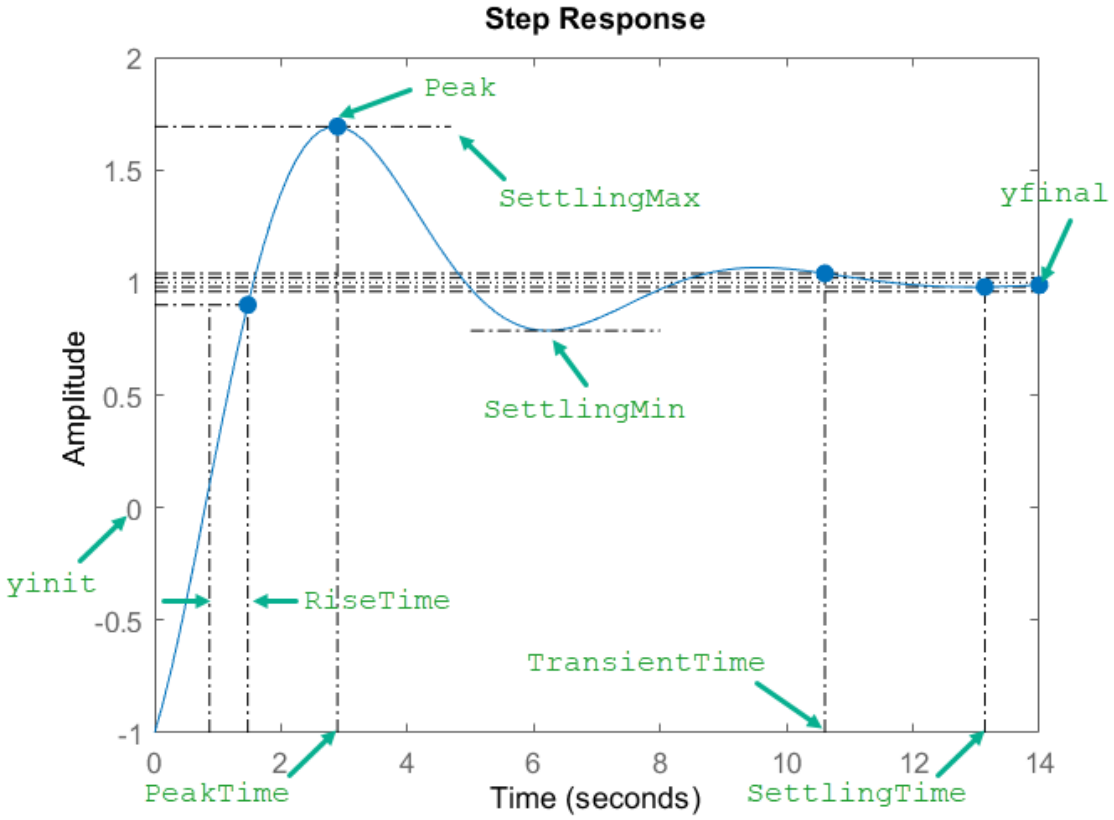

Figure 1.7 Some of the dynamic characteristics for a step response [30].

designing control systems that can regulate the output of the system. They can be determined experimentally by measuring the output of the system in response to a step input or by analyzing the mathematical model of the system.

1.5.3 Fractional Order PID Controller - FOPID

Introduction to Fractional Calculus

The fractional-order differintegral operator D_t^α, with order α, applied to a given function $f(t)$, is defined as follows:

$$D_t^\alpha = \begin{cases} \frac{d^\alpha}{dt^\alpha} f(t) & \text{if } \alpha > 0; \\ f(t) & \text{if } \alpha = 0; \\ \int_0^t f(\tau)\, d\tau & \text{if } \alpha < 0. \end{cases} \tag{1.41}$$

Among the various definitions, the three most commonly used methods for defining the fractional-order derivative D_t^α with order α are Grünwald–Letnikov, Riemann–Liouville, and Caputo, each serving distinct purposes in the analysis of fractional calculus, as

summarized in a review by Bingi et al. [31].

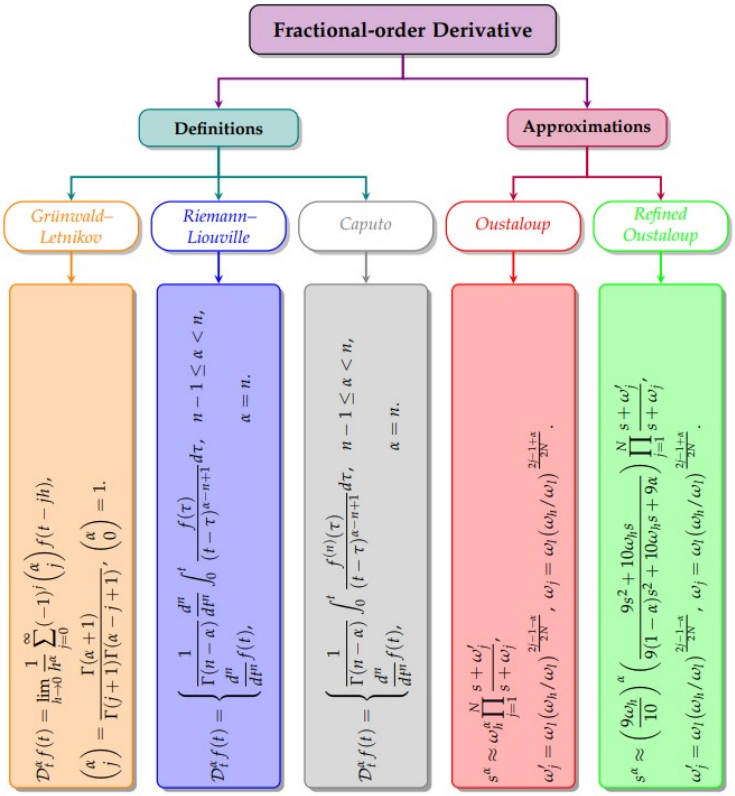

Figure 1.8 Definitions and Approximation Techniques of Fractional-Order Derivatives [31].

Fractional-Order Proportional-Integral-Derivative (FOPID) is represented by $PI^{\lambda}D^{\mu}$. **Mathematical form**:

The overall control function

$$u(t) = K_p \cdot e(t) + K_d D^{-\lambda} e(t) + K_d^{\mu} e(t) \tag{1.42}$$

In general, for closed loop control system, the transfer function of FOPID can be represented by the form:

$$C(s) = \frac{U(s)}{E(s)} = K_p + K_i s^{-\lambda} + K_d s^{\mu} \tag{1.43}$$

Where , involving an integrator of order λ and a differentiator of order μ, where both parameters can be any positive real numbers; K_p is proportional gain, K_i is integral gain, K_d, differential gain constant. When $\lambda = 1$ and $\mu = 1$ we obatain IOPID controller.

$$C(s) = \frac{U(s)}{E(s)} = K_p + K_i \frac{1}{s} + K_d s \tag{1.44}$$

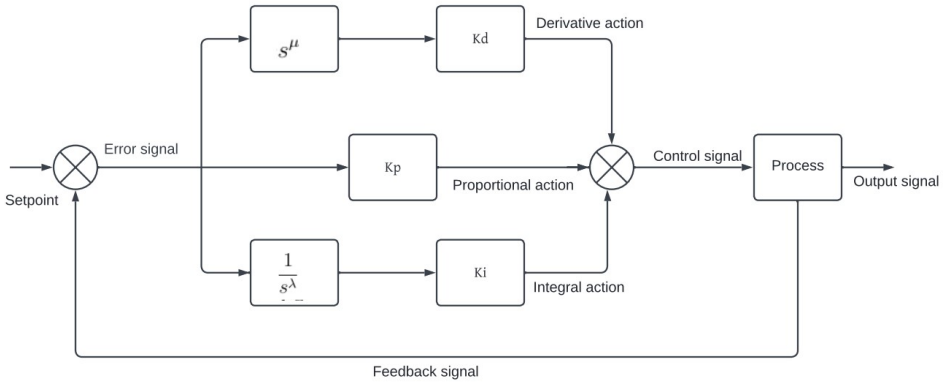

Figure 1.9 Block diagram of Fractional Order PID controller.

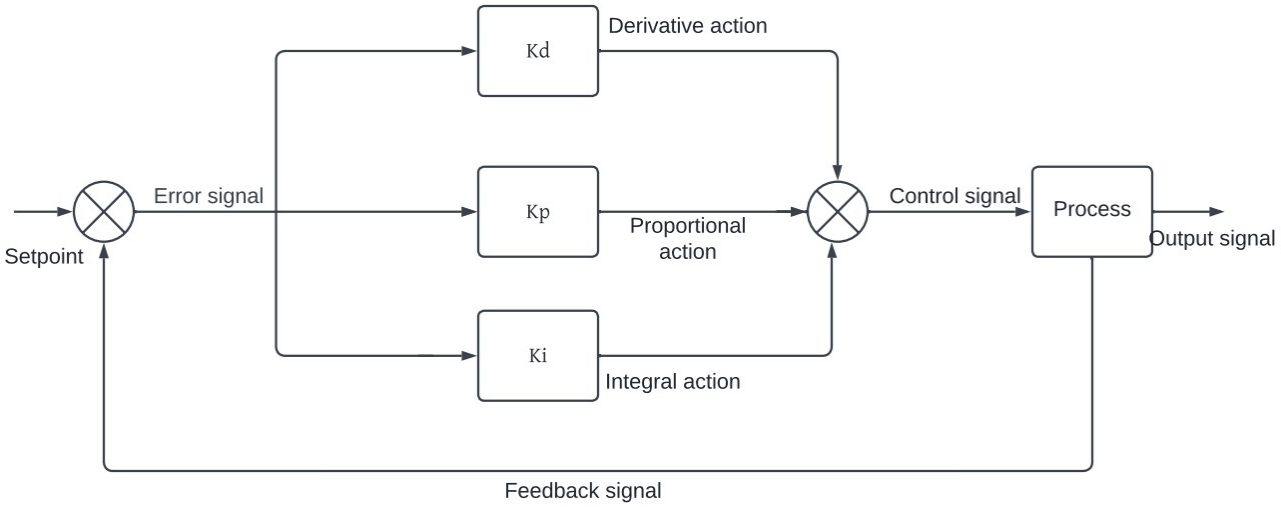

Figure 1.10 Block diagram of Integer Order PID controller.

If $\lambda = 1$ and $\mu = 0$ and $\lambda = 0$ and $\mu = 1$, the convectional PI and PD controller can be recovered respectively. Moreover, for closed loop control system there are four situtations.

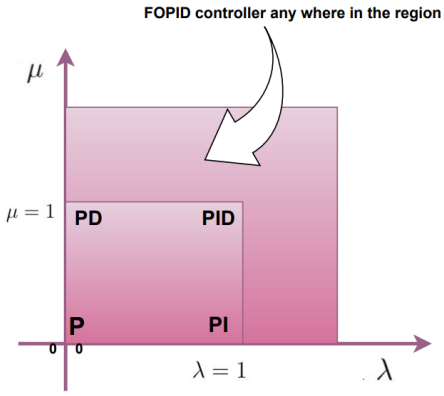

Figure 1.11 FOPID controller region of μ and λ interest.

Integer order plant with integer order controller -An integer order plant with an integer order controller is a type of control system where the plant and the controller are both represented by integer-order transfer functions. In other words, the differential equations governing the dynamics of the plant and the controller are both represented by polynomials with integer exponents.

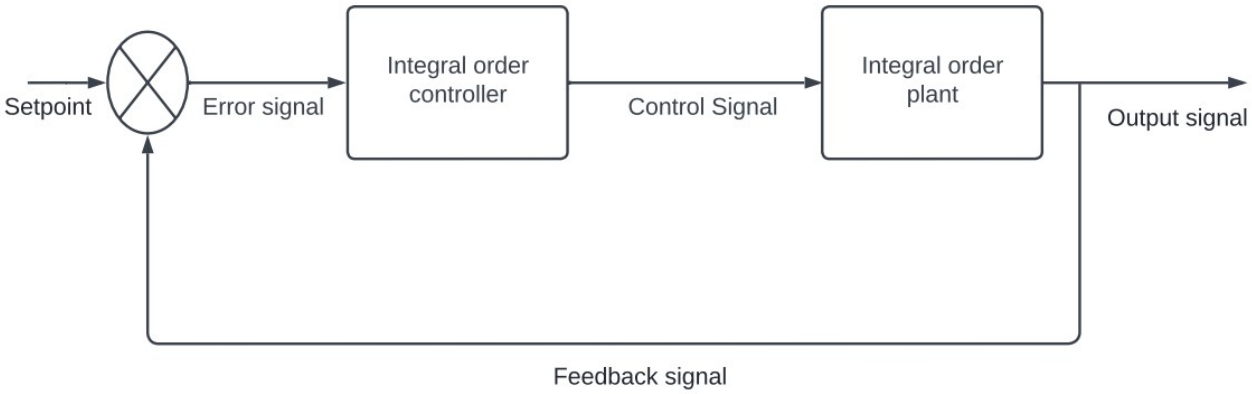

Figure 1.12 Block diagram of integer order plant with integer order controller.

Integer order plant with fractional order controller - An integer order plant with a fractional order controller is a type of control system where the plant is represented by an integer-order transfer function, while the controller is represented by a fractional-order transfer function. In other words, the differential equation governing the dynamics of the controller is represented by a polynomial with a non-integer exponent.

Fractional order plant with integer order controller -In a control system, a fractional order plant with an integer order controller is a system where the plant dy-

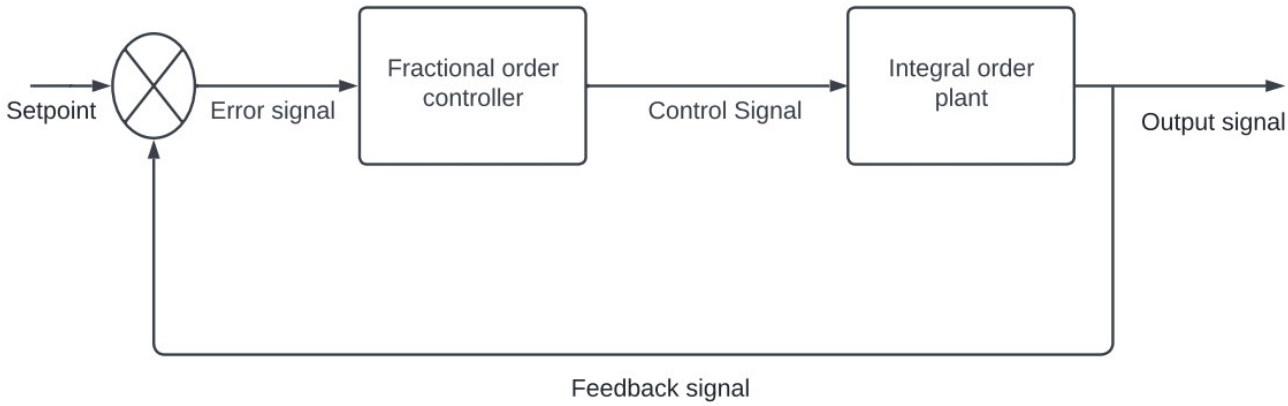

Figure 1.13 Block diagram of integer order plant with fractional order controller.

namics are modeled by a fractional order transfer function and the controller dynamics are modeled by an integer order transfer function.

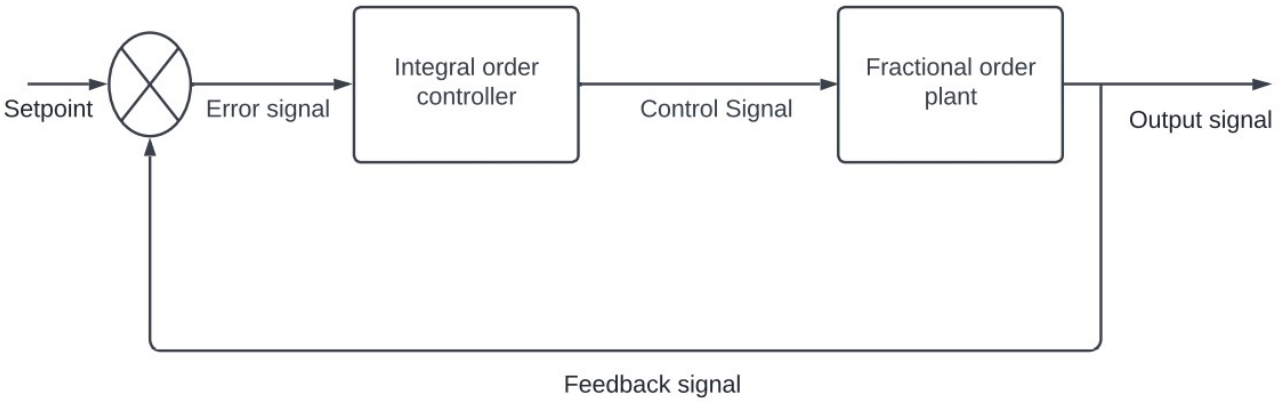

Figure 1.14 Block diagram of fractional order plant with integer order controller.

Fractional order plant with fractional order controller - A fractional order plant with a fractional order controller is a type of control system where both the plant and the controller are represented by transfer functions with non-integer exponents. In this case, the differential equations governing the dynamics of both the plant and the controller are represented by polynomials with fractional exponents.

The use of fractional order control has gained popularity in recent years, as it provides improved control performance compared to traditional integer-order control, particularly for systems with complex dynamics. A fractional order plant with a fractional order controller is particularly useful in such applications where traditional integer-order control cannot achieve the desired performance.

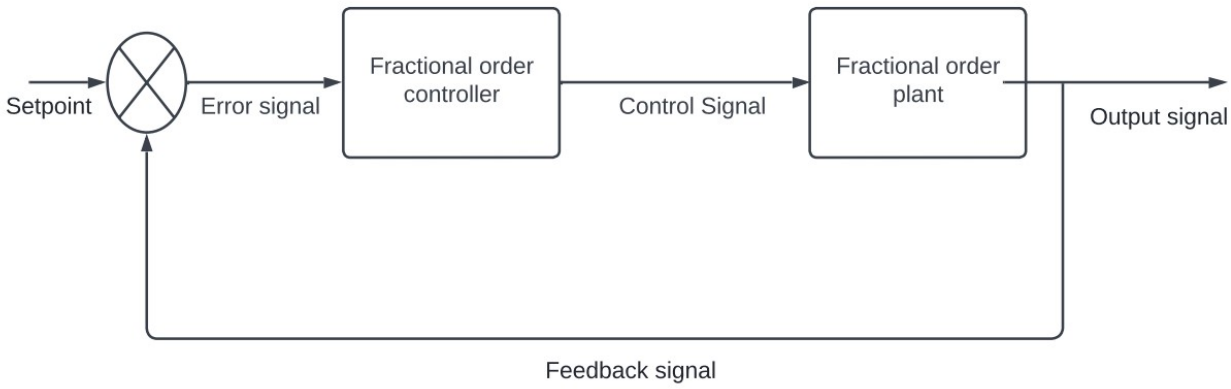

Figure 1.15 Block diagram of fractional order plant with fractional order controller.

This thesis consider both integer order plants with integer order controllers and integer order plants with fractional order controllers in the analysis, utilizing simulations and real-time experiments.

This paper presents an optimization approach to tune FOPID controllers using optimization methods such as PSO, GA, and NM methods. The subsequent sections elaborate on the tuning procedures for the PSO, GA, and NM algorithms.

1.5.4 The Performance of a Control System.

According to [32], in the time domain, various performance criteria are typically used to evaluate and tune the performance of controllers. These include rise time, settling time, overshoot, steady state error, ITSE, ITAE, ISE and IAE.

Integral of the absolute error (IAE): the IAE between the setpoint and the actual output over a specified time interval. A smaller IAE indicates better performance [27] [28] [29].

$$IAE = \int |e(t)|\, dx \tag{1.45}$$

Integral of the squared error (ISE): The ISE between the setpoint and the actual output over a specified time interval. A smaller ISE indicates better performance.

$$ISE = \int e^2(t)\,dx \tag{1.46}$$

Integral of time-weighted absolute error (ITAE): the ITAE between the setpoint and the actual output weighted by time over a specified time interval. A smaller ITAE indicates better performance.

$$ITAE = \int t|e(t)|\,dx \tag{1.47}$$

Integral of time squared error (ITSE): the ITSE between the setpoint and the actual output weighted by time over a specified time interval. A smaller ITSE indicates better performance.

$$ITSE = \int te^2(t)\,dx \tag{1.48}$$

These performance criteria can be used to evaluate and tune the performance of various types of controllers, including IOPID controllers, FOPID controllers, and to compare the performance of different control strategies.

Generally,

In this thesis, two common types of controllers used for control of the TRMS are the IOPID controller and the FOPID controller. The IOPID controller is a classical control technique that is widely used in industrial control systems. The IOPID controller works by computing an error signal that represents the difference between the desired output of the system and the actual output. The controller then adjusts the input to the system based on the error signal, using three components: proportional, integral, and derivative. The proportional component is proportional to the error signal, the integral component is proportional to the integral of the error signal, and the derivative component is proportional to the rate of change of the error signal.

The FOPID controller is an extension of the classical PID controller that includes a fractional-order derivative component. The fractional-order derivative allows the controller to capture the memory and long-term behavior of the system and can improve the controller's performance in handling nonlinear and time-varying systems.

In summary, real-time control of the TRMS using PID and FOPID controllers is an

important research area in control systems engineering, and it requires a deep understanding of the dynamics of the TRMS, as well as the ability to design and implement control algorithms on real-time platforms.

1.5.5 Tips for Optimization Methods: PSO, GA, and NM Algorithms

In the context of optimization for IOPID and FOPID controllers, PSO, GA, and NM refer to different optimization techniques. These techniques are used to tune the parameters of the controllers to achieve optimal or desired performance in control systems.

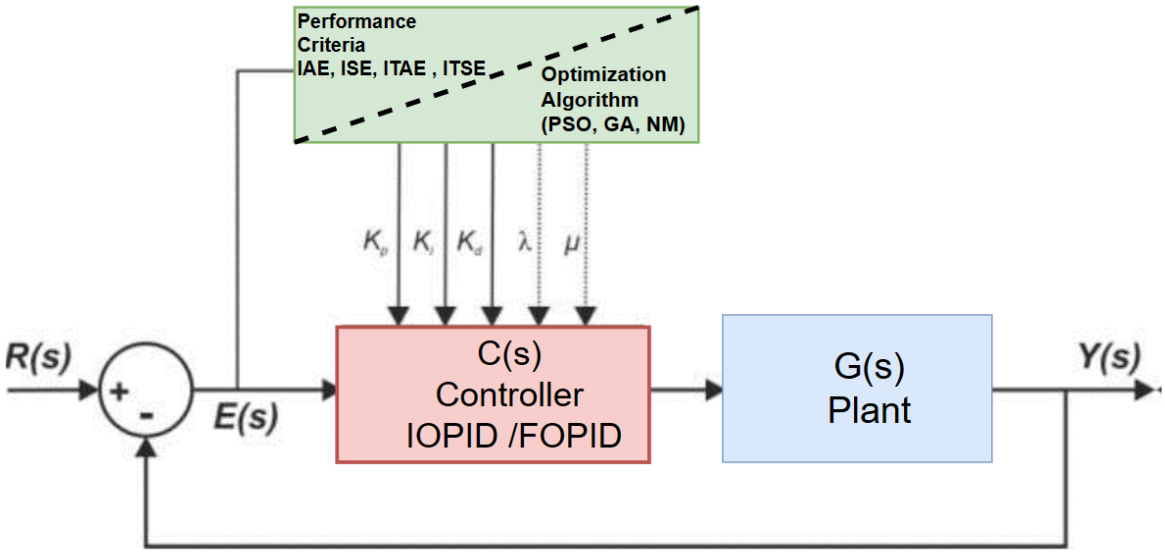

Figure 1.16 Block diagram of Control System used in the Optimization Method.

PSO (Particle Swarm Optimization):

Particle Swarm Optimization (PSO) is an optimization technique that draws inspiration from the behavior observed in bird flocking or fish schooling. It involves a group of particles representing solutions navigating through the search space to find the solution. Each particles position represents a solution and its movement is influenced by its experience (the best solution it has encountered so far) as well, as the experiences of its neighboring particles. Through adjustments PSO continues until a stopping criterion is met or an optimal solution is discovered. This method has found application in optimizing control system parameters, such as FOPID and IOPID controllers to achieve performance and stability.

MATLAB has built-in functions for PSO in the Global Optimization Toolbox. Specifically, this paper use the "particleswarm" function to implement the PSO algorithm for the optimization problems.

```
options = optimoptions('particleswarm', 'SwarmSize', 50);
[x, fval] = particleswarm(@objective_function, num_variables, lb, ub, options);
```

Here, "$objective-function$" is your custom objective function to be optimized, "$num-variables$" is the number of variables in the optimization problem, "lb" and "ub" are the lower and upper bounds of the variables, and "options" is an optional structure containing various settings for the PSO algorithm.

GA (Genetic Algorithm):

Genetic Algorithm (GA) on the hand is another optimization technique inspired by selection and genetics. It simulates a process within a population of solutions using genetic operations like selection, crossover and mutation. The process initiates with a population of generated solutions and in each iteration individuals, with fitness (measured by a fitness function) are more likely to be selected for creating new solutions in the subsequent generation. This iterative process persists until a stopping criterion is met or an optimal solution is identified. GA has been successfully employed for optimizing control system parameters, including FOPID and IOPID controllers.

The Global Optimization Toolbox includes a built function known as "ga" for the Genetic Algorithm.

```
options = optimoptions('ga', 'PopulationSize', 100);
[x, fval] = ga(@objective_function, num_variables, [], [], [], [], lb, ub, [], op
```

Similar to PSO, "$objective-function$" is custom objective function, "$num-variables$" is the number of variables, "lb" and "ub" are the lower and upper bounds, and "options" is an optional structure containing settings for the GA.

NM (Nelder-Mead):

Nelder-Mead is a direct search optimization algorithm that belongs to the class of simplex-based methods. It is also known as the downhill simplex method. NM is a gradient-free optimization technique, which means it does not require information about the gradient (derivative) of the objective function being optimized. The algorithm starts with an initial simplex (a set of points in the search space) and iteratively

moves the simplex to converge towards an optimal solution. The algorithm is guided by the function evaluations at the vertices of the simplex. NM has been used to optimize the parameters of control systems, including FOPID and IOPID controllers.

```
options = optimset('Display', 'iter');
[x, fval] = fminsearch(@objective_function, initial_guess, options);
```

Here, "$objective - function$" is custom objective function, "$initial - guess$" is the starting point for the optimization, and "options" is an optional structure containing settings for the Nelder-Mead algorithm.

1.6 System Identification

System identification is the process of constructing a mathematical model that represents the behavior of a dynamic system, based on measured input and output data, without detailed knowledge of the underlying system's internal structure or physical principles governing its operations. To achieve this, system identification employs an approach known as "black box identification," which enables us to effectively capture and understand the system's characteristics without understanding the internal mechanisms. There are several steps to conduct system identification:

I. **Data Collection**: Collect data from the system by applying input signals and measuring the corresponding output signals. The data should be representative of the operating conditions of the system. For this specific thesis, the input signal consists of several step control input voltages.

II. **Model Structure Selection**: Select a mathematical model structure that is appropriate for the system being identified. The model structure should include all relevant input-output relationships. For this paper, three identification model structures are selected and compared, i.e., identification by "$fminsearch$", ARX and $ARMAX$.

III. **Simulation and Model Validation**: Validate the identified model by comparing the predicted output of the model with the measured output data that is from real laboratory model and nonlinear model.

These steps are crucial in the system identification process, as they enable us to develop accurate models that can be used for analysis, simulation, and control purposes.

II. ANALYSIS PART

2 IMPLEMENTATION OF NONLINEAR MODEL TRMS ON MATLAB SIMULINK

The MATLAB Simulink model of the discussed nonlinear system, as presented in the theory section, is depicted in Figure 2.1. The model's parameters are established using the manual by [25]. This Simulink representation characterizes a MIMO (Multiple-Input, Multiple-Output) plant. It features dual inputs corresponding to rotor voltage inputs and multiple outputs encompassing pitch and yaw angles, alongside their respective angular velocities or rates.

This Simulink model serves as a valuable tool for analyzing and simulating the behavior of the nonlinear TRMS. By considering multiple inputs and outputs, it provides a comprehensive representation of the system's dynamics. This MIMO model enables studying the interdependence between the rotor voltages and the resulting pitch and yaw angles, as well as their respective rates.

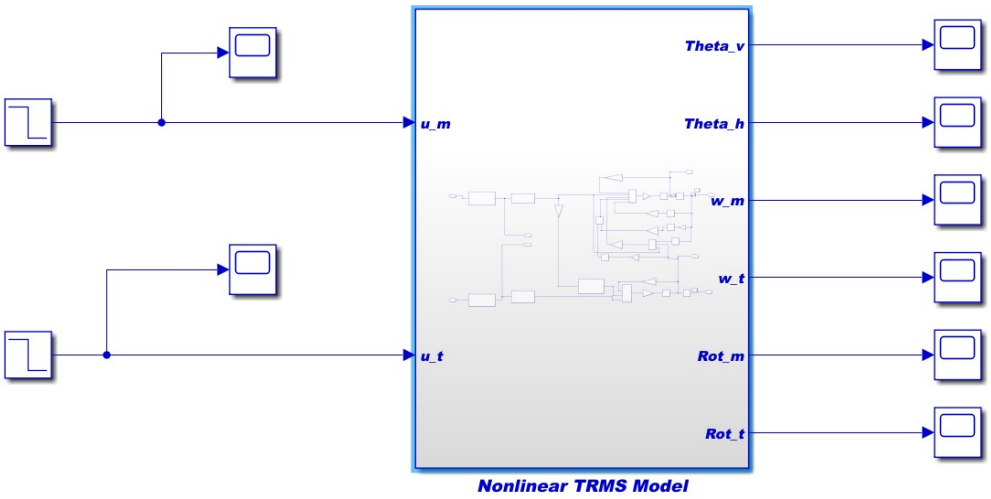

Figure 2.1 The Nonlinear Model of TRMS .

To gain comprehensive insights into the behavior of the system, it is highly recommended to analyze the response of the nonlinear TRMS model under various conditions. A valuable starting point is to examine the system's response without applying any controller, specifically by setting the voltages (u_m and u_t) to different values, i.e., zero, constant, or step input, for both the main and tail rotors. This analysis allows us to understand how changes in the initial angle values for both rotors influence the system's responses.

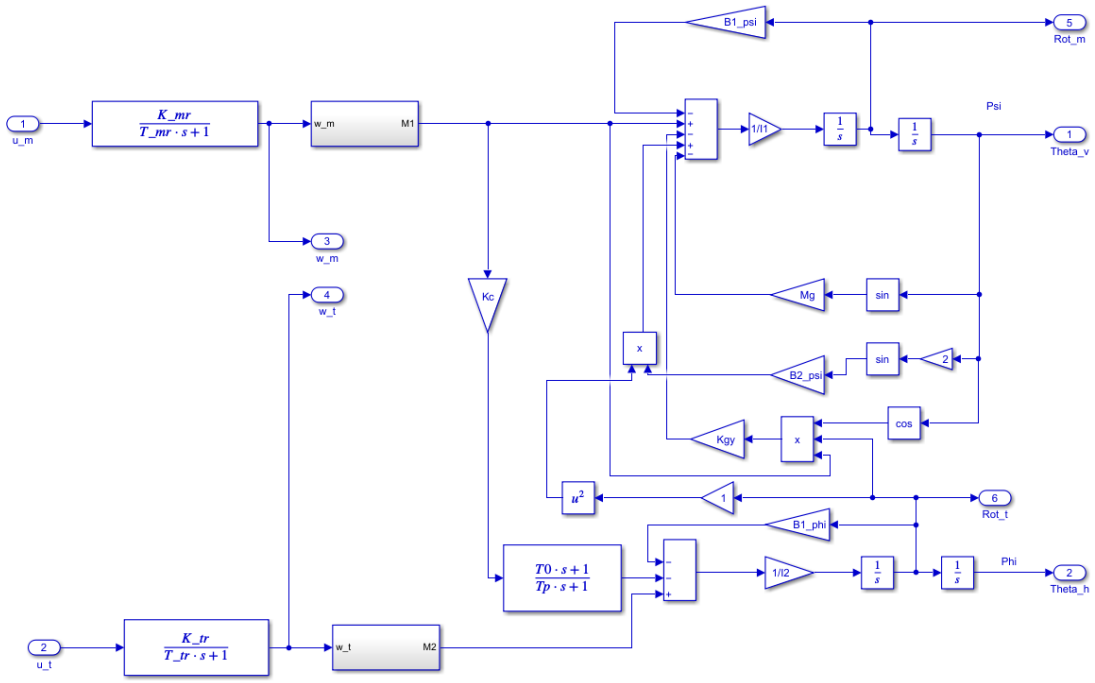

Figure 2.2 The Nonlinear Model of TRMS - Subsystems .

In the case of a nonlinear plant, it is crucial to adhere to the designated input voltage range, which spans from -2.5 to 2.5 volts. Ensuring that the input voltage remains within this acceptable range is of utmost importance. If the input voltage exceeds this range, it may lead to undesirable and aggressive output responses.

For precise control and predictable behavior, the input voltage must be carefully managed. A voltage of -2.5V corresponds to the maximum propeller rotation in a specific direction, typically clockwise. On the other hand, an input voltage of 2.5V results in maximum propeller rotation in the opposite direction, commonly counterclockwise. When the input voltage reaches 0V, the TRMS system remains stationary, indicating that the propeller does not rotate. This stationary outcome aligns with expectations since 0V represents a neutral input voltage, where no external force is applied to the system.

Figure 2.3 illustrates the response of the nonlinear model to step changes in control voltages, specifically transitioning from 1 to 0, for both the main and tail rotors. The plot demonstrates how the system behaves in response to these changes. Furthermore,

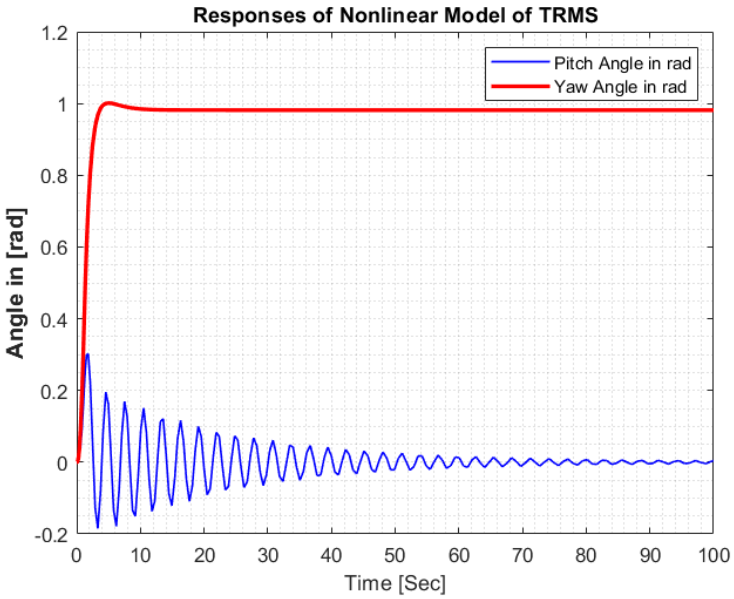

Figure 2.3 The model step response to step control voltage changes from 1 to 0 .

Figure 2.4 shows the step responses of the nonlinear TRMS model for both the pitch angle and yaw angle. The presented data makes it clear that the step response of the TRMS system, when subjected to control voltage changes from 0 to 1 for the main rotor and 0 for the tail rotor, the graphs shows in main rotor adversely affect the yaw angle. Precisely, with the yaw response experiencing an abrupt and unbounded increase. This observation underscores the imperative role of appropriate controllers to establish stability and controlled behaviors within the TRMS system.

Moreover, in Figure 2.5, the step responses of the nonlinear TRMS model are depicted for both the pitch angle and yaw angle. The provided data clarifies that the step response of the TRMS system, when exposed to control voltage shifts from 0 to 1 for the tail rotor and 0 for the main rotor, reveals that the graphs concerning the tail rotor have no impact on the pitch angle. Specifically, the yaw response exhibits a sudden and unbounded escalation. This observation underscores the critical importance of well-suited controllers in establishing stability and desired behaviors within the TRMS system, as also indicated in Figure 2.4.

The step responses of the nonlinear TRMS for the pitch and yaw angles are depicted in Figure 2.6. It's important to note that these responses are observed without the application of any controller but with control voltage changes from 1 to 0. In the case of

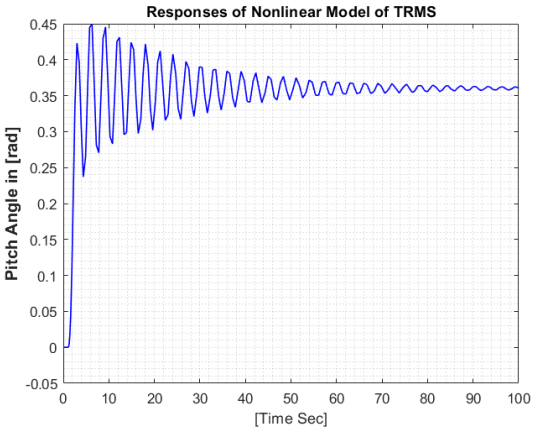

(a) Main response.

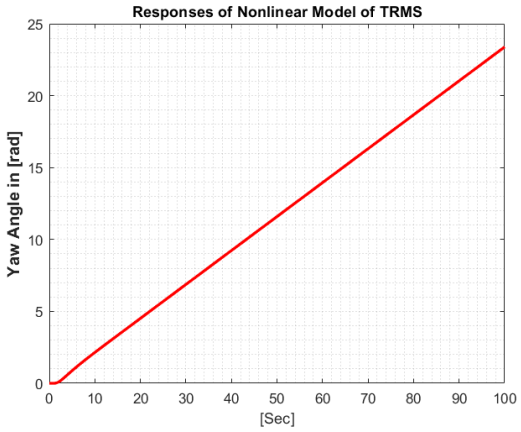

(b) Tail response.

Figure 2.4 Response to step control voltage changes from 0 to 1 for the main rotor and zero for the tail rotor.

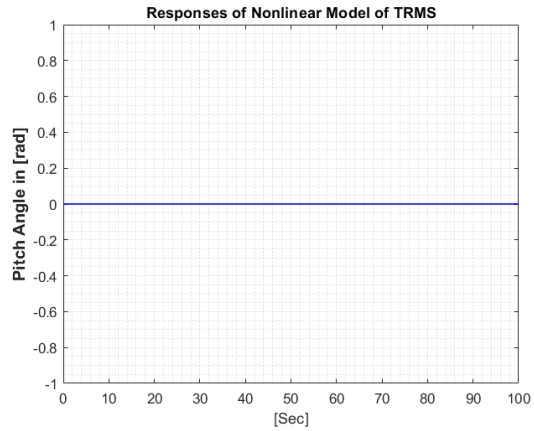

(a) Main response.

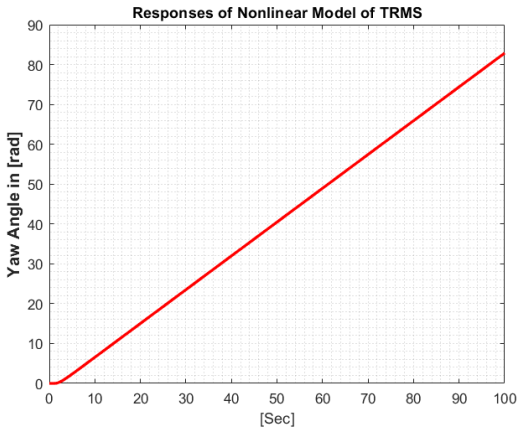

(b) Tail response.

Figure 2.5 Response to step control voltage changes from 0 to 1 for the tail rotor and zero for the main rotor.

the azimuth/yaw angle, the output is limited due to the presence of a stopper in the real laboratory model, causing a bouncing effect. In the MATLAB model, this situation is represented by a limiter, which exhibits nonlinear behavior. The figures vividly illustrate the system's behavior and demonstrate how the pitch and yaw angles respond over time to the specified control voltage changes. The presence of nonlinear behavior in the limiter emphasizes the significance of implementing appropriate controllers to ensure stability and controlled responses in the TRMS system.

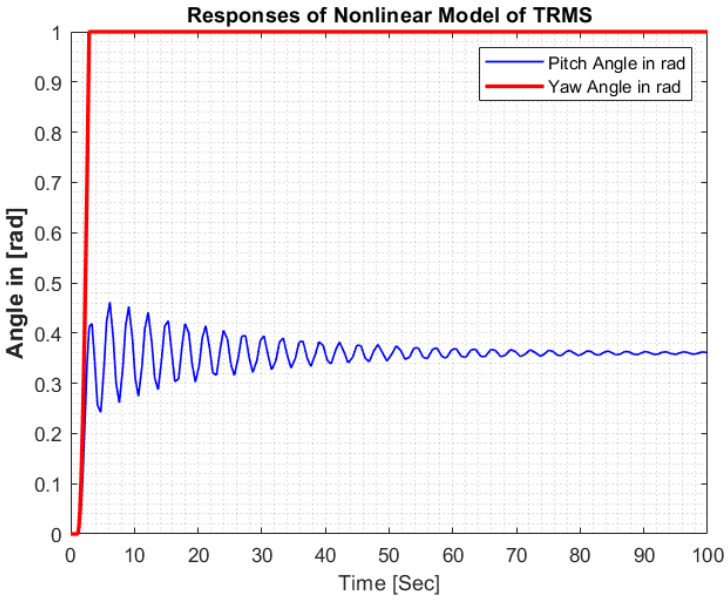

Figure 2.6 Response to step control voltage changes from 0 to 1 for the tail rotor and zero for the main rotor.

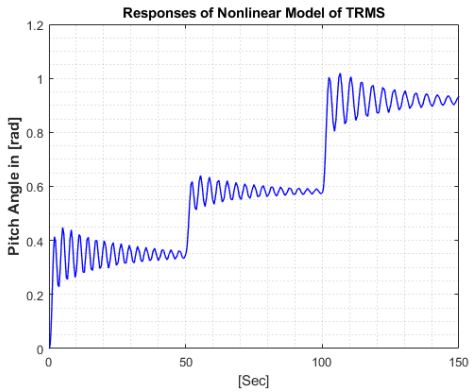

Figure 2.7 Pitch Angle Step Response

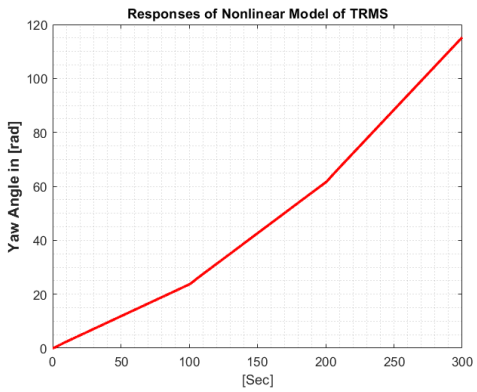

Figure 2.8 Yaw Angle Step Response

Additionally, Figure 2.7 and Figure 2.8 display the step responses of the nonlinear TRMS system for the pitch and yaw angles, respectively, with voltage changes from 1V to 2V in steps of 0.5V for the main rotor and a constant 0V for the tail rotor. These figures illustrate that the system exhibits oscillations in the pitch motion, while the yaw response increases without any bound.

3 IDENTIFICATION OF THE LINEAR TRMS PLANT

System identification is a crucial process in which mathematical models are constructed to accurately describe the behavior of dynamic systems. This is achieved by analyzing and utilizing data collected from experiments. Real-time experiments were conducted for system identification in the Process Control Laboratory at the Faculty of Applied Informatics, Tomas Bata University. The room was sealed, and the temperature was set to room temperature to ensure no external disturbances affected the measurements. However, there are some factors that affect the measurements, which will be addressed later on.

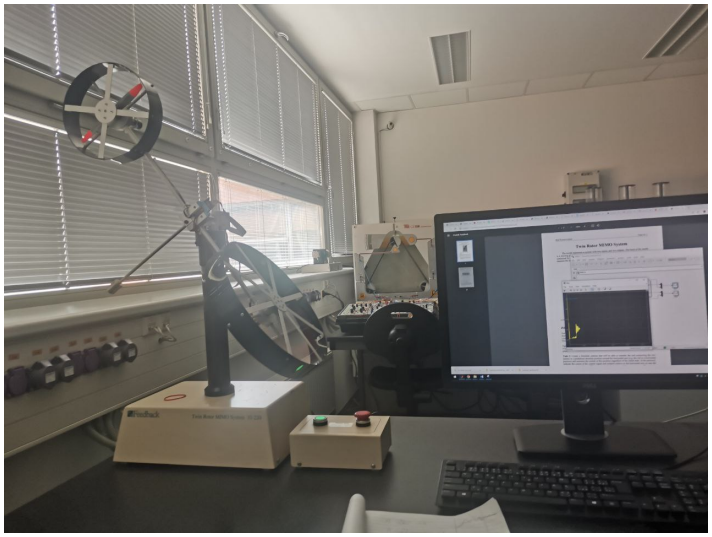

Figure 3.1 Process Control Laboratory- TRMS Model Setup

The block diagram presented below illustrates the general identification method discussed in this paper. However, to simplify the analysis, the effects of each cross-coupling are assumed to be locked, and a Single Input Single Output (SISO) approach is considered. Nevertheless, it is crucial to note that the influence of the main rotor on the azimuth angle, which is cross-coupling effect is acknowledged and recommended for further investigation and future research.

Referring to Figure 3.2, it becomes apparent that u_1 and u_2 denote the input voltages supplied to the TRMS, while y_1 and y_2 correspond to the vertical and horizontal positions of the beam within the system. The paths $G_{pt}(s)$ and $G_{pt}(s)$ influence the main and cross path of pitch, respectively, affecting the azimuth angle, whereas $G_{yt}(s)$ and $G_{yt}(s)$ pertain to the cross path of yaw and the tail path of yaw, respectively. Notably, the input and output channels exhibit a pronounced degree of cross-coupling.

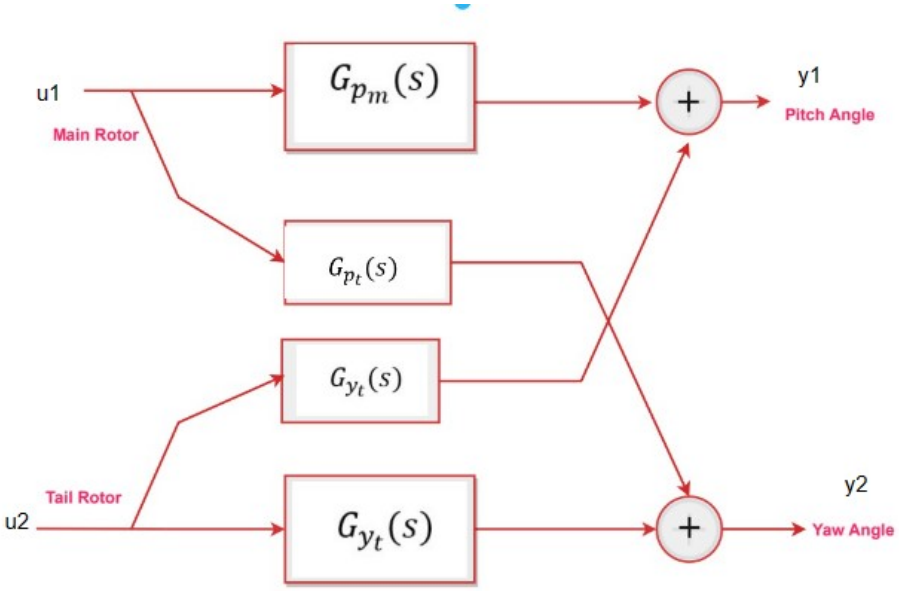

Figure 3.2 Block diagram for proposed identification.

In order to construct a TRMS model using system identification techniques, a well-defined step signal is applied to the TRMS, and the resulting pitch and yaw angle signals are carefully recorded. These recorded input-output data pairs are then used to estimate the parameters of a mathematical model that accurately represents the behavior of the TRMS.

Before directly going to the identification steps, this paper first presents the static characteristics of both elevation and azimuth angles.

3.1 Elevation - Static Characteristics

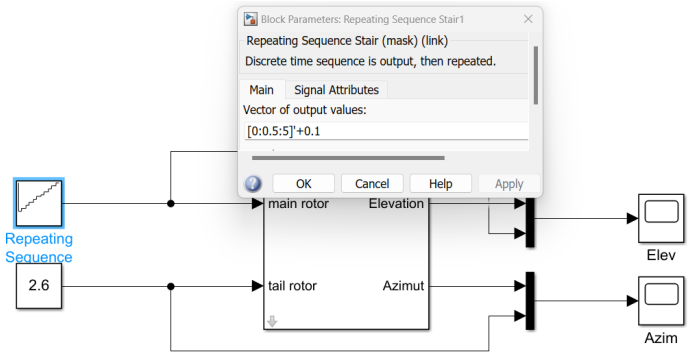

Figure 3.3 Real Model Measurements: Virtual MATLAB Setup for Elevation

The static characteristics of a Twin Rotor MIMO system pertain to the system's behavior under steady-state conditions, specifically in relation to elevation and azimuth

angles.

For the elevation angles, the static characteristics describe the relationship between the input signals (representing the desired elevation angles for each rotor) and the output signals (representing the actual elevation angles of each rotor).

To determine these static characteristics, a step input signal was applied to the system, starting from 0V and increasing in increments of 0.5V up to 5V. Subsequently, the input voltage was decreased in increments of 0.5V from 5V back to 0V. Throughout the experiment, the resulting pitch output signal was recorded while the tail motor remained stationary, i.e, tail motor input voltage is remain 2.6V. The sampling time used in the whole measurement in this paper is 0.01sec.

To gain a deeper understanding of the system's behavior, multiple measurements were conducted, including both short-term and long-term measurements of the entire system. Additionally, measurements were performed to observe the impact of the reference voltage on the non-rotating propeller. Specifically, the following measurements were taken at every 10 minutes to avoid the influence of sensor heating on measurement data:

- **Measurement -1**: Measurements were taken for 30 seconds for each input voltage ranging from 0V to 5V with a step increment of 0.5V.
- **Measurement -2**: Measurements were taken for 30 seconds for each input voltage ranging from 0V to 5V with a step increment of 0.5V plus an additional 0.1V.
- **Measurement -3**: Measurements were taken for 100 seconds for each input voltage ranging from 0V to 5V with a step increment of 0.5V.
- **Measurement -4**: Measurements were taken for 100 seconds for each input voltage ranging from 0V to 5V with a step increment of 0.5V plus an additional 0.1V.

It is important to note that obtaining reliable results may require conducting the experiment multiple times to account for any variations. These measurements provide valuable data to further analyze and understand the behavior of the TRMS system under various input voltage conditions. A comprehensive response involving multiple TRMS measurements is presented below in Figure 3.4a and 3.4b.

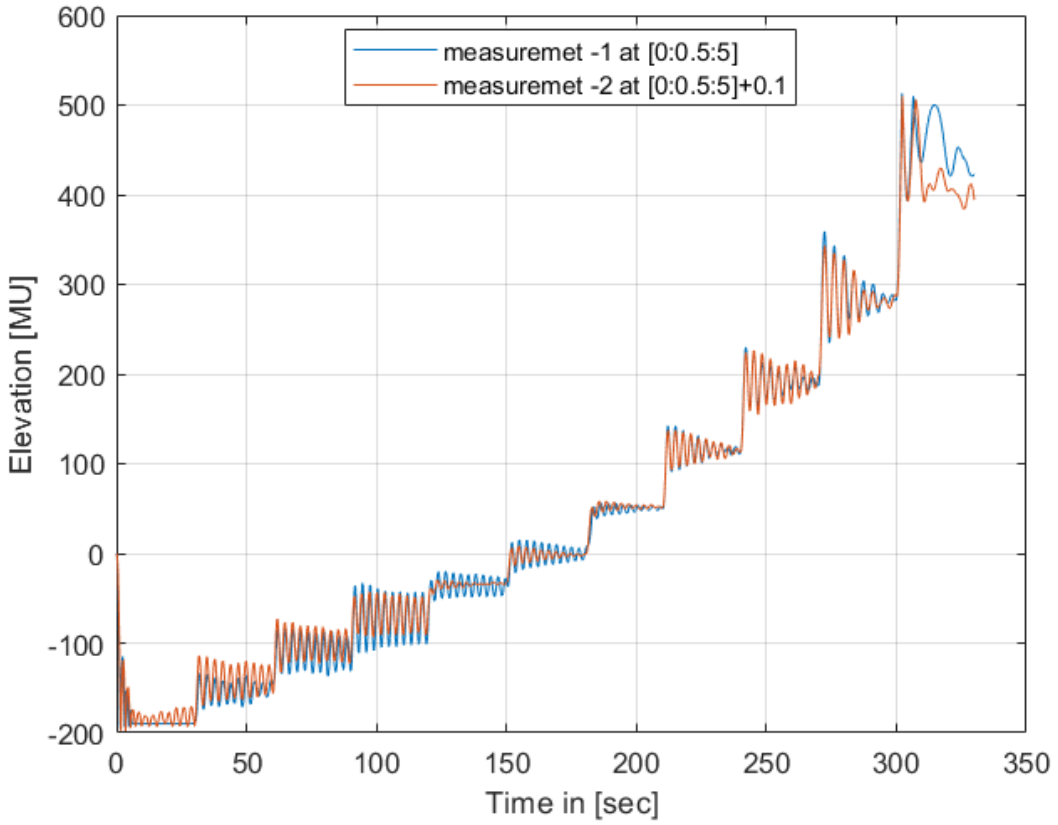

(a) A response TRMS-A measurement for 30sec with input voltage [0:0.5:5] and [0:0.5:5]+0.1

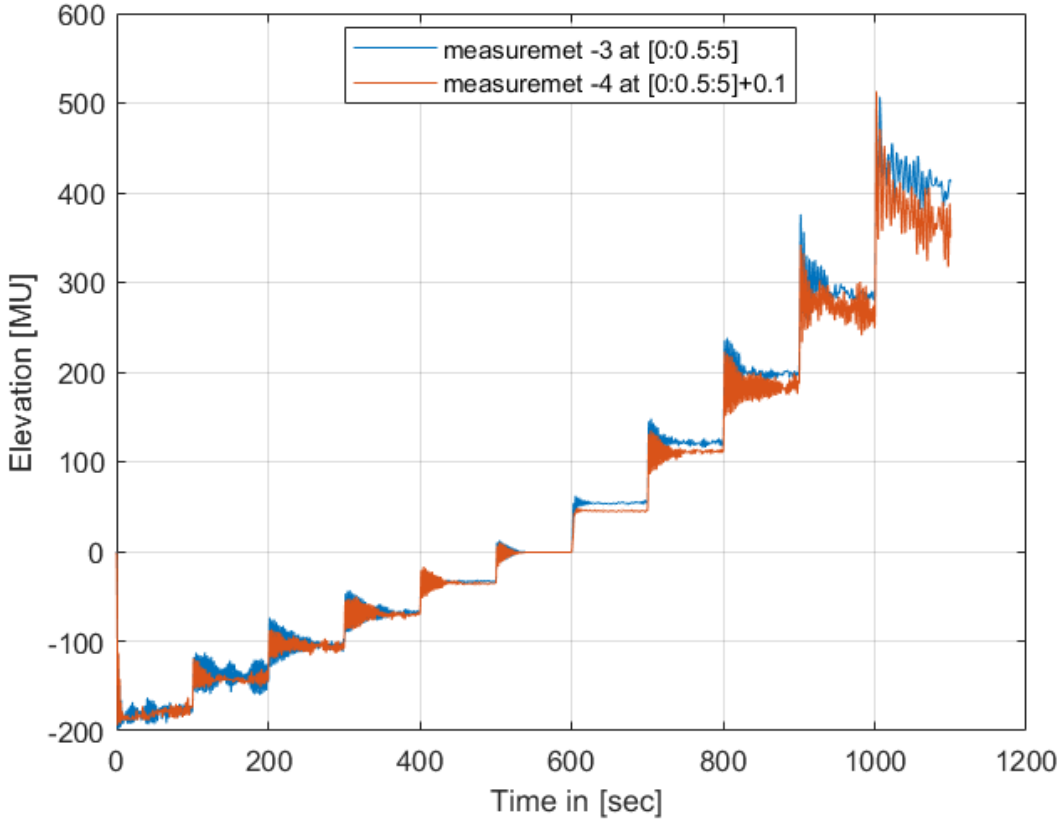

(b) A response TRMS-A measurement for 100sec with input voltage [0:0.5:5] and [0:0.5:5]+0.1

Figure 3.4 Response Measurements

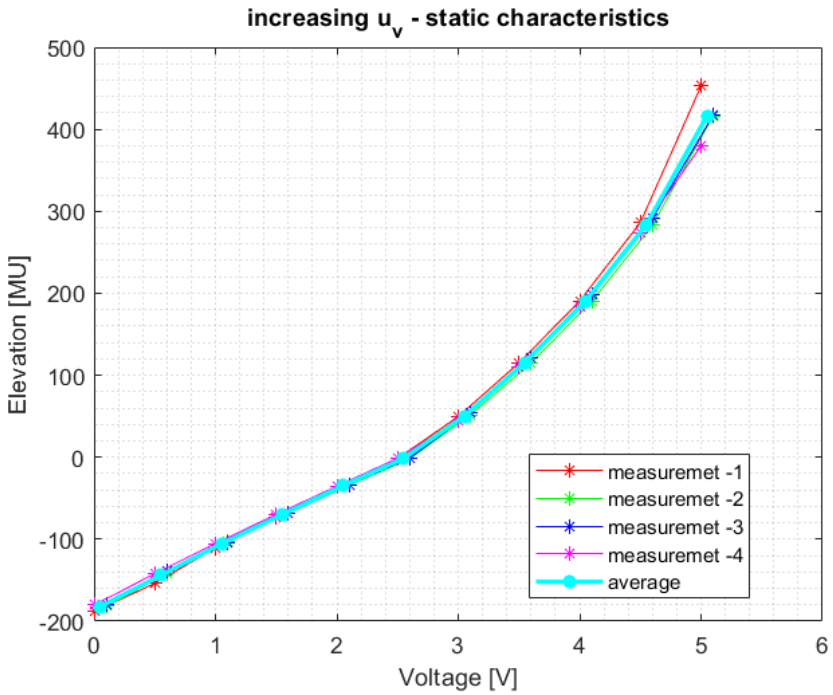

Figure 3.5 Elevation static characteritics for several measurements. -For increasing input voltage.

When the voltage input is 0V, the propeller rotates at maximum speed in one direction, namely clockwise. At 2.5V, the propeller remains stationary, indicating no movement in the TRMS. On the other hand, when the input voltage is 5V, the propeller rotates at maximum speed in the opposite direction, i.e., counterclockwise. It is worth noting that the input voltages mentioned above were adjusted to 0.1V, 2.6V, and 5.1V after conducting careful and repeated measurements. A deviation of $\pm$0.1V from the input voltage is considered acceptable in this case.

The same step was repeated for decreasing step input voltages, and the results of static characteristics for each increasing and decreasing input voltage are shown in Figure 3.5 and 3.6. According to the presented graph, the measurements of different scenarios do not significantly affect the static characteristics of both increasing and decreasing measurements, except for small deviations in some measurements. These deviations are likely due to other factors, which will be discussed in the next sections.

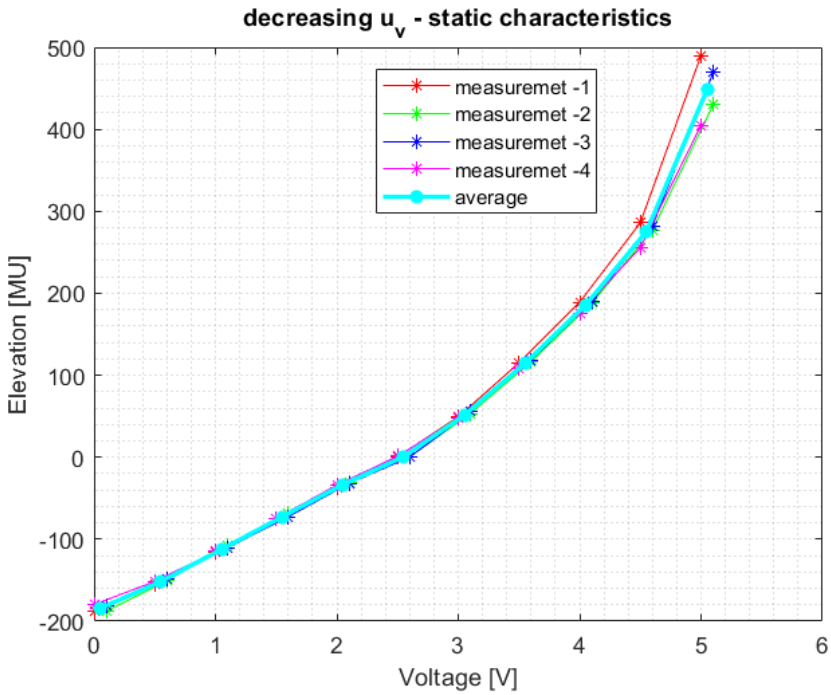

Figure 3.6 Elevation static characteritics for several measurements -For decreasing input voltage.

The following measurements taken for both increasing and decreasing course of control voltage of main rotor. To determine these static characteristics, a step input signal was applied to the system, starting from 0V and increasing in increments of 0.5V up to 5V. Subsequently, the input voltage was decreased in increments of 0.5V from 5V back to 0V. Throughout the experiment, the resulting pitch output signal was recorded while the tail motor remained stationary.

Based on displayed graph, the course of the static characteritics experiment is depicted in Figure 3.8. The experiment suggests that the direction of input voltage change does not have a significant effect on the system's behavior. From presented graph, the static characteristic of the system appears to be piece-wise linear. It mean that the linearity for input voltage ranging from 0V to 2.5V differs from the linearity for input voltage ranging from 2.5V to 5V due to a sudden change in direction of main rotor movements.

Furthermore, it is evident that the gain of the system is significantly influenced when the direction of propeller rotation changes, specifically when the direction of the control voltage changes. Higher voltages appear to result in higher gain.

The corresponding azimuth angle is obtained when the input voltage of the main rotor is set according to Figure 3.7a, with an increasing step input voltage, while keeping

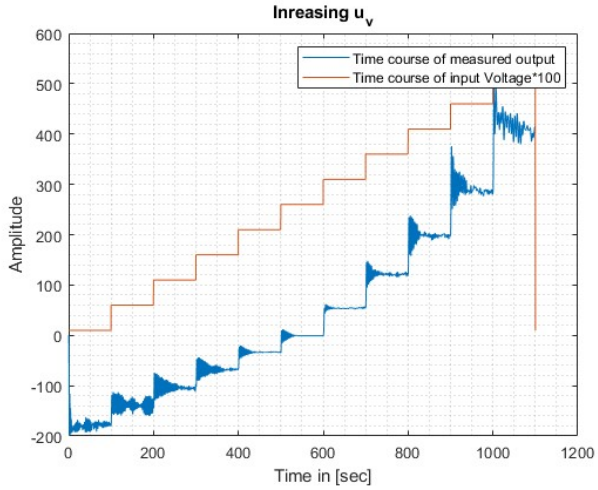

(a) Measurement for increasing voltage.

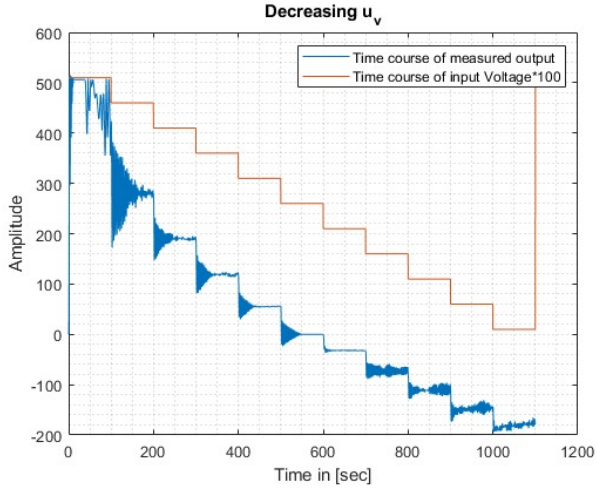

(b) Measurement for decreasing voltage.

Figure 3.7 Step response measurements for both increasing and decreasing input voltage - Elevation.

the tail stationary at 2.6V and unlocked. The measurements were conducted and are depicted in Figure 3.9. The results indicate a significant cross-coupling effect, signifying that the influence of the main rotor on the azimuth angle is highly introduced. A crucial recommendation from this paper is that the impact of the main rotor on azimuth should no longer be ignored when designing controllers to account for cross-coupling. However, it's important to note that the response is nonlinear, proposing linear identification methods ineffective for this particular case.

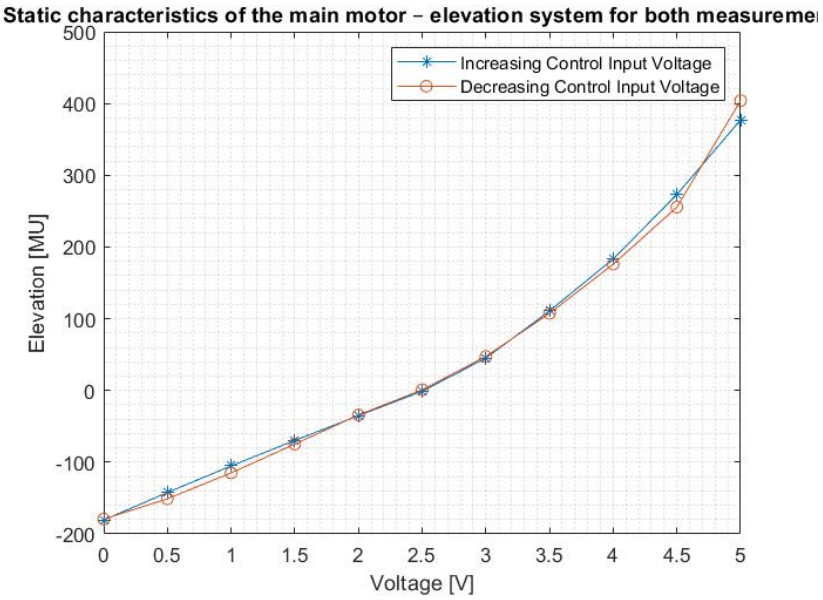

Figure 3.8 Static characteristics of the main motor – elevation system for both increasing and decreasing input voltages - Elevation.

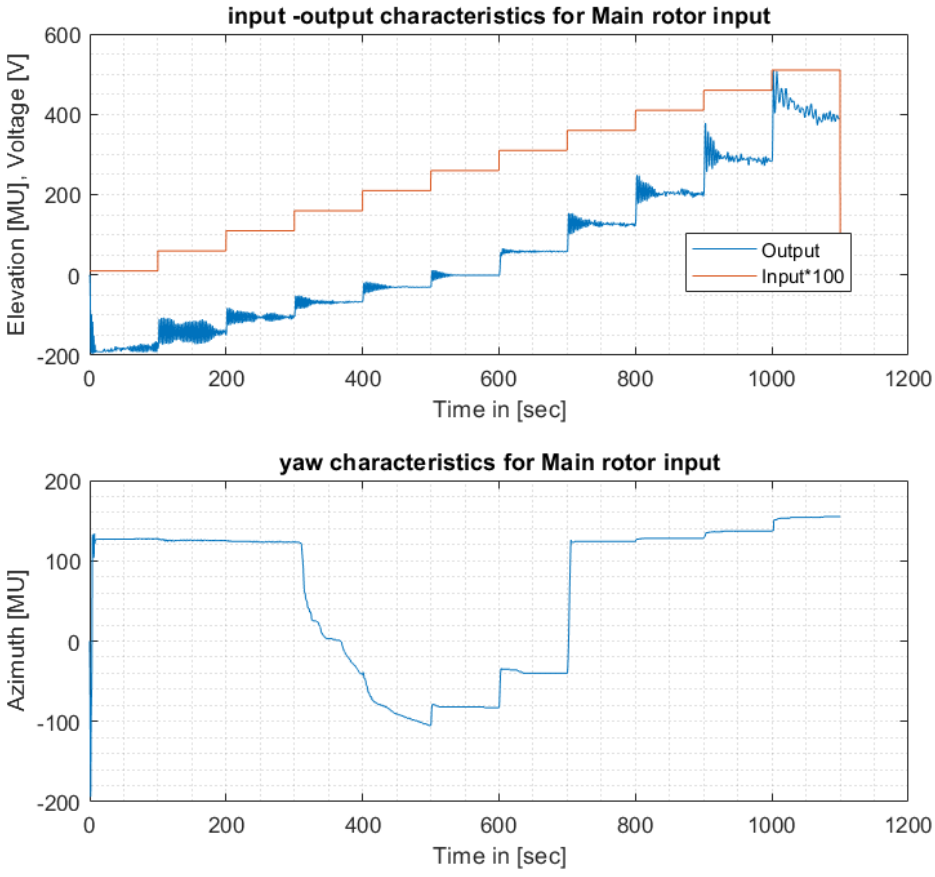

Figure 3.9 Response of Azimuth.

3.2 Azimuth - Static Characteristics

Similarly, the azimuth static characteristics involve the connection between the input signals (representing the desired azimuth angles for each rotor) and the output signals (representing the actual azimuth angles of each rotor).

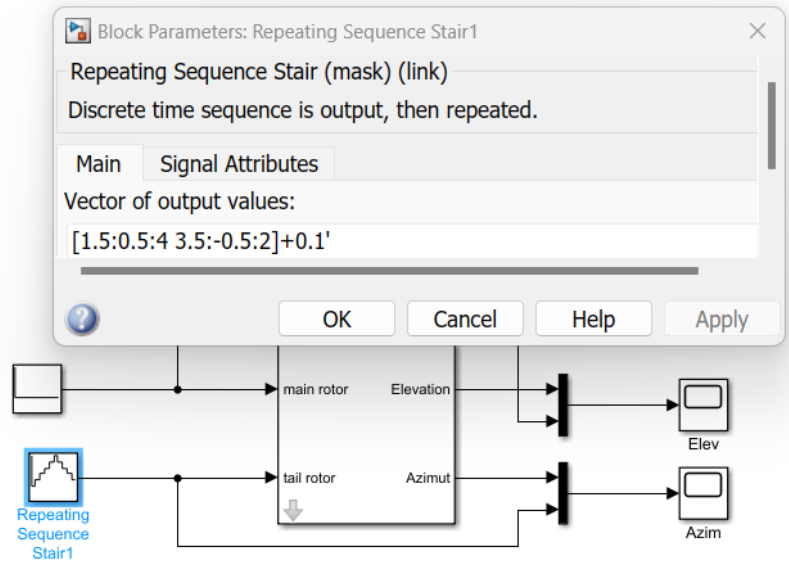

Figure 3.10 Real Model Measurements: Virtual MATLAB Setup for Azimuth

For the azimuth measurements setup shown in Figure 3.10, the control input voltage ranges from 1.5 to 4V for increasing azimuth and 3.5 to 2V for decreasing azimuth. Throughout these measurements, the control input voltage for the main rotor remains at 2.6V, keeping the rotor stationary and screw is unlocked. The corresponding measurement outputs are presented in Figure 3.11. The static characteristics of Azimuth are nonlinear, displaying a resemblance to a hysteresis curve, as shown in Figure 3.12.

An important finding of this study is the elevation angle measurements, which are provided in Figure 3.13. The results indicate that there is almost insignificant cross coupling, meaning that the effect of the tail rotor on the elevation angle is minimal, although not completely absent. In summary, based on real-time experiments and the findings of this paper, the static characteristics of the main rotor-elevation relationship are piecewise linear, while the static characteristics of the tail rotor-azimuth relationship are nonlinear, displaying a large hysteresis curve. These non-linearities and hysteresis significantly affect the control of the system. Furthermore, the influence of the main rotor on the azimuth angle is found to be very high and cannot be ignored, while the influence of the tail rotor on the elevation angle is insignificant. Therefore,

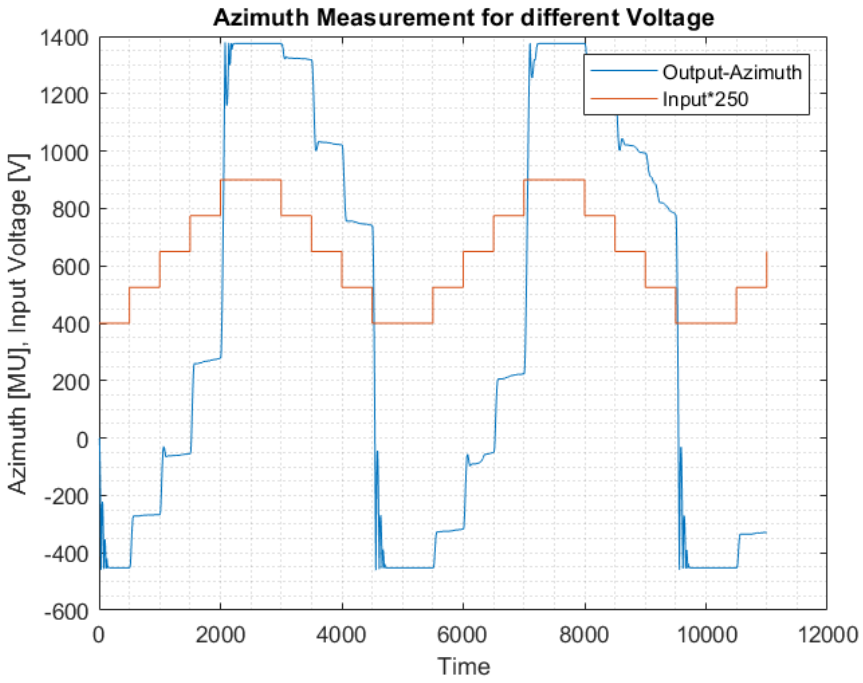

Figure 3.11 Step response measurements for both increasing and decreasing input voltage - Azimuth.

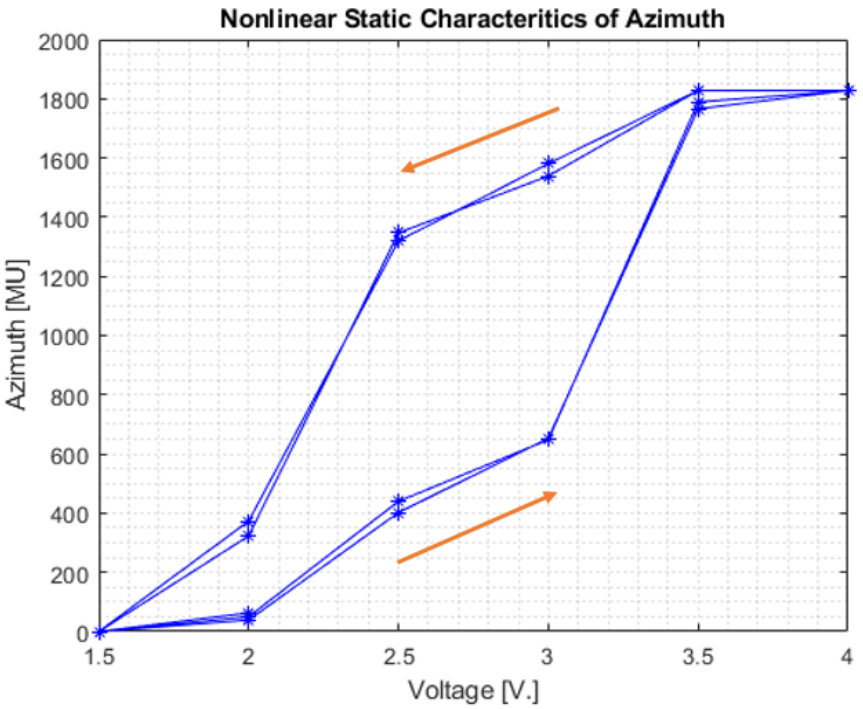

Figure 3.12 Static characteristics of the tail motor – for both increasing and decreasing input voltages - Azimuth.

when considering the cross-coupling effect of the TRMS, it is crucial to acknowledge that the influence of the main rotor on the azimuth angle should never be ignored. Properly accounting for this effect is essential for designing effective controllers that can mitigate cross-coupling and ensure stable and precise control of the system.

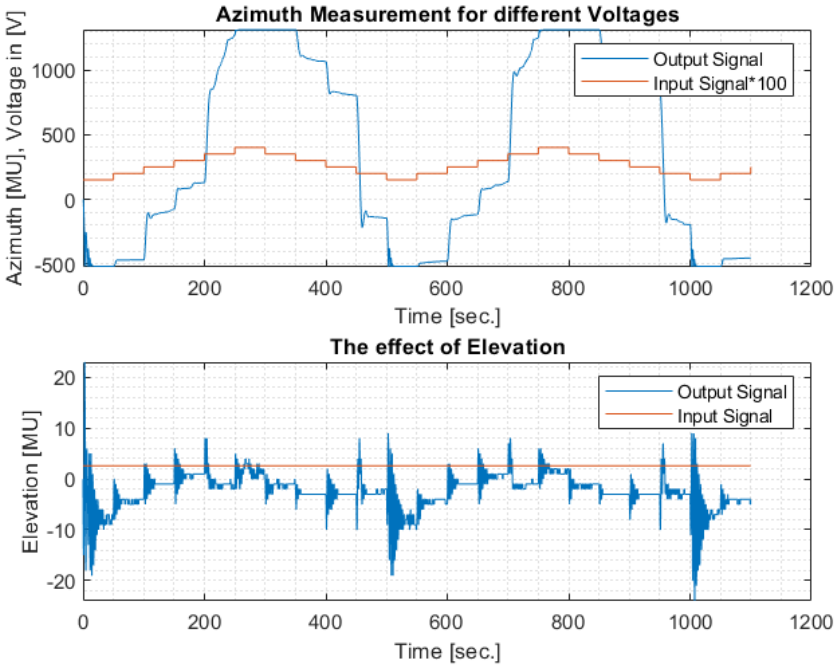

Figure 3.13 The relationship between voltage and azimuth.

3.3 Factors Affecting the Measurements of TRMS

It is important to note that deviations in the static characteristics of a twin rotor MIMO system may arise due to various factors that can alter its physical properties. The following sections discuss some of these factors without deep investigation.

3.3.1 Environmental Factors

External factors, such as temperature, humidity, and air pressure, can significantly impact the behavior of a TRMS [1]. Changes in these environmental factors can affect the system's aerodynamics, material properties, and control performance. For example, variations in air pressure can influence the airflow around the rotor blades, leading to changes in the system's dynamics. Similarly, temperature and humidity can affect the system's material properties, including stiffness and damping, which can alter its overall behavior. Therefore, it is crucial to consider these environmental factors when analyzing the data obtained from a TRMS.

3.3.2 Sensor Heating

In a twin rotor MIMO system, temperature sensors are often used to monitor the temperature of motors, bearings, or other heat-generating components during operation [33]. This is done to ensure that the system can make necessary adjustments or shut down if required to prevent damage or failure caused by overheating. However, it is important to note that the heating of temperature sensors can also affect the behavior of the TRMS, leading to variations in the data obtained.

3.3.3 Integrative Nature of the System

Another factor that can affect the data from a TRMS is its integrative nature. The current data obtained from the system can be influenced by previous data [34] [35]. This integration of information can introduce dependencies and nonlinearities in the system's behavior, which may result in variations in the data obtained.

Considering these factors is crucial for accurately interpreting and analyzing the data obtained from a TRMS. By accounting for these influences, researchers and engineers can gain a better understanding of the system's behavior and make more informed decisions regarding its design, control, and optimization.

Although further study is needed to determine the extent to which the above-mentioned factors influence the measurements, it is possible that these factors can affect the data from TRMS or influence the behavior of TRMS.

The following measurements are taken for step input control voltage to main rotor from 3 to 4V at different time. Notably, the tail rotor input voltage remains at zero, and the TRMS tail remains unsrewed / not locked throughout the measurement process. The response of elevation is indicated in the Figure 3.14a and the corresponding azimuth response is given in the Figure 3.14b. From experimental observations, the course of measurements obtained during the experiments, which could potentially support the explanations mentioned above. In essence, the TRMS Laboratory model is subject to multiple influencing factors. These factors should be taken into careful consideration by academics and researchers when working on the implementation of controls for the TRMS model. Hence, certain measurement deviations in this thesis are arise due to the factors discussed in this section.

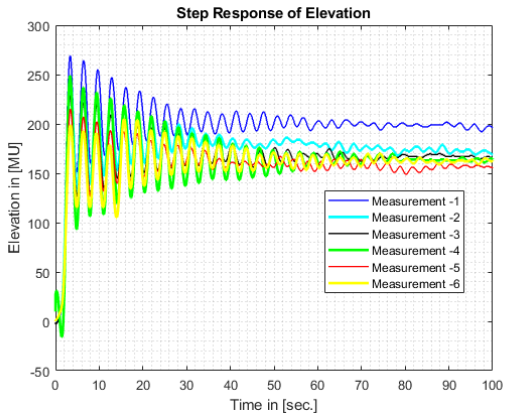

(a) Performance degradation of step response of elevation.

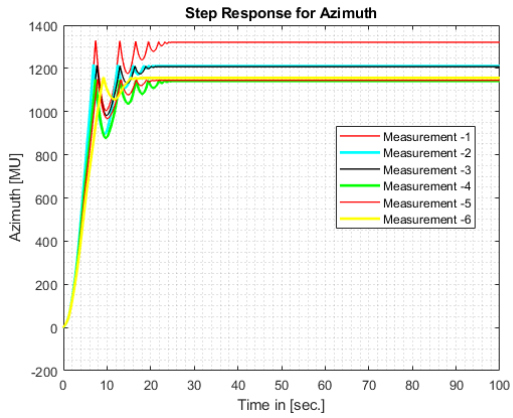

(b) Performance degradation of step response of azimuth.

Figure 3.14 Impact on Performance Degradation

3.4 Identification of Linear Model of Elevation/Azimuth

As mentioned in the subsection on static characteristics, the elevation output/step responses were measured when a series of step changes in the control voltage of the main rotor of a TRMS in the input were applied. Based on these step responses, a linear model of the main motor-elevation system was identified using proposed system identification techniques such as the "fminsearch" MATLAB function, ARX model, ARMAX model.

In this section, consider a simplified model of a 1-degree-of-freedom (1-DOF) system without the influence of coupling. In this model, assume that the tail rotor is locked / screw TRMS, meaning it has no effect on the vertical motion. Therefore, only the main rotor affects the vertical motion, while the tail rotor has no contribution. This paper focuses on a Single Input Single Output (SISO) scenario. Specifically, the elevation /pitch angle is influenced solely by the input voltage applied to the main rotor, while the azimuth /yaw angle is influenced by the input voltage applied to the tail rotor of TRMS.

3.4.1 Identification using the "fminsearch" MATLAB function

In this task, step changes in the control voltage of the main rotor of a TRMS were observed to induce an oscillatory response in the system's elevation output. To model this behavior, a 3rd order linear system that captures the system's characteristics was employed and 2nd order linear system proposed for system's azimuth output, and identification was performed using the MATLAB function "fminsearch."

The "fminsearch" function in MATLAB is aiming to find the minimum or maximum value of a given function. It is analogous to the Solver function in Excel and is employed in this context to determine the optimal parameters that best fit the model to the observed data during the identification process.

```
par2 = fminsearch(@(par) Criterion(par, y, u, t), [140, 0.5, 0.1, 1])
```

Using the step response elevation data obtained from a step input ranging from 3V to 4V, it is feasible to derive the transfer function of the system utilizing the "fminsearch" function in MATLAB. The "fminsearch" function performs numerical optimization to find the parameters that minimize the difference between the system's response and the desired step response. By iteratively adjusting the parameters, the function aims to

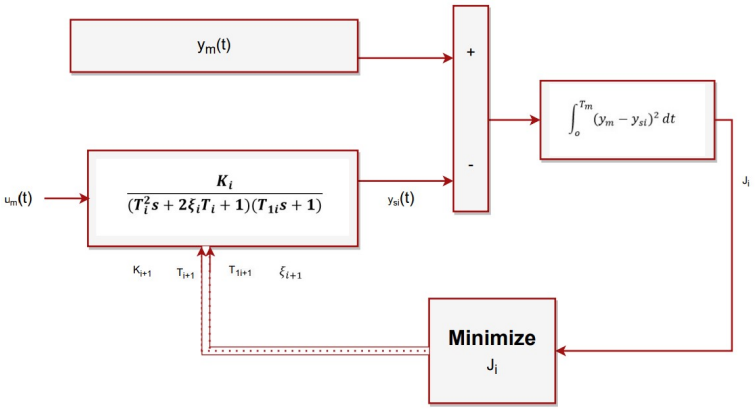

Figure 3.15 fminsearch algorithm for elevation (Modification of [36]).

find the best-fitting transfer function that represents the system's behavior accurately.

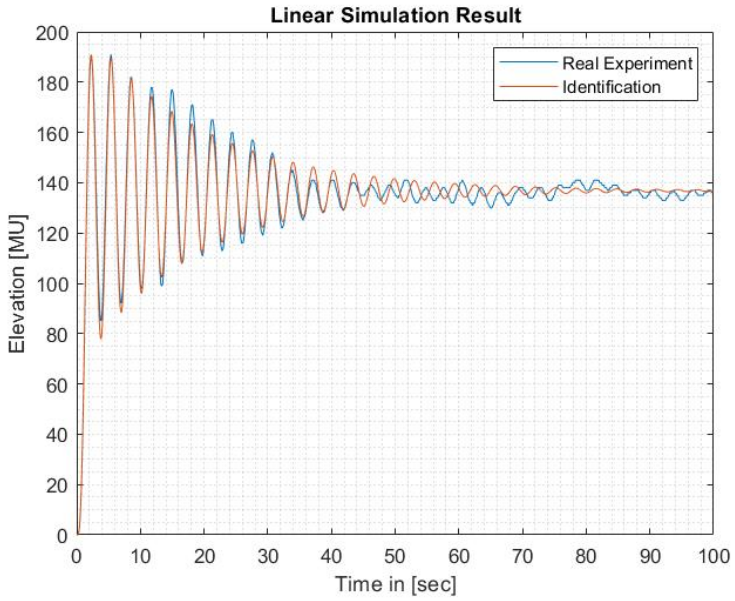

Figure 3.16 Elevation Step response identified by fminsearch.

Thus, the transfer function for the elevation can be expressed as follows:

$$G(s) = \frac{136.84}{0.2182s^3 + 0.2785s^2 + 0.8832s + 1} \tag{3.1}$$

To identify Azimuth, the measurements of step input voltages ranging from 3V to 3.5V were used for identification. Thus, the corresponding transfer function for the azimuth can be expressed as follows:

```
par = fminsearch (@(par) criteria(par, u, t, y), [500 4 2])
```

$$G(s) = \frac{583.5}{5.128s^2 + 3.286s + 1} \tag{3.2}$$

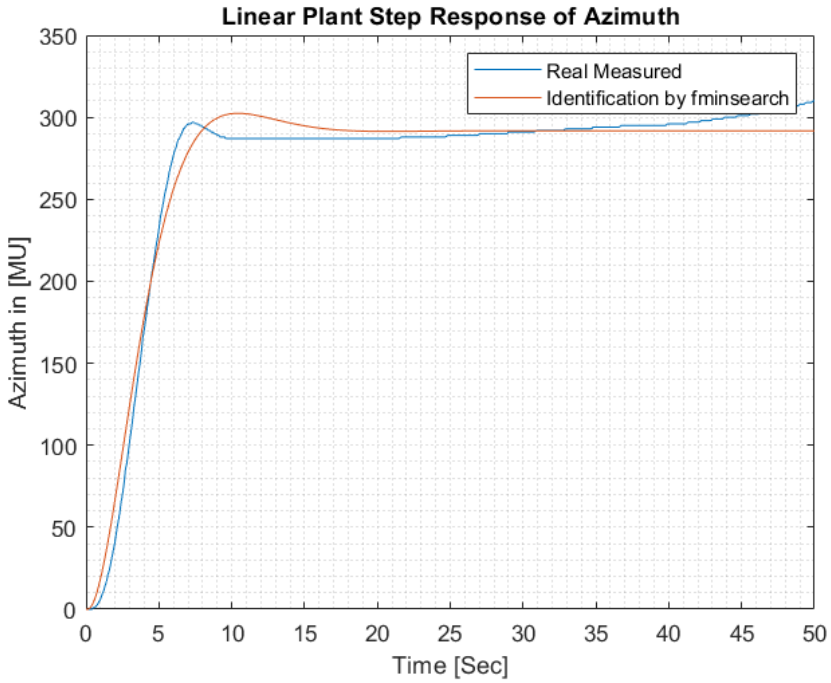

Figure 3.17 Azimuth Step response identified by fminsearch.

3.4.2 Autoregressive with Exogenous Input (ARX) and Autoregressive and Moving Average with Exogenous input (ARMAX) methods of parameter estimation

To obtain a mathematical model of the system, we apply an input signal u(k) to the system and record the corresponding response as y(k). The error term is then calculated as the difference between the actual system output and the output predicted by the model. A comprehensive representation of the system, considering these components, can be described as follows:

$$A(z^{-1})y(k) = \frac{B(z^{-1})}{F(z^{-1})}u(k) + \frac{C(z^{-1})}{D(z^{-1})}e(k) \tag{3.3}$$

This equation can be rearranged to obtain the following expression:

$$y(k) = \frac{B(z^{-1})}{A(z^{-1})F(z^{-1})}u(k) + \frac{C(z^{-1})}{A(z^{-1})D(z^{-1})}e(k) \tag{3.4}$$

In the above equations, u(k), y(k), and e(k) represent the input, output, and zero-mean white noise, respectively. The white noise represents the disturbance acting on the system. This relationship is illustrated in the following block diagram:

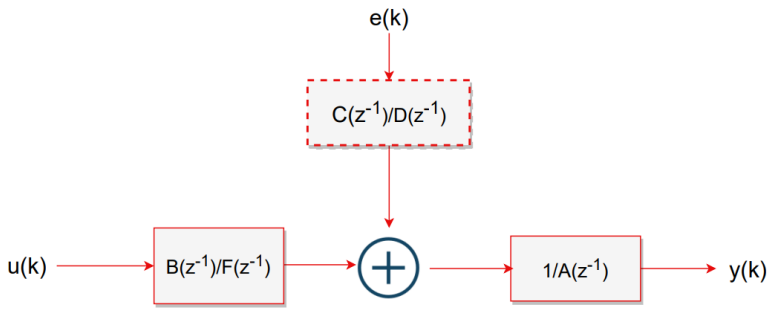

Figure 3.18 System as a general linear model structure.

The individual polynomials in the system have the following form:

$$
\begin{aligned}
A(z^{-1}) &= 1 + a_1 z^{-1} + ... + a_{n_a} z^{-n_a} \\
B(z^{-1}) &= 1 + b_1 z^{-1} + ... + b_{n_b} z^{-n_b} \\
C(z^{-1}) &= 1 + c_1 z^{-1} + ... + c_{n_c} z^{-n_c} \\
D(z^{-1}) &= 1 + d_1 z^{-1} + ... + d_{n_d} z^{-n_d} \\
F(z^{-1}) &= 1 + f_1 z^{-1} + ... + f_{n_f} z^{-n_f}
\end{aligned} \tag{3.5}
$$

It is important to note that the memory depths must satisfy the conditions: $n_f \geq n_b$ and $n_d \geq n_c$.

ARX Model: The ARX model is a widely used and efficient model for estimation methods, particularly advantageous when dealing with high-order systems. The ARX model assumes that discrete transfer functions have polynomials in the numerator and denominator with the same degree, denoted as n. Additionally, it assumes that changes in the input value do not instantaneously affect changes in the output value, which is a realistic assumption for most physical systems where there is no direct input-to-output link. Thus, the weight of the current input value is assumed to be zero.

Based on these assumptions, we can define the polynomials A and B as follows. By making the substitution C = D = F = 1 in the general stochastic model, we obtain the ARX model in the following form:

$$
y(k) = \frac{B(z^{-1})}{A(z^{-1})} u(k) + \frac{1}{A(z^{-1})} e(k) \tag{3.6}
$$

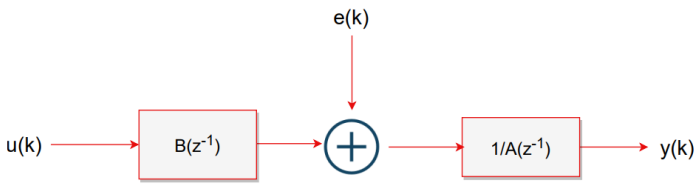

Figure 3.19 Scheme of ARX model.

ARMAX Model: The ARMAX model is a widely used time-series model, ranking as the second most common after the ARX model. It is a more complex model compared

to ARX, but it offers greater versatility as it incorporates an extended noise model. In the ARMAX model, the noise entering the system is correlated, which is a more general assumption.

By making the following substitution in the general stochastic model (D = F = 1), we obtain an ARMAX model in the following form:

$$y(k) = \frac{B(z^{-1})}{A(z^{-1})}u(k) + \frac{C(z^{-1})}{A(z^{-1})}e(k) \tag{3.7}$$

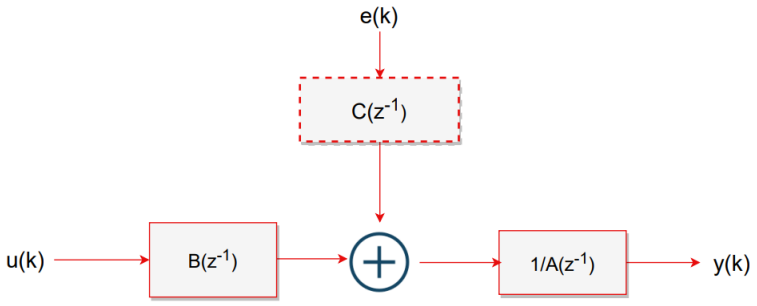

Figure 3.20 Scheme of ARMAX model.

Like fminsearch , the identification of system parameters of elevation channel using ARX and ARMAX models is conducted by analyzing the step response of the system to input voltages ranging from 3V to 4V.

```
% identification based on ARX
z=[y,u];
sys_arx=arx(z,[3 3 1])
sys_arx.Ts=0.01;
sysD_arx=tf(sys_arx)
sysC_arx=d2c(sysD_arx)
y_sim_arx=lsim(sysD_arx,u);
```

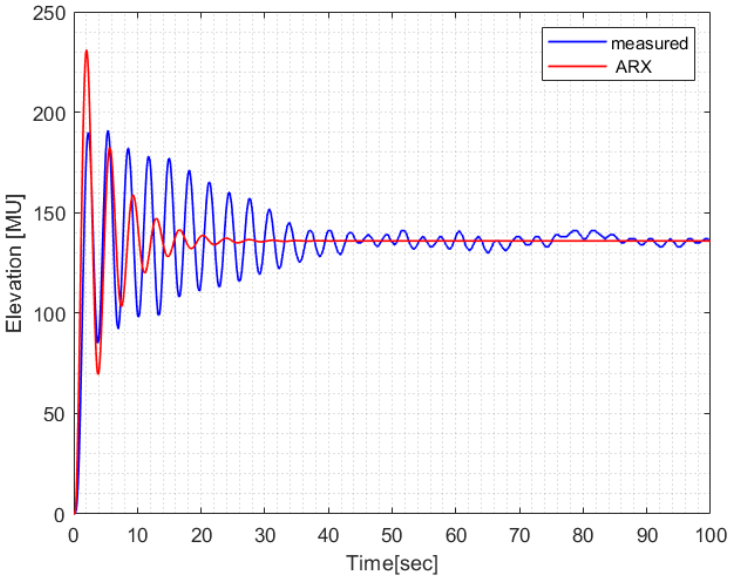

Figure 3.21 ARX model identification for elevation.

$$G_{ARX}(s) = \frac{-229.4s^3 + 1.596e05s^2 - 2.967e07s + 4.238e09}{s^4 + 149.7s^3 + 1.049e05s^2 + 4.49e05s + 3.118e07} \tag{3.8}$$

```
sys_armax = armax(z,[3 3 3 1])
sys_armax.Ts=0.01;
sysD_armax=tf(sys_armax)
sysC_armax=d2c(sysD_armax)
y_sim_armax=lsim(sysD_armax,u);
```

$$G_{ARMAX}(s) = \frac{-7.993s^2 - 953.5s + 6.227e05}{s^3 + 12.73s^2 + 406.8s + 4550} \tag{3.9}$$

The identification using an ARMAX model yields similar results to the measurement model, it implies that the ARMAX model is capable of accurately capturing the dynamics of the system and producing outputs that closely match the measurements obtained from the system. In this case, it suggests that the estimated parameters of the ARMAX model align well with the true parameters of the system's measurement model. The ARMAX model successfully captures the system's input-output relationship, allowing it to generate outputs that closely resemble the actual measurements.

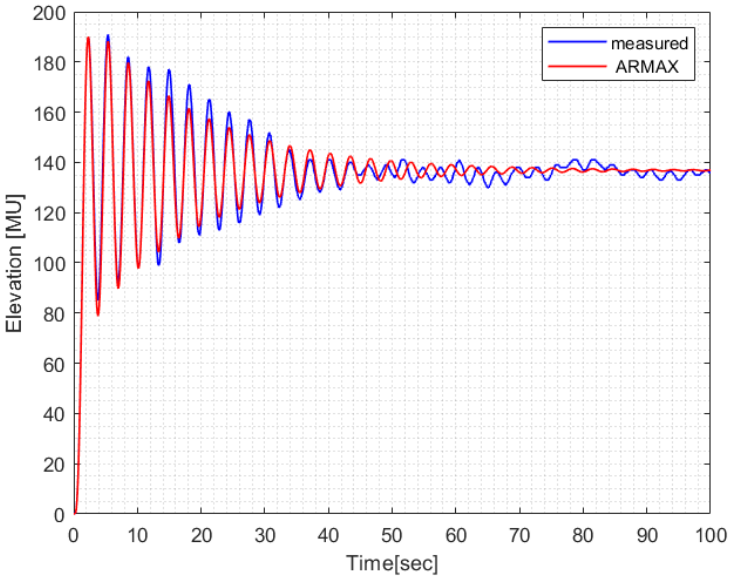

Figure 3.22 ARMAX model identification for elevation.

Based on the graph, it is evident that the identification using the fminsearch algorithm yields a superior model response. Therefore, for this specific thesis, the fminsearch-based identification is chosen for the entire controller design process due to its simplicity and effectiveness.

Similiarly, the step response Azimuth data obtained from the measurements of step input voltages ranging from 3V to 3.5V were used for identification, it is feasible to derive the transfer function of the system utilizing the ARX and ARMAX model.

```
% identification based on ARX
z=[y,u];
sys_arx=arx(z,[2 2 1])
sys_arx.Ts=0.01;
sysD_arx=tf(sys_arx)
sysC_arx=d2c(sysD_arx)
y_sim_arx=lsim(sysD_arx,u);
```

$$G_{ARX}(s) = \frac{-113.1s + 2.201e04}{s^2 + 16.54s + 36.68} \tag{3.10}$$

```
% identification based on ARMAX
sys_armax = armax(z,[2 2 2 1])
sys_armax.Ts=0.01;
sysD_armax=tf(sys_armax)
sysC_armax=d2c(sysD_armax)
y_sim_armax=lsim(sysD_armax,u);
```

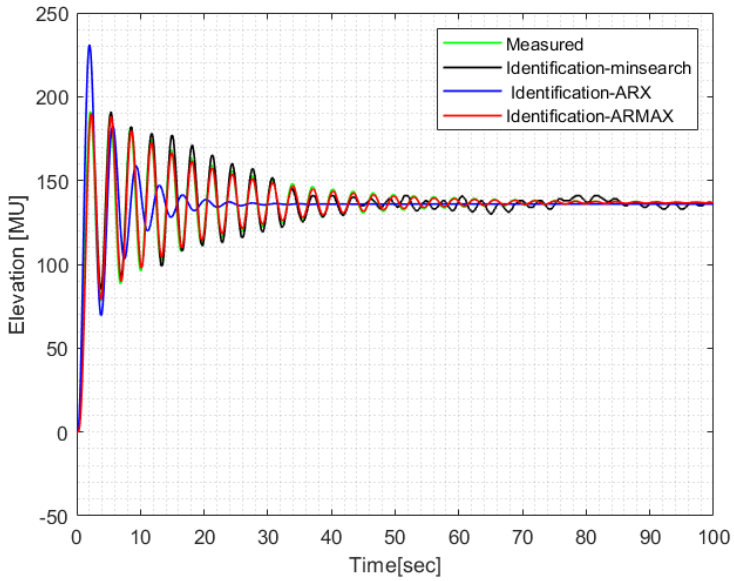

Figure 3.23 fminsearch ARX and ARMAX model identification for elevation-comparison.

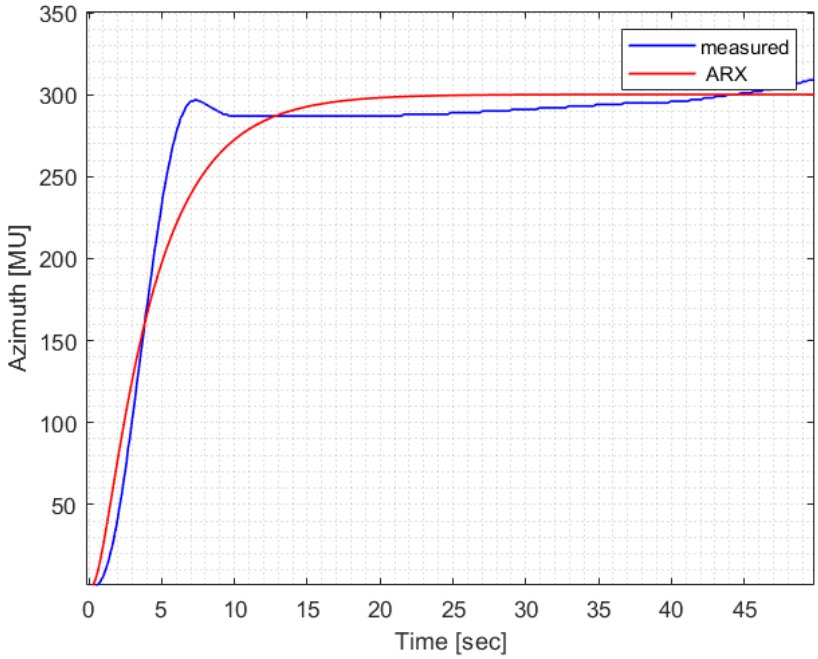

Figure 3.24 Azimuth Step response identified by ARX.

$$G_{ARMAX}(s) = \frac{-144.2s + 8852}{s^2 + 4.173s + 15.28} \tag{3.11}$$

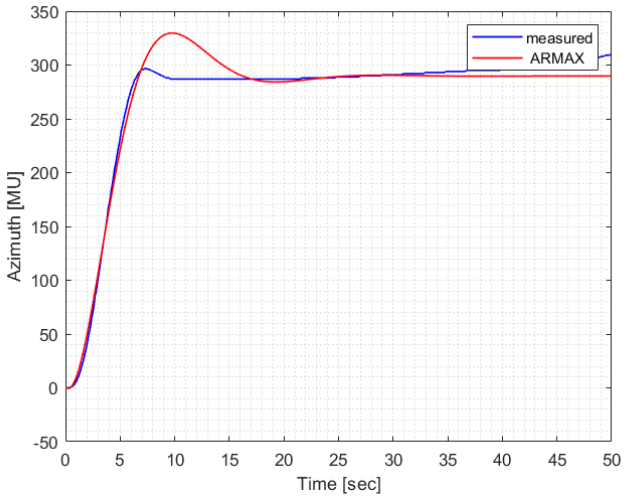

Figure 3.25 Azimuth Step Response Identified by ARMAX.

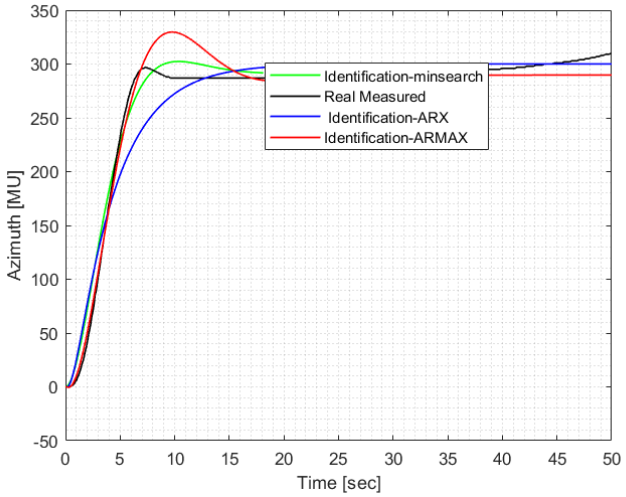

Figure 3.26 Azimuth Step Response Identified by fminsearch, ARX, ARMAX, and Real Plant Measurement - Comparison.

An Important Note: First, it is crucial to acknowledge that the identification of azimuth angle and elevation angle is not feasible at the stopper, which restricts the movements of TRMS and causes bounce back, leading to nonlinear behavior.

The second critical point is that identification should only be carried out at stable points during TRMS measurements. Therefore, it is essential to wait for a sufficiently long period of time to ensure that the measurement data has reached a stable state

before proceeding with the identification process. Utilizing fluctuating measurement data for identification may lead to inaccurate modeling results.

To generalize, in this paper, the identification achieved through the fminsearch optimization algorithm is utilized throughout the entire controller design process.

3.4.3 Analysis of Hurwitz Stability, State Controllability, Output Controllability, Observability -of Elevation

The transfer function for the elevation is as follows:

$$G(s) = \frac{136.84}{0.2182s^3 + 0.2785s^2 + 0.8832s + 1} \tag{3.12}$$

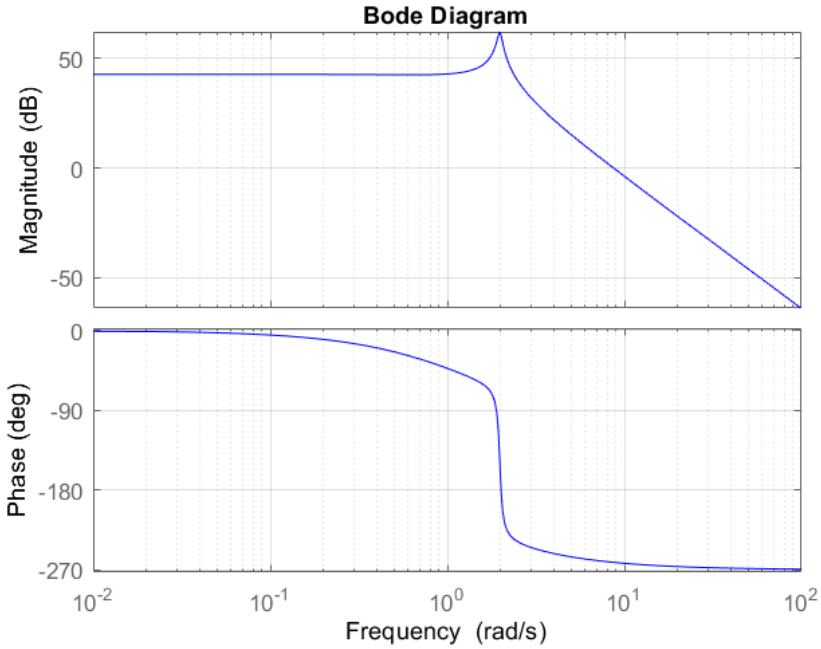

Figure 3.27 Bode Plot of Plant - Elevation.

According to the Bode plot, the frequency range extends from 0.01 rad/sec to 100 rad/sec, encompassing both the lower and upper frequencies.
To check the stability of the given plant, we use the Hurwitz criteria. The plant transfer function is:

$$G(s) = \frac{136.84}{0.2182s^3 + 0.2785s^2 + 0.8832s + 1}$$

1. Rewrite the transfer function as a characteristic equation by setting the denominator equal to zero:

$$0.2182s^3 + 0.2785s^2 + 0.8832s + 1 = 0$$

2. Obtain the coefficients of the characteristic equation:

$$a_0 = 1, \quad a_1 = 0.8832, \quad a_2 = 0.2785, \quad a_3 = 0.2182$$

3. Construct the Hurwitz matrix:

$$\begin{array}{ll} s^3: & a_3 \quad a_1 \\ s^2: & a_2 \quad a_0 \\ s^1: & \frac{a_2 a_1 - a_3 a_0}{a_2} \\ s^0: & a_0 \end{array}$$

Substituting the coefficients, we have:

$$\begin{array}{ll} s^3: & 0.2182 \quad 0.8832 \\ s^2: & 0.2785 \quad 1 \\ s^1: & \frac{0.2785 * 0.8832 - 0.2182}{0.2785} = 0.0997 \\ s^0: & 1 \end{array}$$

Check the signs of all coefficients .Since all the coefficients in the first column are of the same sign, i.e., positive, the given equation has no roots with positive real parts; therefore, the system is said to be stable.

Therefore, based on the Hurwitz criteria, the system described by the transfer function $G(s) = \frac{136.84}{0.2182s^3 + 0.2785s^2 + 0.8832s + 1}$ is indeed stable.
For further analysis, roots of the characteristic equation
$0.2182s^3 + 0.2785s^2 + 0.8832s + 1 = 0$
$s_1 = -0.0539 + 1.9795i$
$s_2 = -0.0539 - 1.9795i$
$s_3 = -1.1686$
Negative real parts of the roots indicate that the system is stable, while the presence of imaginary parts suggests that the system is oscillatory and marginally stable system. This observation aligns with the measurements conducted on the TRMS plant, which exhibited noticeable oscillations. Thus, the analysis of the roots reinforces the understanding that the TRMS system displays stable in the long run and yet oscillatory behavior.

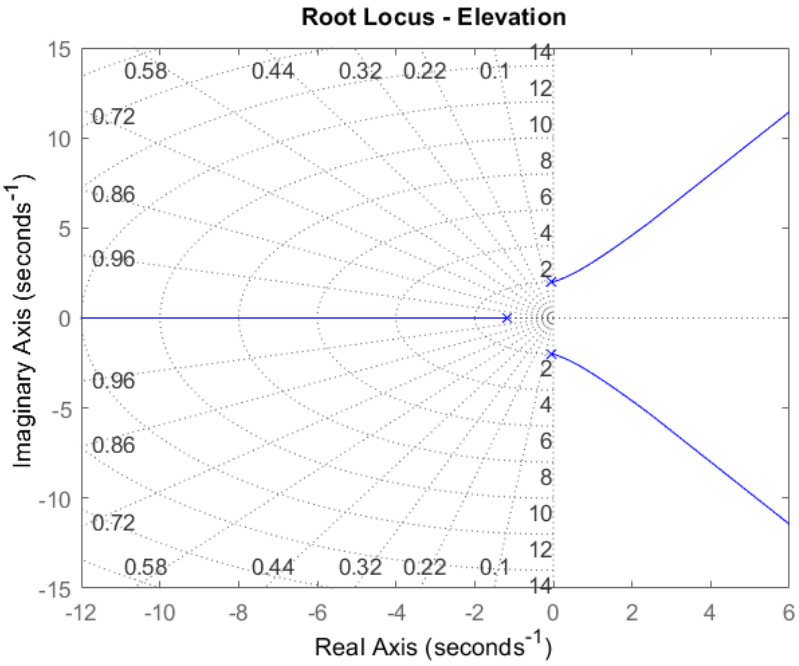

Figure 3.28 Root Locus - Elevation.

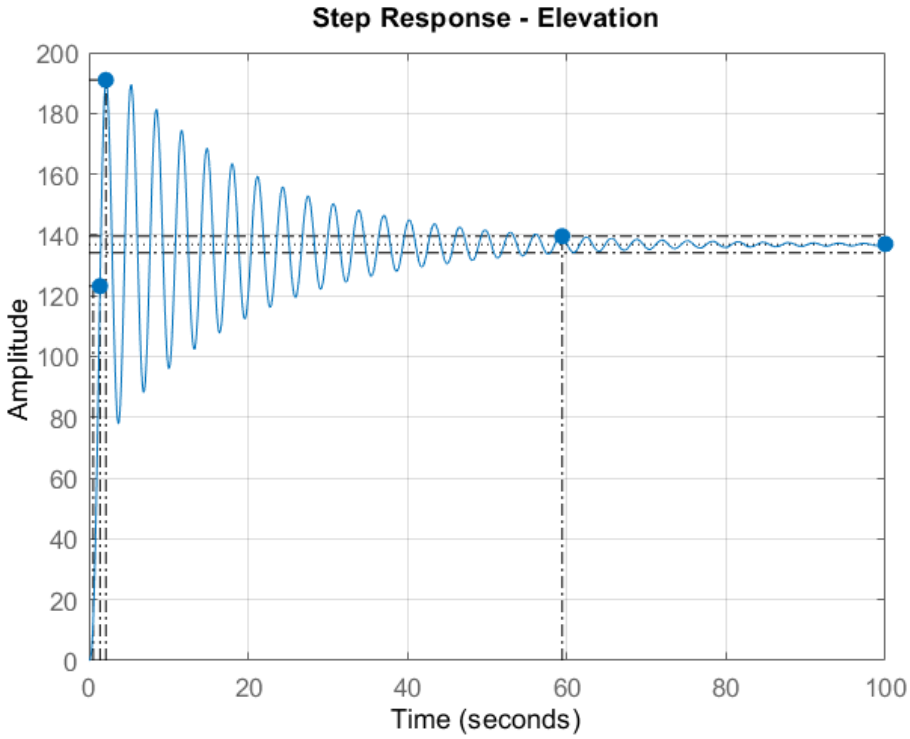

Figure 3.29 Step Response -Elevation.

The response characteristics of the system can be summarized as follows: The rise time is 0.8462, indicating the time it takes for the response to rise from 10% to 90% of its final value. The settling time is 59.4240, representing the time it takes for the response

to reach and stay within a specified error band. The overshoot is 39.5633, indicating the percentage by which the response exceeds its final value before settling. There is no undershoot observed. The peak value is 190.9785, representing the highest value reached by the response. The peak time is 2.1279, indicating the time at which the peak value occurs.

The State Space Representation

Additionally, the given transfer function can be represented in the state-space form as follows:

Given transfer function:

$$G(s) = \frac{136.84}{0.2182s^3 + 0.2785s^2 + 0.8832s + 1}$$

Let's rewrite it in the standard form:

$$G(s) = \frac{136.8}{0.2182} \times \frac{1}{s^3 + \frac{0.2785}{0.2182}s^2 + \frac{0.8832}{0.2182}s + \frac{1}{0.2182}}$$

$$G(s) = \frac{627}{s^3 + 1.2764s^2 + 4.076s + 4.583}$$

The state-space representation of the above transfer function is given by:

$$\dot{x}(t) = Ax(t) + Bu(t)$$
$$y(t) = Cx(t) + Du(t)$$

where:

$x(t) = \begin{bmatrix} x_1(t) \\ x_2(t) \\ x_3(t) \end{bmatrix}$ is the state vector, $u(t)$ is the input vector, $y(t)$ is the output vector.

Indeed, the state-space representation for any system is not unique. In fact, there are many (infinitely many) state-space representations that can describe the same system. One possible state-space representation is

The state matrix A and the input-to-state matrix B are as follows:

$$A = \begin{bmatrix} 0 & 1 & 0 \\ 0 & 0 & 1 \\ -4.583 & -4.076 & -1.2764 \end{bmatrix}$$

$$B = \begin{bmatrix} 0 \\ 0 \\ 627 \end{bmatrix}$$

The output-to-state matrix C and the state-to-output matrix D are as follows:

$$C = \begin{bmatrix} 1 & 0 & 0 \end{bmatrix}$$

$$D = \begin{bmatrix} 0 \end{bmatrix}$$

Another possible state-space representation (among infinitely many alternatives) is

$$A = \begin{bmatrix} -1.2764 & -4.0476 & -4.583 \\ 1 & 0 & 0 \\ 0 & 1 & 0 \end{bmatrix}$$

$$B = \begin{bmatrix} 1 \\ 0 \\ 0 \end{bmatrix}$$

The output-to-state matrix C and the state-to-output matrix D are as follows:

$$C = \begin{bmatrix} 0 & 0 & 627 \end{bmatrix}$$

$$D = \begin{bmatrix} 0 \end{bmatrix}$$

The basic system properties: (State Controllability, Output Controllability, Observability, Stabilization)

To analyze the basic system properties, it is better to examine the controllability, observability, and stabilization of the system represented by the given matrices A, B, C, and D.

1. State Controllability: The controllability matrix is given by:

$$\mathcal{C} = \begin{bmatrix} B & AB & A^2B \end{bmatrix}$$

Evaluating $\mathcal{C}$:

$$\mathcal{C} = \begin{bmatrix} 1 & -1.2764 & -2.4180 \\ 0 & 1 & -1.2764 \\ 0 & 0 & 1 \end{bmatrix}$$

The rank of $\mathcal{C}$ is 3, which is equal to the number of states (3). Since the number of state of matrix is the same with the number of rank of state controllable matrix, thus the system is completely controllable in terms of states. i.e., the number of uncontrollable states is zero.

2. Output Controllability: The output controllability matrix is given by:

$$\mathcal{C}_{\text{output}} = \begin{bmatrix} CB & CAB & CA^2B \end{bmatrix}$$

Evaluating $\mathcal{C}_{\text{output}}$:

$$\mathcal{C}_{\text{output}} = \begin{bmatrix} 0 & 0 & 627 \end{bmatrix}$$

The rank of matrix is 1, which is similar with the number of outputs. Since the number of outputs of matrix is the same with the number of ranks of output controllable matrix, thus the system is completely controllable in terms of output.

3. Observability: The observability matrix is given by:

$$\mathcal{O} = \begin{bmatrix} C \\ CA \\ CA^2 \end{bmatrix}$$

Evaluating $\mathcal{O}$:

$$\mathcal{O} = \begin{bmatrix} 0 & 0 & 627 \\ 0 & 627 & 0 \\ 627 & 0 & 0 \end{bmatrix}$$

The rank of $\mathcal{O}$ is 3, which is equal to the number of states (3). Since the number of states of matrix is the same with the number of rank of observable matrix, thus the system is completely observable in terms of states. i.e., number of unobservable states is zero

4. Stability: To check the stability, we find the eigenvalues of matrix A:

$$A = \begin{bmatrix} -1.2764 & -4.0476 & -4.583 \\ 1 & 0 & 0 \\ 0 & 1 & 0 \end{bmatrix}$$

The characteristic equation is given by:

$$\det(\lambda I - A) = \det\left(\begin{bmatrix} \lambda + 1.2764 & 4.0476 & 4.583 \\ -1 & \lambda & 0 \\ 0 & -1 & \lambda \end{bmatrix} \right)$$

Evaluating the determinant, we get:

$$4.583 + 4.0476\lambda + 1.2764\lambda^2 + \lambda^3$$

The roots of the characteristic equation are: $\lambda_1 = -0.0539 + 1.9795i$

$\lambda_2 = -0.0539 - 1.9795i$

$\lambda_3 = -1.1686$

Since all eigenvalues have negative real parts, the system is stable, as stated in the Hurwitz stability criterion discussed earlier.

In summary, the given state-space representation is state controllable, output controllable, observable, and stable.

The Relationship Between Transfer Functions and State-Space Equations the relationship between the transfer function and state space representation of the identified elevation plant system is presented. Let us consider transfer function given by:

$$G(s) = \frac{Y(s)}{U(s)}$$

This system can be represented in state space by the following equations:

$$\dot{x} = Ax + Bu$$
$$y = Cx + Du$$

where: x is the state vector of the system, $\dot{x}$ is the derivative of the state vector x with respect to time, A is the state matrix, B is the input matrix, C is the output matrix, D is the direct transmission matrix. Taking the Laplace transform of the first equation gives:

$$sX(s) = AX(s) + BU(s)$$

Next, we can solve for $X(s)$ to get:

$$(sI - A)X(s) = BU(s)$$

where I is the identity matrix.

$$X(s) = (sI - A)^{-1}BU(s)$$

$$Y(s) = CX(s) + DU(s) = C(sI - A)^{-1}BU(s) + DU(s)$$

Finally, express the transfer function $G(s)$ as the ratio of the Laplace transform of the output to the Laplace transform of the input:

$$G(s) = \frac{Y(s)}{U(s)} = C(sI - A)^{-1}B + D$$

This is the relationship between the transfer function $G(s)$ and the state space representation of the system. Conversely, the state space representation can be obtained from the transfer function by inverting the Laplace transform and rearranging the equations.

3.4.4 Analysis of Hurwitz Stability, State Controllability, Output Controllability, Observability -of Azimuth

$$G(s) = \frac{583.5}{5.128s^2 + 3.286s + 1} \tag{3.13}$$

According to the Bode plot, the frequency range extends from 0.01 rad/sec to 10 rad/sec, encompassing both the lower and upper frequencies.

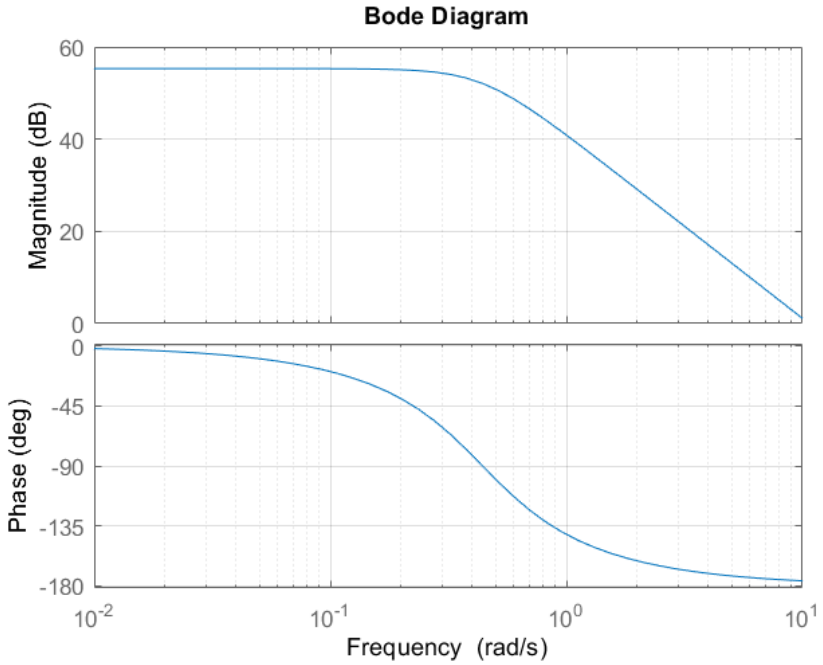

Figure 3.30 Bode Plot of Plant - Azimuth.

1. Rewrite the transfer function as a characteristic equation by setting the denominator equal to zero:

$$5.128s^2 + 3.286s + 1 = 0$$

2. Obtain the coefficients of the characteristic equation:

$$a_0 = 1, \quad a_1 = 3.286, \quad a_2 = 5.128$$

3. Construct the Hurwitz matrix:

$$\begin{array}{lll} s^2: & a_2 & a_0 \\ s^1: & a_1 & 0 \\ s^0: & \frac{a_1 a_0 - 0}{a_1} & \end{array}$$

Substituting the coefficients, we have:

$$\begin{array}{lll} s^2: & 5.128 & 1 \\ s^1: & 3.286 & 0 \\ s^0: & \frac{3.286-0}{3.286} = 1 & \end{array}$$

4. Check the signs of all coefficients .Since all the coefficients in the first column are of the same sign, i.e., positive, the given equation has no roots with positive real parts; therefore, the system is said to be stable.

Therefore, based on the Hurwitz criteria, the system described by the transfer function $G(s) = \frac{583.5}{5.128s^2+3.286s+1}$ is stable.

For further analysis, roots of the characteristic equation
$5.128s^2 + 3.286s + 1 = 0$
$s_1 = -0.32 + 0.304i$
$s_2 = -0.32 - 0.304i$

The presence of poles on the imaginary axis indicates that the system is marginally stable.

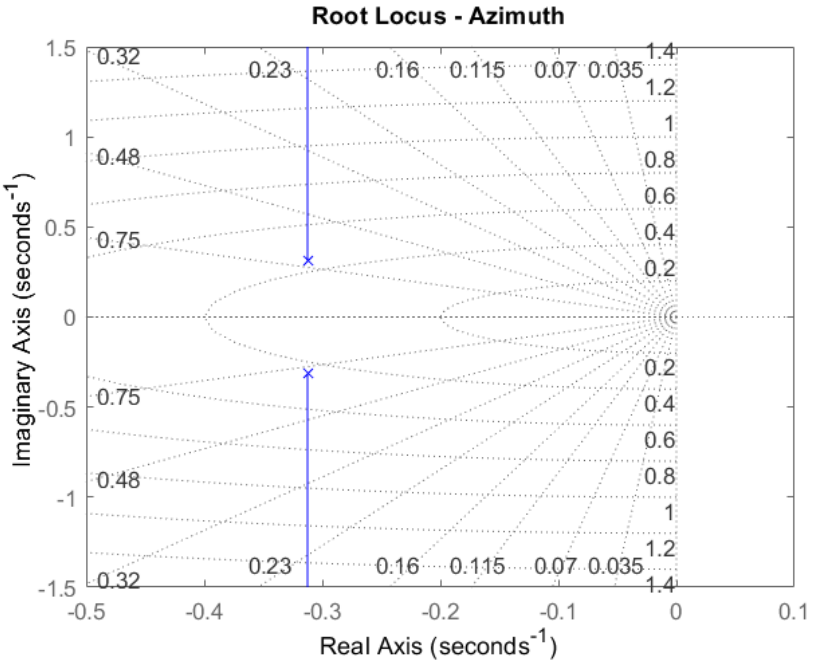

Figure 3.31 Root Locus - Azimuth.

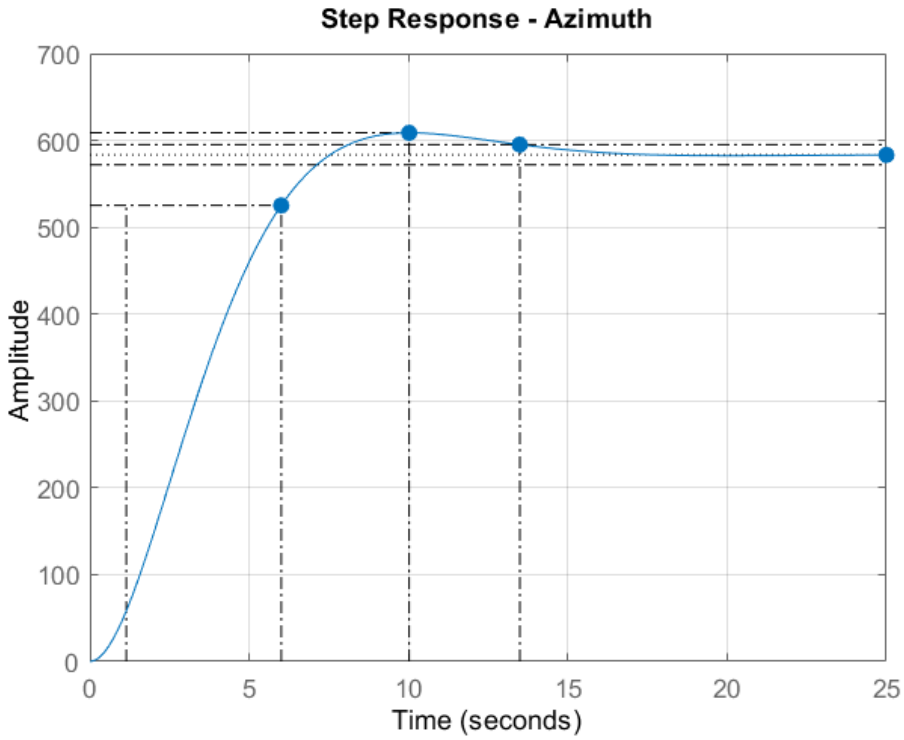

Figure 3.32 Step Response -Azimuth.

The response characteristics of the system can be summarized as follows: The rise time is 4.86, indicating the time it takes for the response to rise from 10% to 90% of its final value. The settling time is 13.49, indicating the duration takes for the response to attain and remain within a predefined error margin. The overshoot is 4.32, indicating the percentage by which the response exceeds its final value before settling. There is no undershoot observed. The peak value is 608.7, representing the highest value reached by the response. The peak time is 10.02, indicating the time at which the peak value occurs.

The State Space Representation

Additionally, the given transfer function can be represented in the state-space form as follows:

Given transfer function:

$$G(s) = \frac{583.5}{5.128s^2 + 3.286s + 1}$$

Let's rewrite it in the standard form:

$$G(s) = \frac{583.5}{5.128} \times \frac{1}{s^2 + \frac{3.286}{5.128}s + \frac{1}{5.128}}$$

$$G(s) = \frac{113.78}{s^2 + 0.64s + 0.195}$$

The state-space representation of the above transfer function is given by:

$$\dot{x}(t) = Ax(t) + Bu(t)$$
$$y(t) = Cx(t) + Du(t)$$

$$A = \begin{bmatrix} -0.64 & -0.195 \\ 1 & 0 \end{bmatrix}$$

$$B = \begin{bmatrix} 1 \\ 0 \end{bmatrix}$$

$$C = \begin{bmatrix} 0 & 113.78 \end{bmatrix}$$

$$D = \begin{bmatrix} 0 \end{bmatrix}$$

The basic system properties: (State Controllability, Output Controllability, Observability, Stabilization)

To analyze the basic system properties, it is better to examine the controllability, observability, and stabilization of the system represented by the given matrices A, B, C, and D.

1. State Controllability: The controllability matrix is given by:

$$\mathcal{C} = \begin{bmatrix} B & AB \end{bmatrix}$$

Evaluating $\mathcal{C}$:

$$\mathcal{C} = \begin{bmatrix} 1 & -0.64 \\ 0 & 1 \end{bmatrix}$$

The rank of $\mathcal{C}$ is 2, which is equal to the number of states (2). Since the number of state of matrix is the same with the number of rank of state controllable matrix, thus the system is completely controllable in terms of states. i.e., the number of uncontrollable states is zero.

2. Output Controllability: The output controllability matrix is given by:

$$\mathcal{C}_{\text{output}} = \begin{bmatrix} CB & CAB \end{bmatrix}$$

Evaluating $\mathcal{C}_{\text{output}}$:

$$\mathcal{C}_{\text{output}} = \begin{bmatrix} 0 & 113.78 \end{bmatrix}$$

The rank of matrix is 1, which is similar with the number of outputs. Since the number

of outputs of matrix is the same with the number of ranks of output controllable matrix, thus the system is completely controllable in terms of output.

3. Observability: The observability matrix is given by:

$$\mathcal{O} = \begin{bmatrix} C \\ CA \end{bmatrix}$$

Evaluating $\mathcal{O}$:

$$\mathcal{O} = \begin{bmatrix} 0 & 113.78 \\ 113.78 & 0 \end{bmatrix}$$

The rank of $\mathcal{O}$ is 2, which is equal to the number of states (2). Since the number of states of matrix is the same with the number of rank of observable matrix, thus the system is completely observable in terms of states. i.e., number of unobservable states is zero

4. Stability: To check the stability, we find the eigenvalues of matrix A:

$$A = \begin{bmatrix} -0.64 & -0.195 \\ 1 & 0 \end{bmatrix}$$

The characteristic equation is given by:

$$\det(\lambda I - A) = \det\left(\begin{bmatrix} \lambda + 0.64 & 0.195 \\ -1 & \lambda \end{bmatrix}\right)$$

Evaluating the determinant, we get:

$$0.195 + 0.64\lambda + \lambda^2$$

The roots of the characteristic equation are:

$\lambda_1 = -0.32 + 0.304i$
$\lambda_2 = -0.32 - 0.304i$
Since all poles lie on the imaginary axis, the system is marginally stable, as stated in the earlier-discussed Hurwitz stability criterion..

In summary, the given state-space representation is state controllable, output controllable, observable, and stable.

3.5 Comparative Analysis of Nonlinear, Linear, and Real Laboratory Models for the Twin Rotor MIMO System

Comparing the Twin Rotor MIMO System's nonlinear, linear, and real laboratory models can yield valuable insights into its behavior under diverse conditions. Among the linear models studied, the one obtained using the "fminsearch" MATLAB Toolbox exhibits the strongest fit to the data. Its accurate results make it an ideal candidate for controller design.

During comprehensive laboratory investigations, the operating point for the input voltage of the real laboratory model was determined to fall within the range of 0 to 5 volts. Staying within this voltage range is crucial to achieve desired and stable results. Operating the plant with input voltage beyond this specified range may lead to aggressive and undesirable outcomes.

The linear plant, obtained through an identification method from the real laboratory model, also follows an input voltage range of 0 to 5 volts.

As for the nonlinear plant, the acceptable input voltage range is from -2.5 to 2.5 volts, a range also stated in the manual [25]. It is equally essential to ensure that the input voltage remains within this designated range for the nonlinear model. Exceeding this range could lead to aggressive and unfavorable output responses.

To maintain stability and ensure proper functioning of all three models, it is of utmost importance to adhere to the specified input voltage ranges and avoid operating them outside of these boundaries.

Based on the above explanation, the relationship between the input voltage ranges for the nonlinear, linear, and real plants is as follows:

- For the nonlinear plant, an input voltage of -2.5 volts corresponds to 0 volts for both the linear and real plants.
- Conversely, an input voltage of 0 volts for the nonlinear plant corresponds to 2.5 volts for both the linear and real plants.
- Furthermore, an input voltage of 2.5 volts for the nonlinear plant corresponds to 5 volts for both the linear and real plants, and so forth.

This correlation allows us to understand how the input voltage values relate across

the different models, enabling us to make appropriate adjustments when working with each plant.

3.5.1 Step Response Comparison

The comparison of step responses for the Nonlinear, Linear, and Real Laboratory Models of the Twin Rotor MIMO System is illustrated in Figure 3.33.

The course data was obtained for a step change of control voltage from 0.5 volts to 1.5 volts for the nonlinear plant and from 3 to 4 volts for the main motor in both the linear and real plant models.The corresponding output course is depicted in Figure 3.34. In this scenario, the tail is not locked it unskrew TRMS measurements.

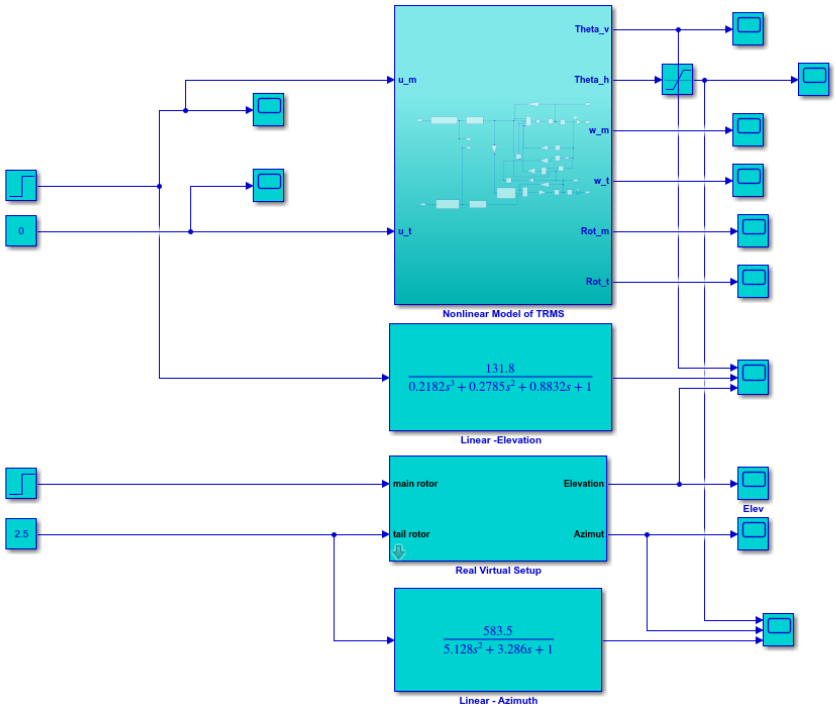

Figure 3.33 MATLAB implementation for Comparison of each Plants

For the tail motor, the input voltage is 0 volts for the nonlinear plant and 2.5 volts for both the linear and real plant models. The corresponding output graph is illustrated in Figure 3.35.

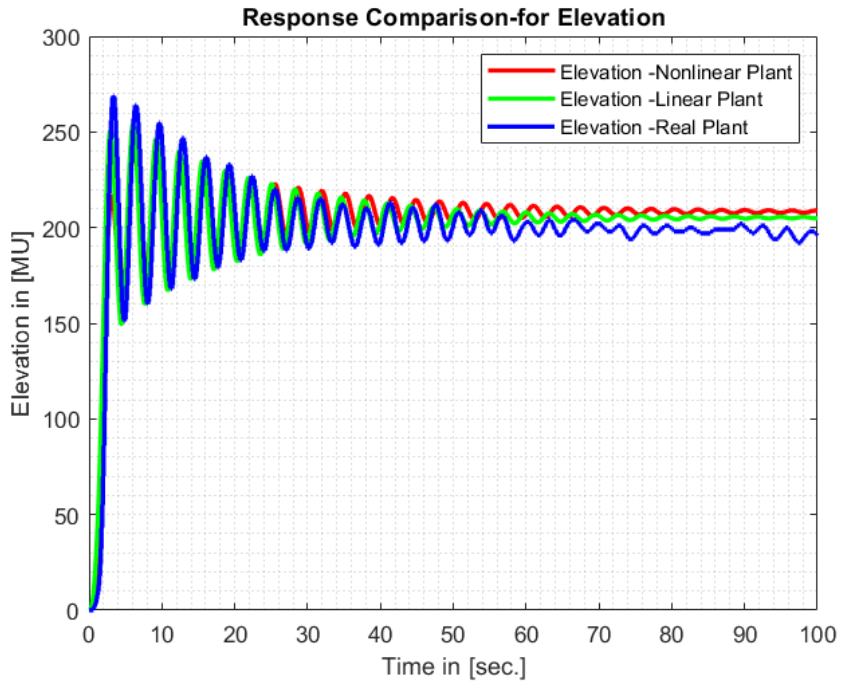

Figure 3.34 Response Comparison -for Elevation

In the case of the azimuth, after reaching a certain level, it encountered a stopper and bounced back. However, this bouncing behavior is not modeled in the nonlinear plant at all.

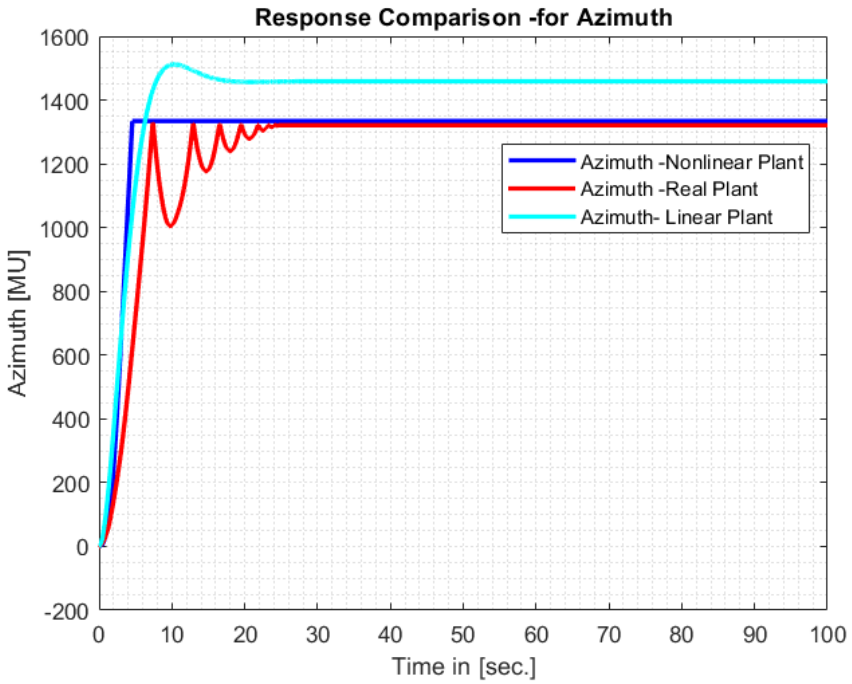

Figure 3.35 Response Comparison -for Azimuth

Furthermore, it is noticeable from the graph that the performance of the nonlinear plant is superior to that of the linear plant, as the linear model deviates more from the real time labolatory model's course.

4 CONTROLLER ALGORITHM IMPLEMENTATION

Since the primary objective of this thesis is not to develop a novel algorithm for PSO, GA, or NM. Instead, the main focus of this paper is that the use these algorithms to tune parameters of IOPID or FOPID controllers and control the TRMS model without deep investigation for each algorithm. Instead of creating new algorithms from scratch, the MATLAB toolbox is employed for implementing the overall system. The following section describes the MATLAB implementation of the entire system.

This section presents the implementation of several integer order and fractional order PID controllers. The controllers are implemented and their respective results are compared for further analysis.

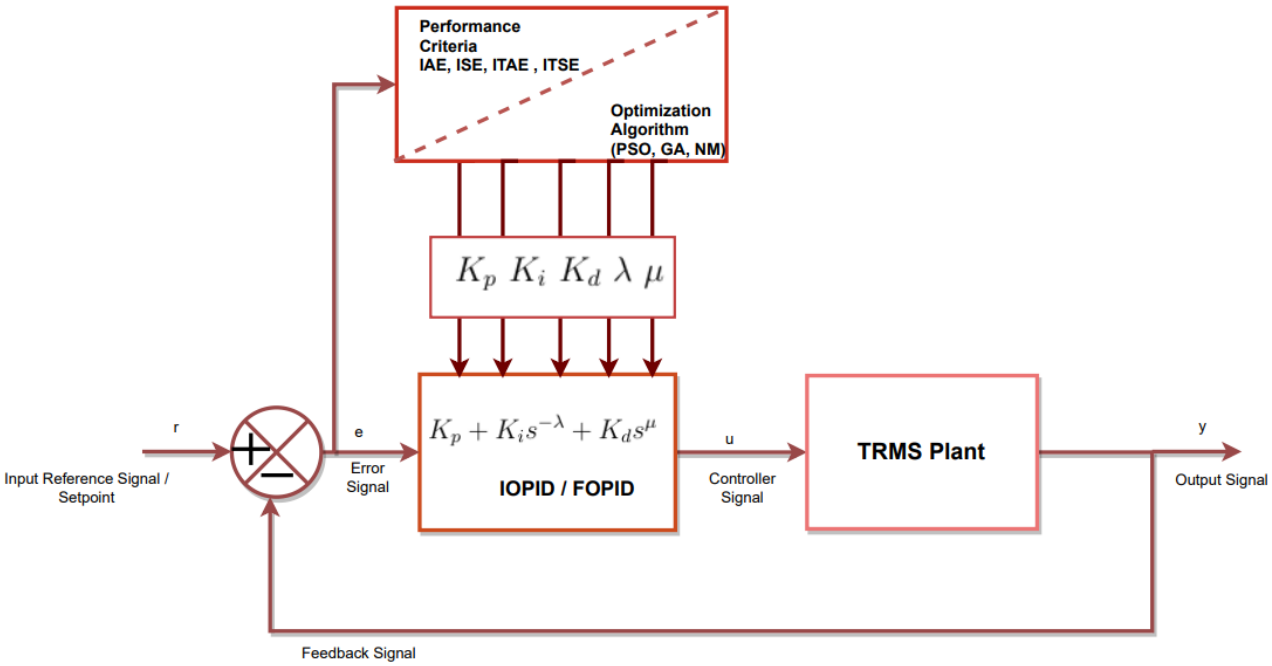

Figure 4.1 Block diagram of Control System used in the Optimization Method.

Where the following definitions hold for both IOPID and FOPID controller:

r : Input reference signal or setpoint.It represents the desired value or target for the controlled system.

e : Error signal. It is the difference between the reference signal (r) and the actual output signal (y).

u : Control signal. It is the output signal from the controller that is applied to the plant.

y : Output signal. It represents the measured or observed response of the controlled system.

The block diagram illustrates the PSO/GA/NM-based IOPID/FOPID controller tuning technique that minimizes time domain performance indices: The block diagram consists of the following components:

- IOPID/FOPID Controller: The controller that is being tuned by the PSO/GA/NM-based technique. Both λ and μ =1 in the case of IOPID.
- TRMS Plant: The controlled system or process.
- Performance Criteria (J): Represents the time domain integral performance indices, acting as the objective function to be minimized.

The objective function is implemented based on IAE, ITSE, ISE and ITAE, which have a relationship with the error values and specified time intervals, as discussed in the theory part (From Equation 1.45- 1.48).

The performance criteria are calculated for each PSO/GA/NM algorithm, and the results of each criterion are compared across the algorithms. The MATLAB code for implementing the PSO/GA/NM-based IOPID and FOPID controller tuning technique can be derived from the block diagram and the desired fitness evaluation function. In this section, the design of both IOPID and FOPID controllers has been focused on the time domain.

4.1 MATLAB Implementation

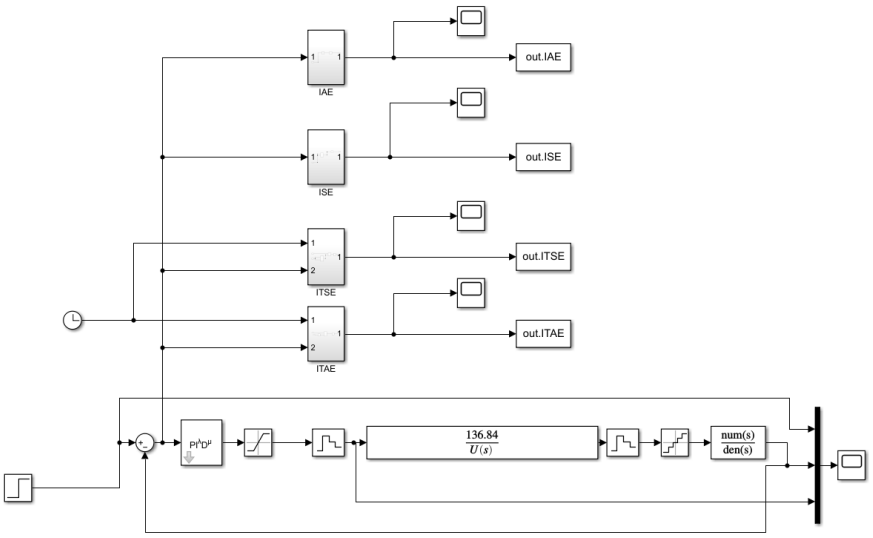

Figure 4.2 MATLAB Simulink Implementation for Elevation - Linear Plant Control.

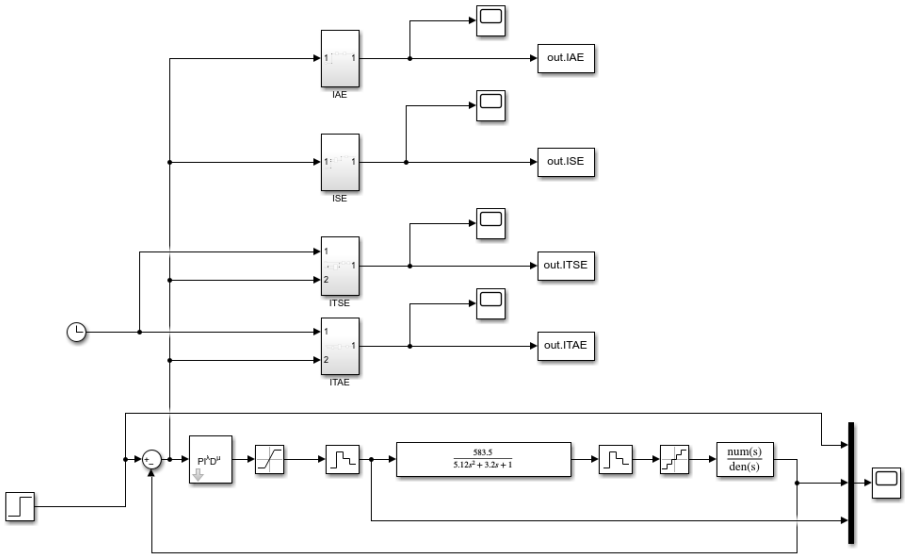

Figure 4.3 MATLAB Simulink Implementation for Azimuth - Linear Plant Control.

The implementation of $PI^{\lambda}D^{\mu}$ is based on MATLAB toolboxes Fractional-order Modeling and Control (FOMCON) [37].

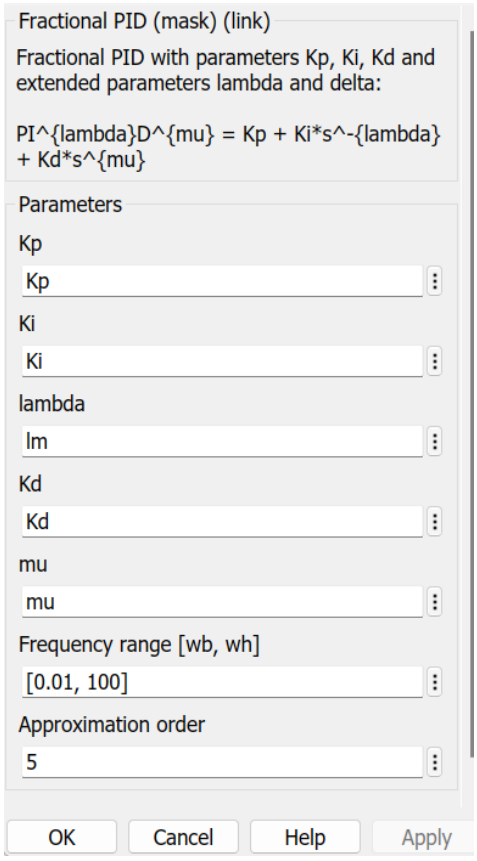

Figure 4.4 Parameters of controller based on FOMCON.

Parameter	IOPID	FOPID	Description
K_p	0 to 0.01	0 to 0.01	Proportional Gain
K_i	0 to 0.1	0 to 0.1	Integral Gain
K_d	0 to 0.1	0 to 0.1	Derivative Gain
λ	-	0 to 2	Integral Order
μ	-	0 to 2	Differentiator Order

Table 4.1 The lower and upper bounds for the IOPID/FOPID controller parameters for both elevation and azimuth

This paper investigates a system governed by five key parameters: K_p, K_i, K_d, λ, and μ, as outlined in the FOMCON implementation [37] without deep investigation in to its implementation, depicted in Figure 4.4. Notably, the IOPID controller implementation sets λ and μ to a fixed value of 1. Table 4.1 provides the upper and lower parameter ranges.

from bode plot of closed loop system, the selected frequency range stems from the Bode plot and spans from 0.01 to 100 for elevation, and 0.001 to 100 for azimuth. This

frequency range particularly applies to the elevation analysis, visualized in Figure 3.27, and azimuth analysis, shown in Figure 4.5.

The elevation control employs an IOPID/FOPID controller, realized through a MATLAB Simulink implementation depicted in Figure 4.2. Similarly, the azimuth control integrates an IOPID/FOPID controller, demonstrated through a MATLAB Simulink implementation illustrated in Figure 4.3.

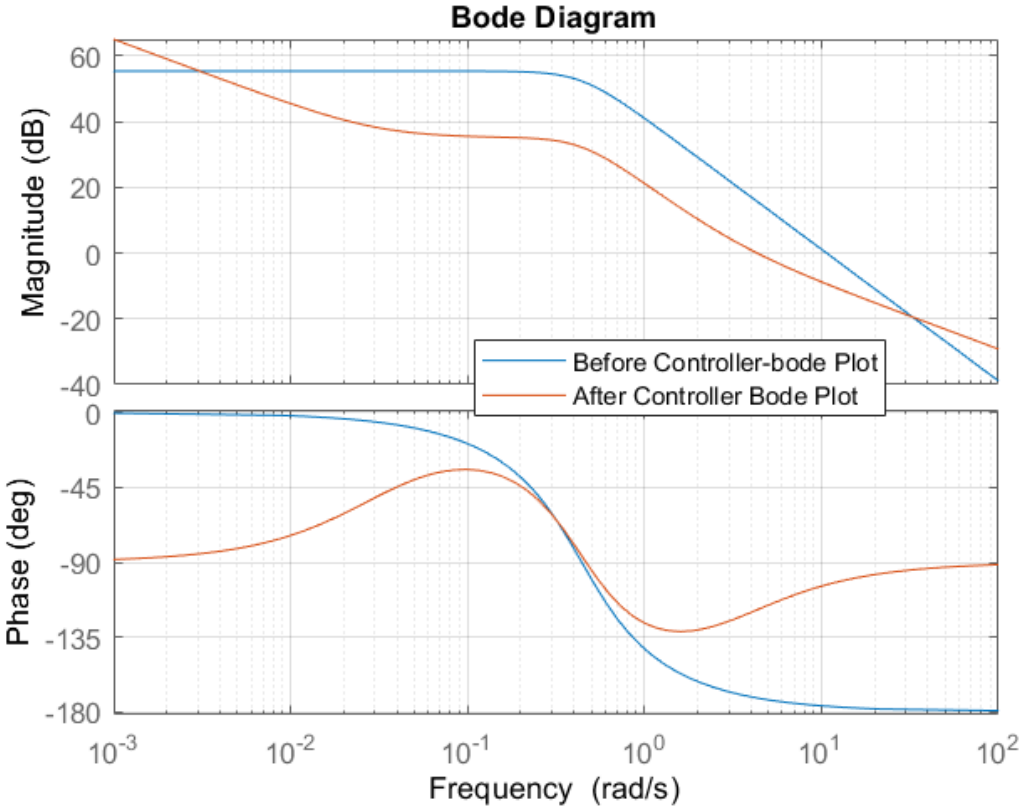

Figure 4.5 Bode plot before and after controller applied.

The tuning of controller parameters, which includes K_p, K_i, K_d, λ, and μ, is carried out for both IOPID and FOPID using the PSO/GA/NM algorithms. For IOPID, the controller has three parameters, while for FOPID, it has five parameters, requiring optimization in three and five-dimensional spaces, respectively. The subsequent flowchart outlines the implementation of these algorithms accordingly.

Each algorithm is limited to a maximum of 20 iterations or 20 generations, and the simulation time is set to run for 60 seconds for elevation and 100 seconds for azimuth. The optimization process continues until the stopping conditions are met, which can occur when the number of generations is reached or when the fitness value becomes

less than 1e-6. In case the simulation fails, a return cost of J=1e3 is assigned.

The best-optimized parameters obtained from each algorithm will be considered the final solution for each respective problem. These parameters represent the optimal values that yield the desired control performance for the given system.

4.2 GA /PSO/NM based IOPID and FOPID based Tunning Technique.

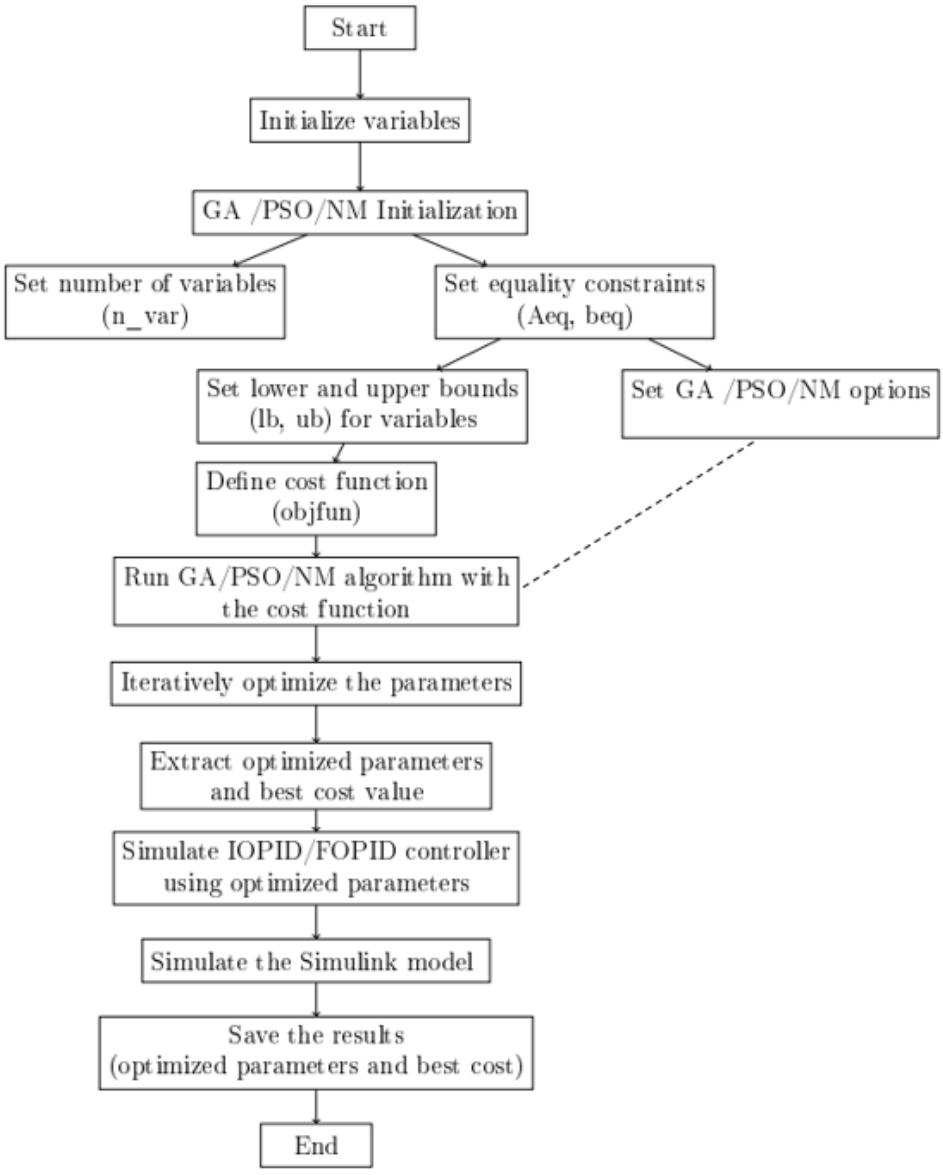

Figure 4.6 Flowchart for the GA/PSO/NM-based IOPID /FOPID controller tuning technique

4.3 Results of GA /PSO/NM based IOPID and FOPID Controller Responses for Linear and Real Time Experiments.

In this subsection, MATLAB simulation results were initially generated for both IOPID and FOPID controllers. The most favorable simulation outcomes were then applied to actual experiments.

4.3.1 Results of GA IOPID and FOPID Controller Responses for Elevation Linear Model

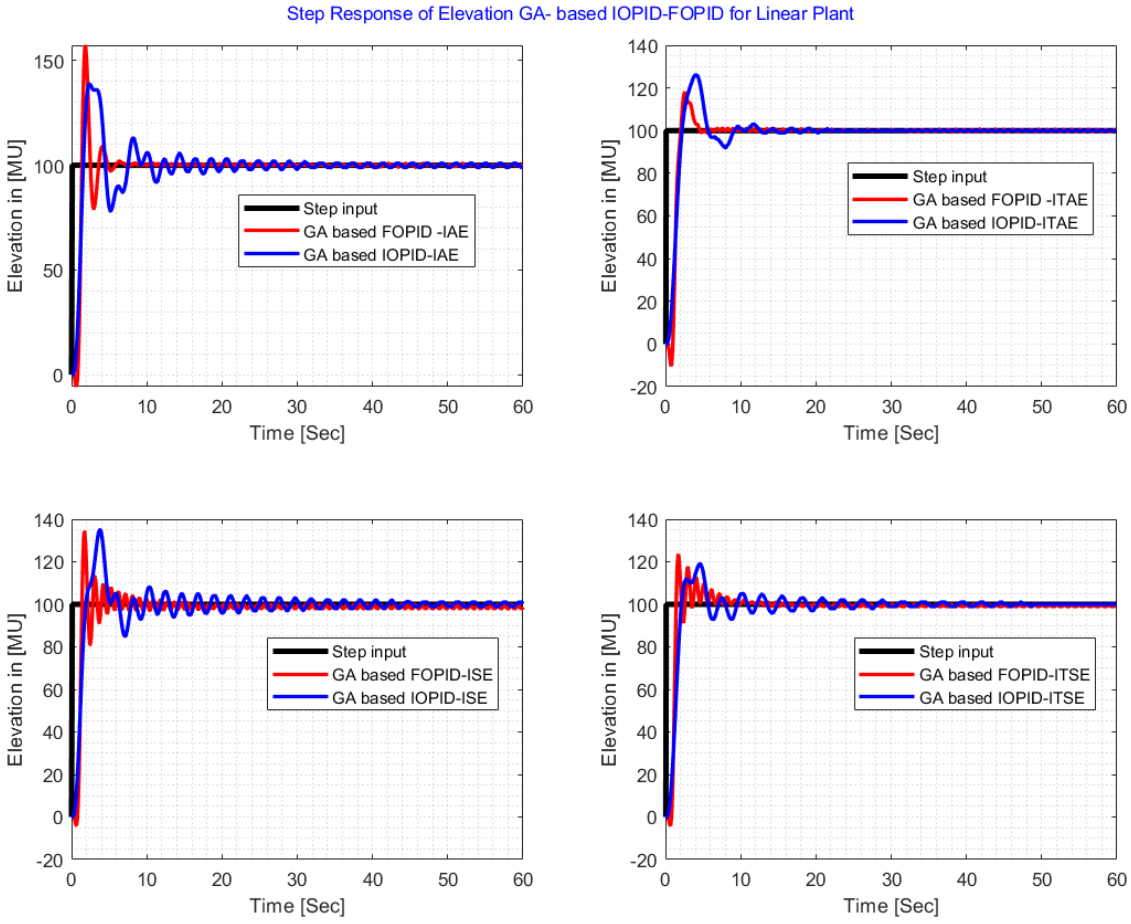

Figure 4.7 GA based IOPID/FOPID Elevation Response for various Performance Indices.

According to the step response of elevation for GA based IOPID controller algorithm, the ITSE performance index offers the advantage of yielding smaller overshoots (20.7250%) compared to other performance indices. However, it is accompanied by a longer settling time (18.9353 seconds) in contrast to the ITAE (11.5748 seconds)

IOPID Controller - GA based tuning - for Elevation						
Performance Index	K_p	K_i	K_d	$\%M_p$	$t_r(sec.)$	$t_s(sec.)$
ITSE	0.0018	0.0083	0.0043	20.7250	2.7133	18.9353
ITAE	0.0015	0.0093	0.0059	25.7128	2.6103	11.5748
ISE	0.0037	0.0123	0.0092	37.5025	0.5672	12.2036
IAE	0.0033	0.0193	0.0109	40.3485	0.5056	12.5622
IOPID Controller - PSO based tuning - for Elevation						
Performance Index	K_p	K_i	K_d	$\%M_p$	$t_r(sec.)$	$t_s(sec.)$
ITSE	0.0011	0.0085	0.0041	18.9433	2.6248	16.2758
ITAE	1.9784e-4	0.0049	0.0020	14.4838	2.8247	16.3071
ISE	1.9047e-4	0.0073	0.0025	23.7832	2.1154	15.0789
IAE	6.7809e-4	0.0062	0.0032	17.3441	2.7975	15.6666
IOPID Controller - NM based tuning - for Elevation						
Performance Index	K_p	K_i	K_d	$\%M_p$	$t_r(sec.)$	$t_s(sec.)$
ITSE	3.6803e-4	0.0057	0.0020	15.0796	2.7453	17.4269
ITAE	1.7278e-5	0.0044	0.0016	8.8182	2.8692	13.7324
ISE	1.9047e-4	0.0073	0.0025	24.5633	0.7483	15.8195
IAE	2.8145e-4	0.0053	0.0022	15.4363	2.7997	16.1780

Table 4.2 Parameter ranges for the IOPID controller (GA, PSO, NM) for elevation

performance index, as an illustrative in Table 4.2

According to the step response of elevation for GA based FOPID controller algorithm, The ITAE performance index offers the advantage of yielding smaller overshoots (15%) compared to other performance indices. However, it is accompanied by a undershoot as performance index of others, as an illustrative in Figure 4.7.

Upon comparing the GA-based IOPID and FOPID controller algorithms, particularly focusing on the performance index ITAE, it is evident that the performance index ITAE during GA-based FOPID controller optimization shows significant improvement. This observation is demonstrated in Figure 4.7. This demonstrates the effectiveness of using FOPID controller for achieving better control performance in the GA-based tuning approach.

FOPID Controller - GA based tuning - for Elevation				
Performance Index	K_p	K_i	K_d	λ
ITSE	0.0806	0.0192	0.0312	0.8749
ITAE	0.0665	0.0067	0.0322	1.0097
ISE	0.0870	0.00387	0.0388	0.5742
IAE	0.0925	0.0097	0.0192	1.0284
FOPID Controller - PSO based tuning - for Elevation				
Performance Index	K_p	K_i	K_d	λ
ITSE	0.0028	0.0127	0.0086	0.9021
ITAE	0.0086	0.0062	0.0084	1.0251
ISE	0.0080	0.0944	0.0386	0.2018
IAE	0.0099	0.1000	0.0379	0.3714
FOPID Controller - NM based tuning - for Elevation				
Performance Index	K_p	K_i	K_d	λ
ITSE	1.8671e-4	0.0081	0.0034	1.0017
ITAE	3.6833e-4	0.0055	0.0026	1.0057
ISE	0.0014	0.0150	0.0101	0.8203
IAE	5.8010e-4	0.0059	0.0027	1.0128

Table 4.3 Parameter ranges for the FOPID controller (GA, PSO, NM) for elevation

4.3.2 Results of PSO IOPID and FOPID Controller Responses for Elevation Linear Model.

In the case of the PSO tuning algorithm, the ITAE performance index offers the advantage of yielding smaller overshoots (14.5%) compared to other performance indices. Additionally, it exhibits fewer oscillations compared to other indices, as illustrated in Figure 4.8. This demonstrates the effectiveness of using ITAE as a performance metric for achieving better control performance in the PSO-based IOPID tuning approach.

In the case of the PSO-based FOPID controller tuning algorithm, the ITSE performance index offers the advantage of yielding smaller overshoots (22%) compared to other performance indices. Furthermore, it exhibits fewer oscillations compared to the other indices, as illustrated in Figure 4.8. This clearly demonstrates the effectiveness of using ITSE as a performance metric for achieving superior control performance in the PSO-based FOPID tuning approach.

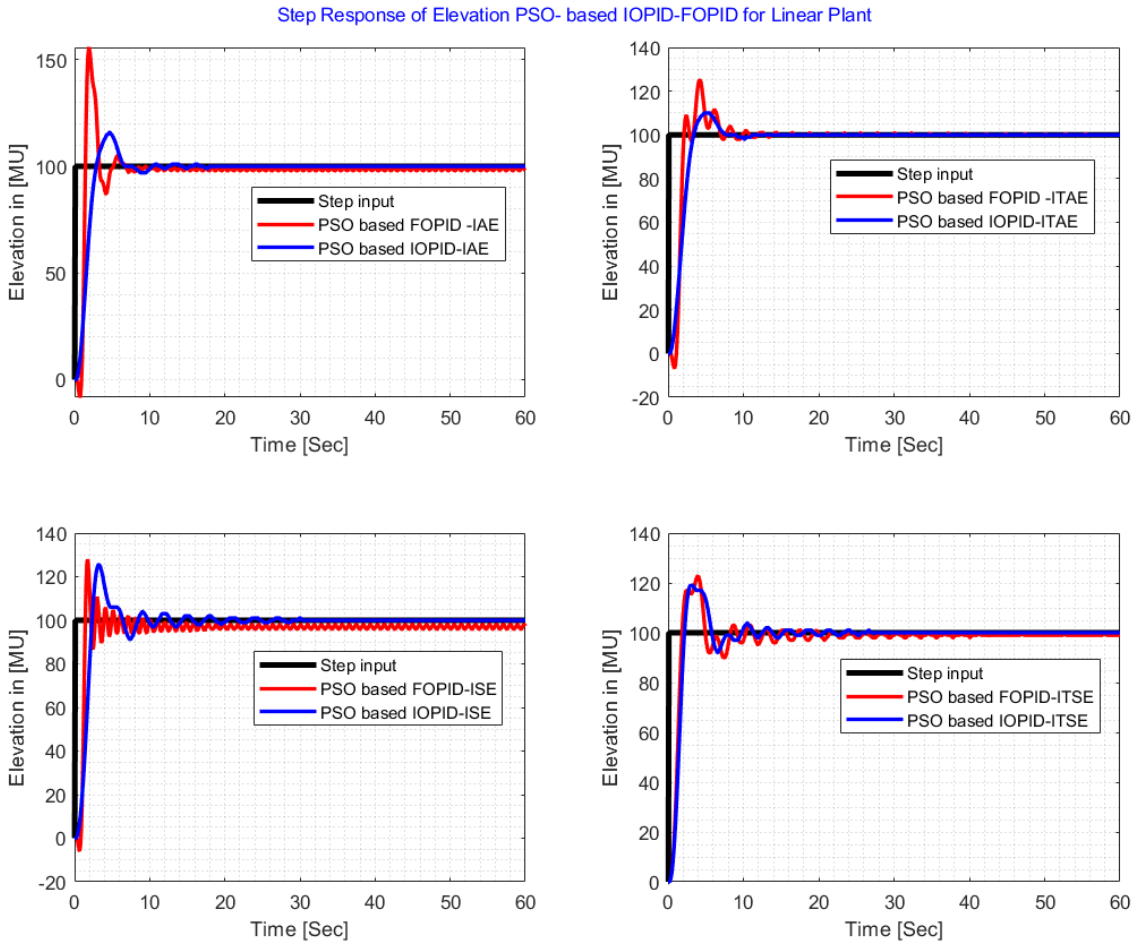

Figure 4.8 PSO based IOPID/FOPID Elevation Response for various Performance Indices.

4.3.3 Results of NM IOPID and FOPID Controller Responses for Elevation Linear Model.

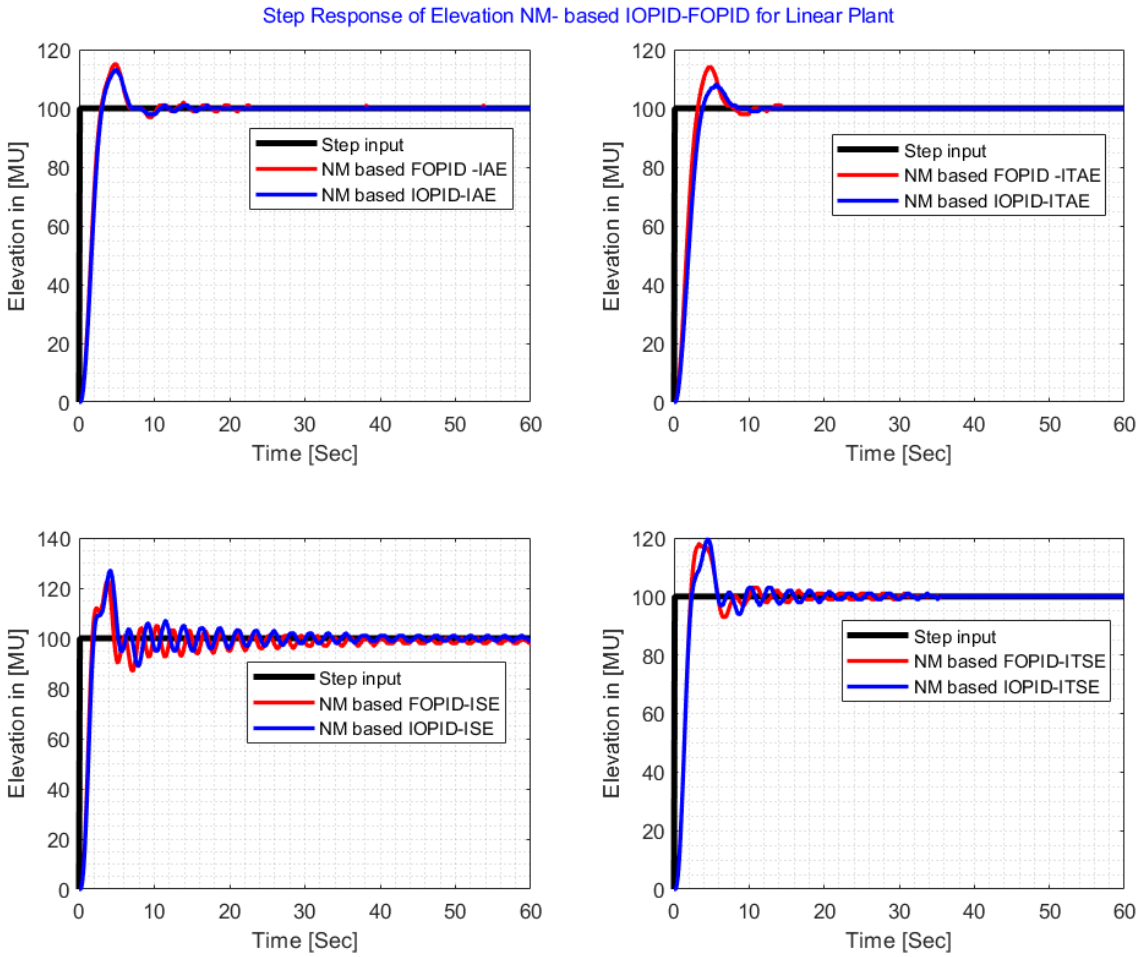

Figure 4.9 NM based IOPID/FOPID Elevation Response for various Performance Indices.

In the case of the NM tuning algorithm, both the ITAE and IAE performance indices offer the advantage of yielding smaller overshoots (9% and 10%, respectively) when compared to other performance indices. Additionally, they exhibit fewer oscillations compared to the other performance indices, as illustrated in Figure 4.9. However, it is worth noting that for the NM-based IOPID tuning approach, the IAE metric provides better results in terms of rise time and settling time.

This clearly demonstrates the effectiveness of using IAE as a performance metric for achieving superior control performance in the NM-based IOPID tuning approach. By considering IAE, the control system can achieve better response characteristics.

In the case of the NM-based FOPID tuning, the performance indices ITAE and IAE offer the advantage of yielding smaller overshoots (18%) compared to other performance indices. Moreover, they exhibit fewer oscillations compared to the other performance indices, as illustrated in Figure 4.9. This clearly demonstrates the effectiveness of using ITAE and IAE as performance metrics for achieving superior control performance in the NM-based FOPID tuning approach. These metrics help in achieving better control stability and precision for the given system.

4.3.4 IOPID/FOPID Controller Comparison -Linear Model for Elevation

The comparison of the IOPID/FOPID controller algorithms based on ITAE optimization is presented in Figure 4.10. The figure illustrates that the NM-based FOPID-ITAE approach delivers a favorable controller response, indicating the potential of this FOPID method in effectively controlling the TRMS model.

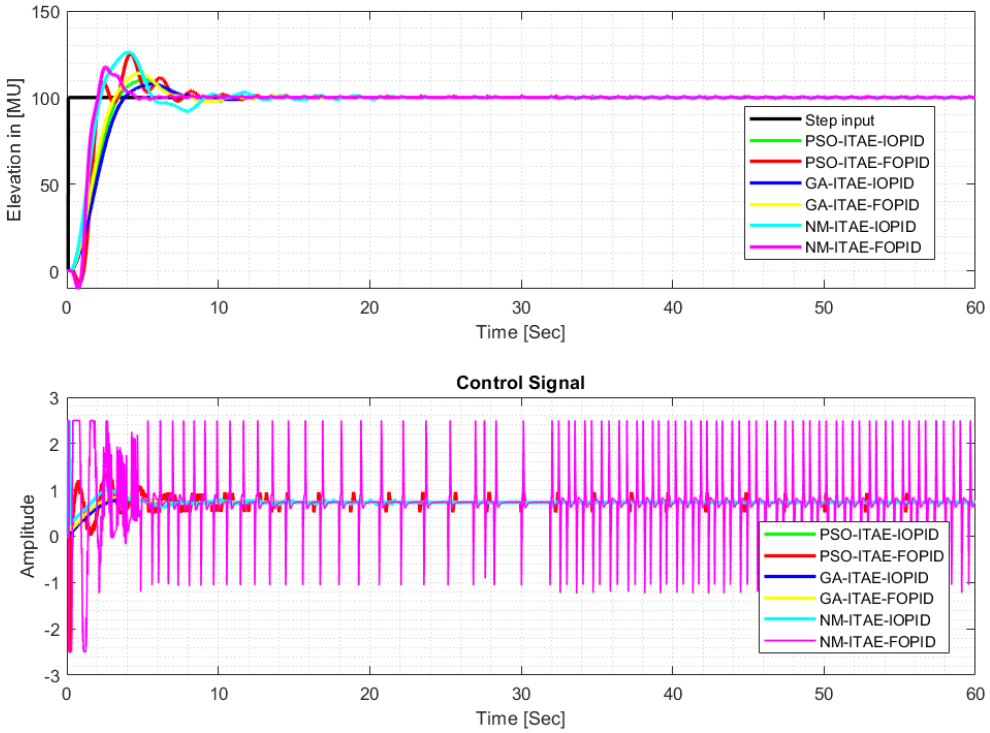

Figure 4.10 IOPID/ FOPID Controller Response for various Controller Tunning Algorithm.

4.3.5 IOPID Controller Comparison -Real Time Experiment for Elevation

The identical controller parameters were used IOPID in both simulation and real-time experiments. As illustrated in Figure 4.11, the implementation approach was employed, and the measurement results are compared in Figure 4.12. The inputs included both step input and ramp input signals.

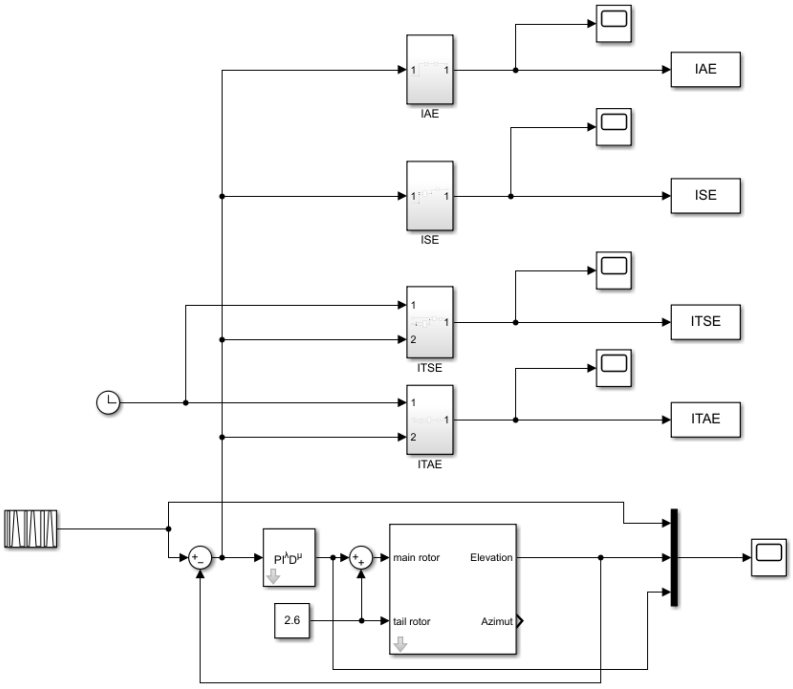

Figure 4.11 Structure of MATLAB Simulink embedded with Real Time Experiment for Elevation.

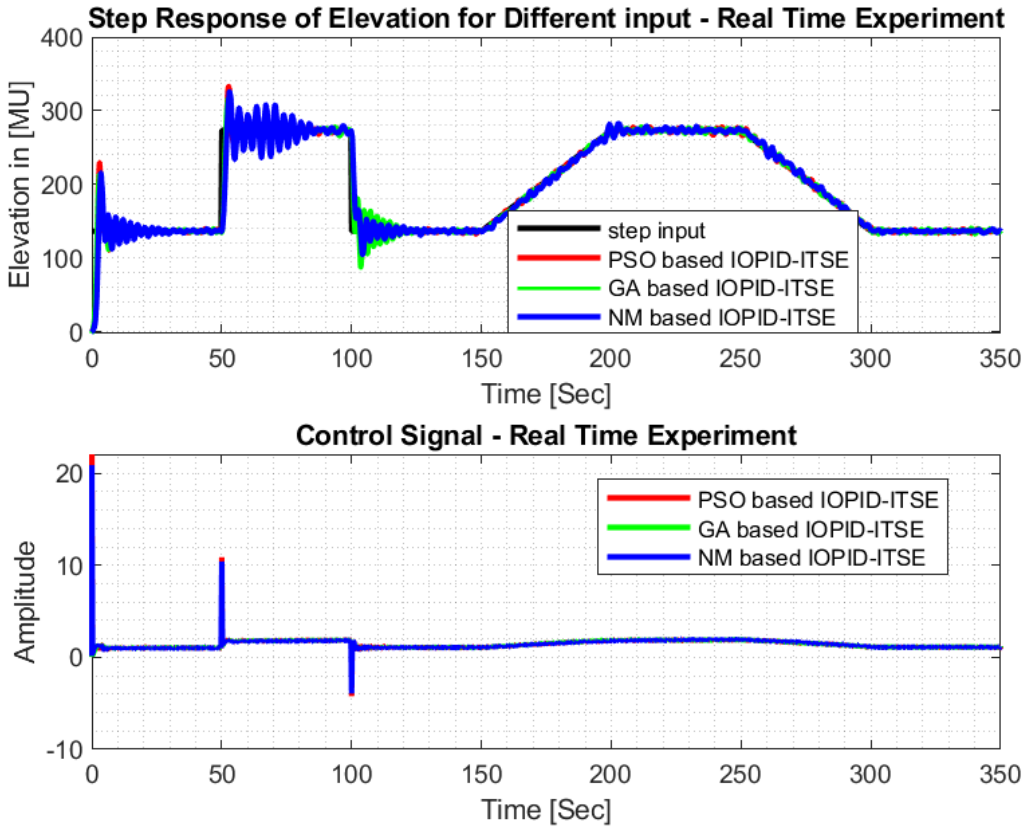

Figure 4.12 IOPID Controller Response for various Controller Tunning Algorithm-Real Time Experiment.

4.3.6 FOPID Controller Comparison -Real Time Experiment for Elevation

The identical controller parameters were used FOPID in both simulation and real-time experiments. As illustrated in Figure 4.11, the implementation approach was employed, the inputs included both step input and ramp input signals and the measurement results are compared in Figure 4.13.

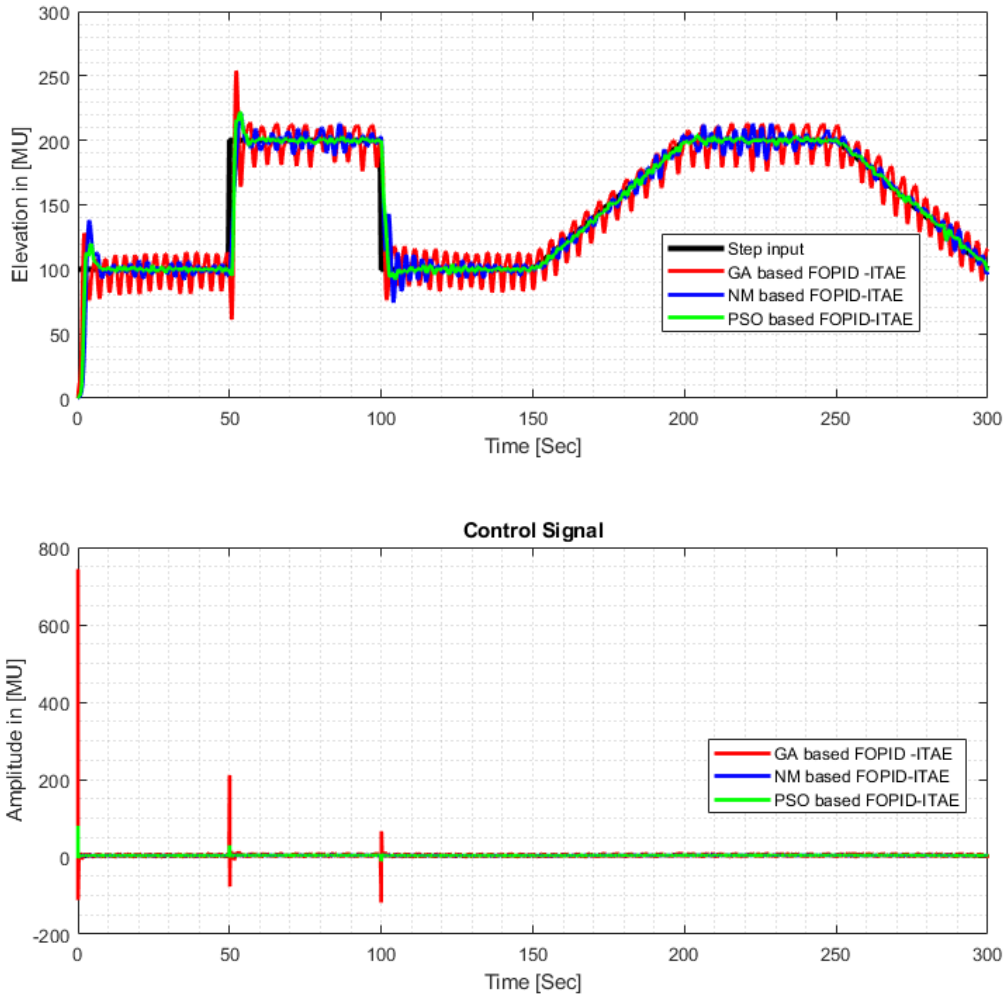

Figure 4.13 FOPID Controller Comparison - for Elevation

Based on the responses observed during the real-time experiment, the FOPID controller demonstrates promising outcomes when implemented on the TRMS model. Specially PSO based FOPID controller with ITAE performance index gives a better results than others.

4.3.7 Results of GA IOPID and FOPID Controller Responses for Azimuth Linear Model

According to the step response of Azimuth for GA based IOPID controller algorithm, the ITSE performance index offers the advantage of yielding smaller overshoots (7.7709%) and offers best settling and rise time as given in Table 4.4. Also, in the case of the GA-based FOPID tuning, the performance indices ISE and IAE offer the advantage of yielding smaller overshoots (10%) compared to other performance indices as illustrated in Figure 4.14. This clearly demonstrates the effectiveness of using ISE and IAE as performance metrics for achieving superior control performance in the GA-based FOPID tuning approach.

IOPID Controller - GA based tuning - for Azimuth						
Performance Index	K_p	K_i	K_d	$\%M_p$	$t_r(sec.)$	$t_s(sec.)$
ITSE	0.0098	0.0014	0.0059	7.7709	1.3951	13.0948
ITAE	0.0096	0.0020	0.0049	14.2635	1.3591	8.3896
ISE	0.0100	0.0012	0.0050	9.4683	1.3801	15.6546
IAE	0.0100	0.0024	0.0166	12.3214	1.2443	5.8363
IOPID Controller - PSO based tuning - for Azimuth						
Performance Index	K_p	K_i	K_d	$\%M_p$	$t_r(sec.)$	$t_s(sec.)$
ITSE	0.0099	0.0014	0.0066	5.9938	1.3898	13.1295
ITAE	0.0098	0.0012	0.0105	1.2315	1.4238	16.3083
ISE	0.0100	0.0014	0.0053	9.5381	1.3710	13.5362
IAE	0.0100	0.0017	0.0075	5.6498	1.3581	10.2391
IOPID Controller - NM based tuning - for Azimuth						
Performance Index	K_p	K_i	K_d	$\%M_p$	$t_r(sec.)$	$t_s(sec.)$
ITSE	0.0197	0.0025	0.0115	10.9792	0.8390	9.1057
ITAE	0.0073	0.0011	0.0078	1.3654	4.3986	14.5584
ISE	0.0994	0.0026	0.0337	2.5911	0.2956	2.3816
IAE	0.0255	0.0025	0.0122	14.0440	0.7217	10.0553

Table 4.4 Performance and parameter values for the IOPID controller (GA, PSO, NM) for azimuth

FOPID Controller - GA based tuning - for Azimuth					
Performance Index	K_p	K_i	K_d	λ	μ
ITSE	0.0991	0.0019	0.0382	1.0353	1.0635
ITAE	0.0097	0.0638	0.0541	0.9039	0.4643
ISE	0.0098	0.0912	0.0962	0.2296	0.6384
IAE	0.0100	0.0781	0.0.0992	0.3642	0.5566
FOPID Controller - PSO based tuning - for Azimuth					
Performance Index	K_p	K_i	K_d	λ	μ
ITSE	0.0100	00996	0.1000	0.4036	0.6388
ITAE	0.0071	0.0200	0.0338	1.0045	0.3775
ISE	0.0100	0.100	0.100	0.2311	0.6457
IAE	0.0100	0.0956	0.0977	0.3325	0.6667
FOPID Controller - NM based tuning - for Azimuth					
Performance Index	K_p	K_i	K_d	λ	μ
ITSE	0.0100	0.0051	0.0211	1.0210	0.5201
ITAE	0.0083	0.0013	0.0077	1.0040	0.9640
ISE	0.0099	0.0053	0.0402	0.8582	0.4286
IAE	0.0100	0.0042	0.0187	1.0371	0.5338

Table 4.5 Performance and parameter values for FOPID controller tuning (GA, PSO, NM) for elevation and azimuth

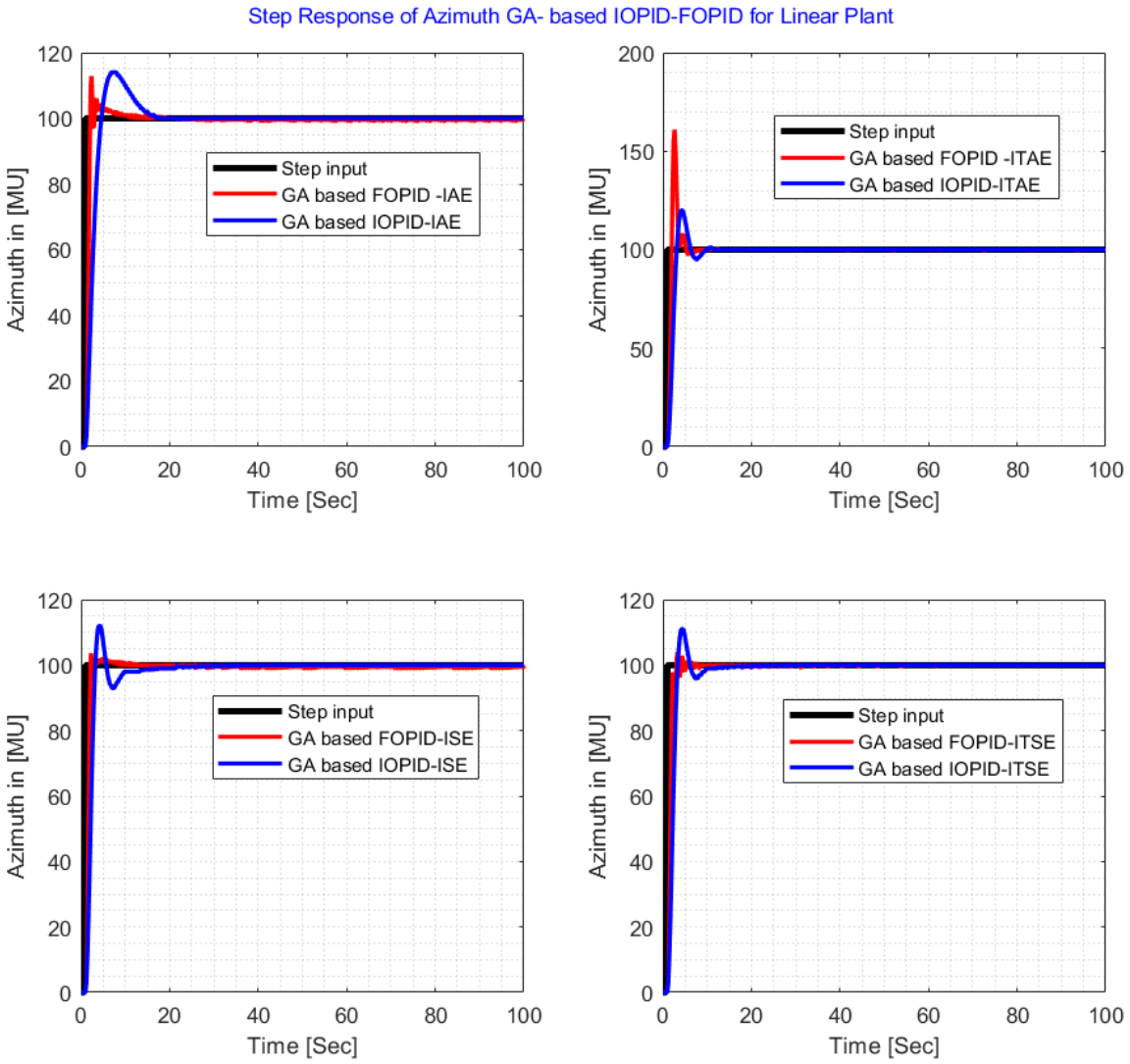

Figure 4.14 GA based IOPID/FOPID Azimuth Response for various Performance Indices.

4.3.8 Results of PSO IOPID and FOPID Controller Responses for Azimuth Linear Model

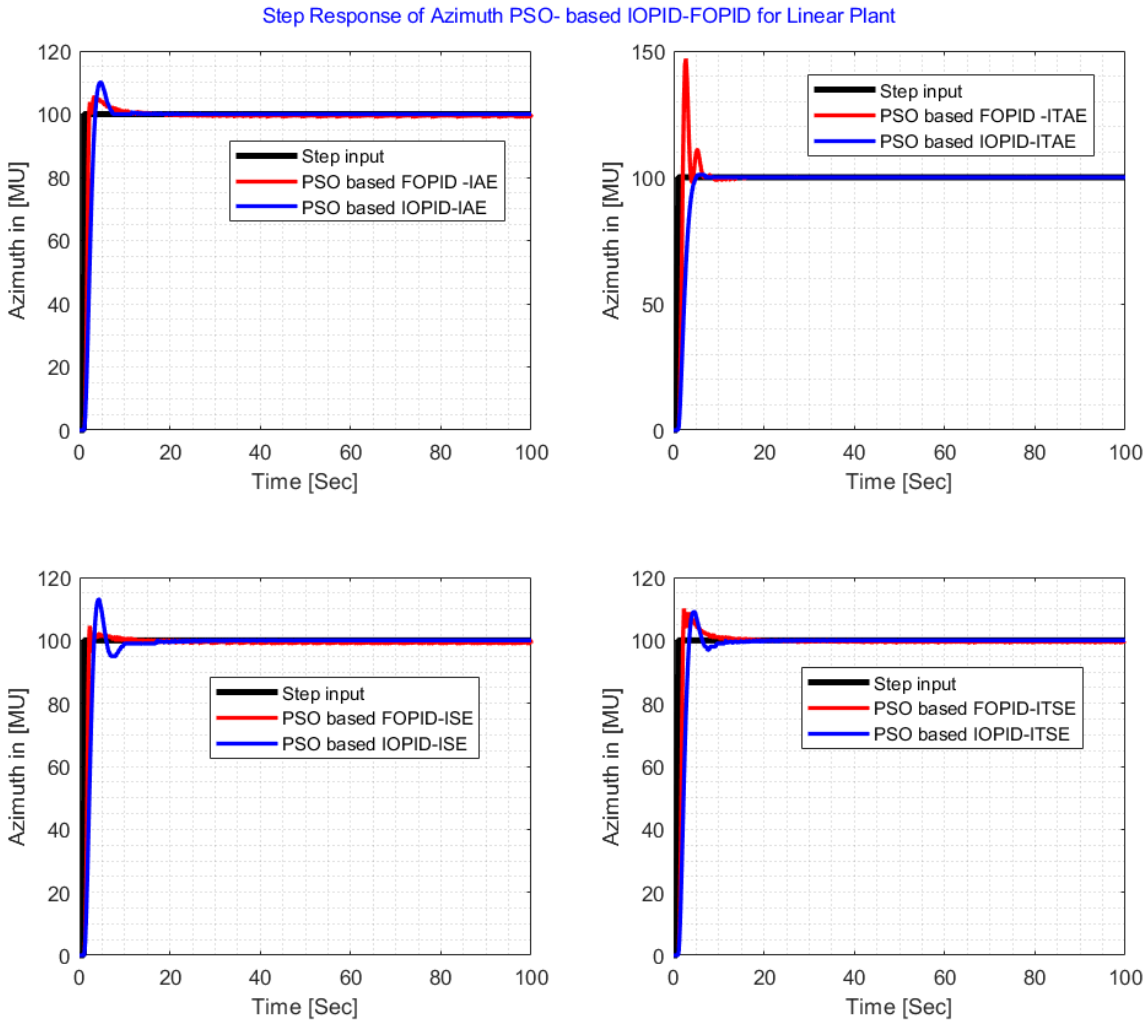

Figure 4.15 PSO based IOPID/FOPID Azimuth Response for various Performance Indices.

According to the step response of Azimuth for PSO based IOPID controller algorithm, the ITAE performance index offers the advantage of yielding smaller overshoots (1.2315%) as given in Table 4.4.

According to the step response of Azimuth for PSO based FOPID controller algorithm, the ISE performance index offers the advantage of yielding smaller overshoots (10%) as depicted in Figure 4.15.

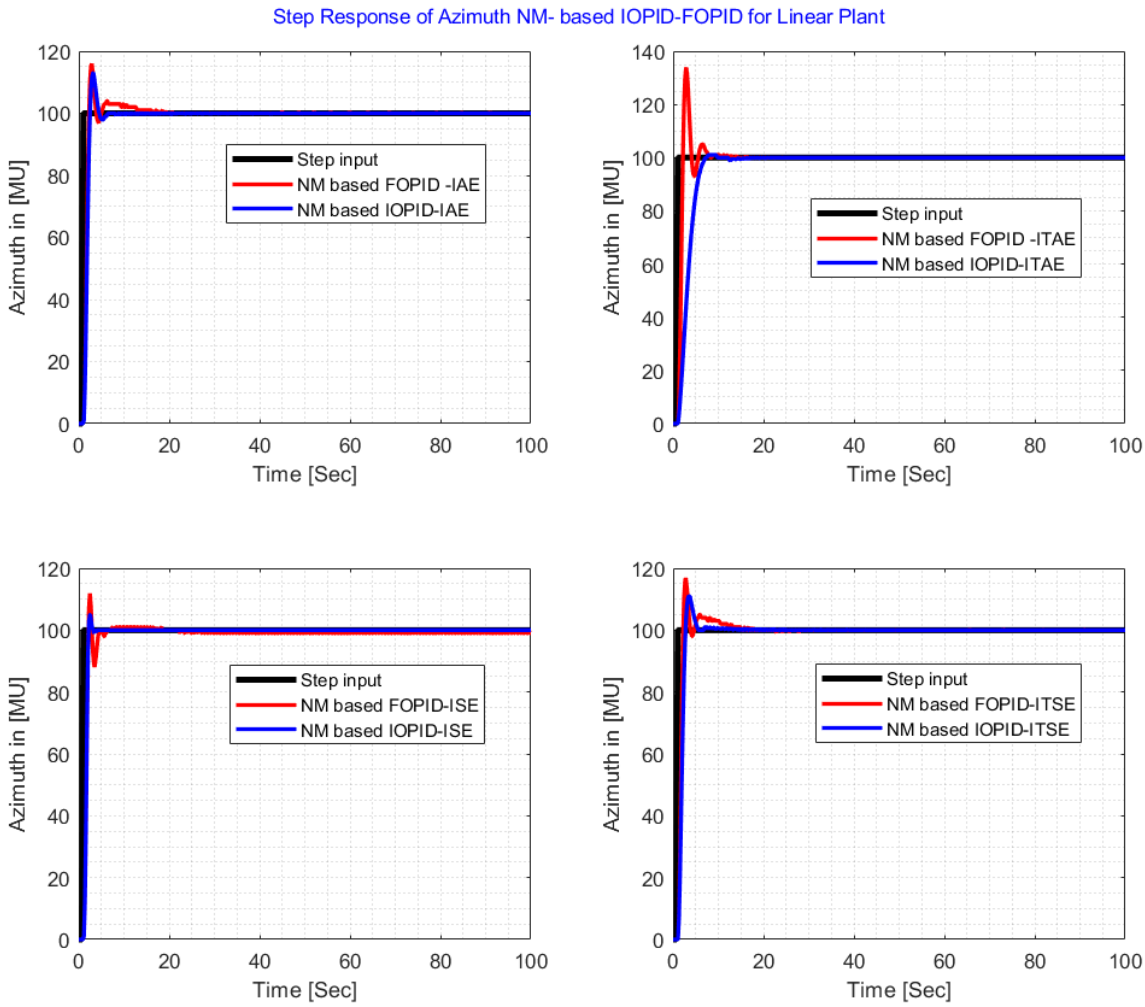

Figure 4.16 NM based IOPID/FOPID Azimuth Response for various Performance Indices.

According to the step response of Azimuth for the NM-based IOPID controller algorithm, the ITAE performance index offers the advantage of yielding smaller overshoots (1.3654%) and shorter rise time 4.3986 sec) and settling time (14.5584 sec) compared to other performance indices, as given in Table 4.14. This demonstrates that the NM-based IOPID controller with the ITAE performance index provides a more favorable response in terms of overshoot, resulting in better control performance and stability for the Azimuth system.

4.3.9 IOPID/FOPID Controller Comparison -Real Time Experiment for Azimuth

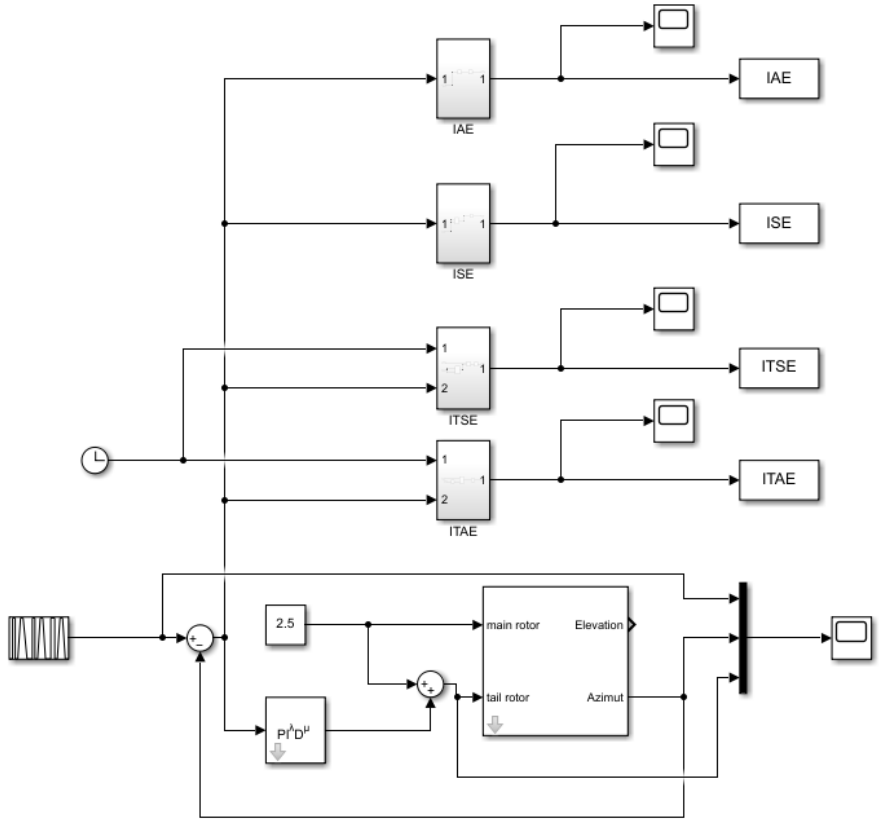

Figure 4.17 Structure of MATLAB Simulink embedded with Real Time Experiment for Azimuth.

The identical controller parameters were used for both IOPID and FOPID in both simulation and real-time experiments. As illustrated in Figure 4.17, the implementation approach was employed, and the measurement results are compared in Figure 4.18. The inputs included both step input and ramp input signals. Based on the responses observed during the real-time experiment, the FOPID controller demonstrates promising outcomes when implemented on the TRMS model.

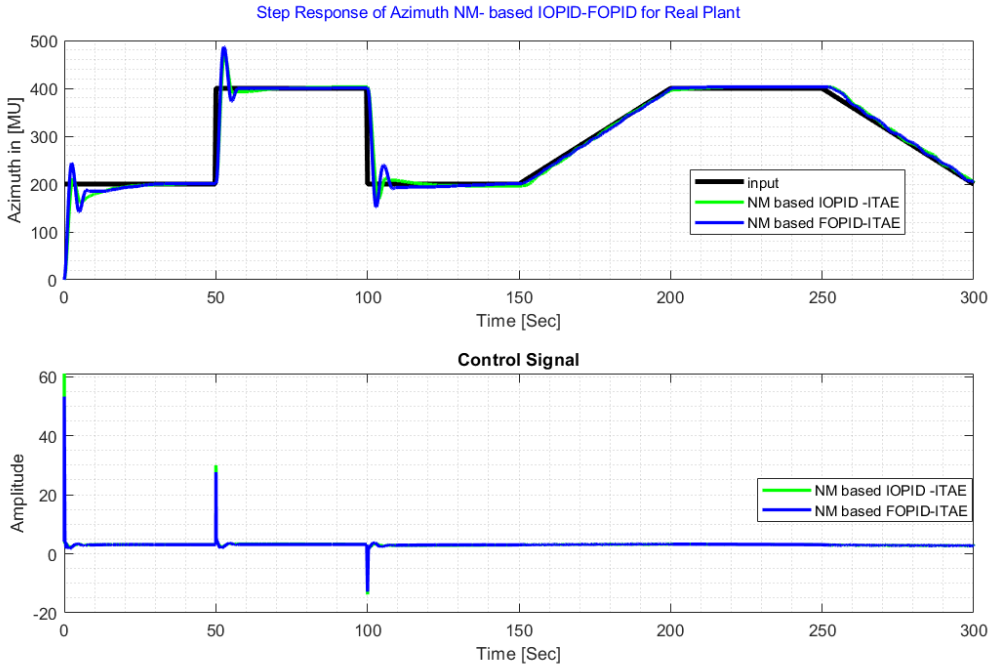

Figure 4.18 IOPID/FOPID Controller Comparison - Azimuth

CONCLUSIONS AND RECOMMENDATIONS

Conclusions

According to this paper a best approach for skillfully implementing nonlinear mathematical modeling based on the physical analysis of TRMS - first principles. The results obtained from the model align closely with the outcomes of real-time experiments, demonstrating the effectiveness of the proposed approach. The study also aims to compare the nonlinear model with the linear and real-time plant. According to these comparison, nonlinear plant has a promising result than linear and real time model, due to the fact that the performance real time plant degraded due several factors like temperature, heat sensor and other factors discussed in this paper.

Additionally, the static characteristics of each main and tail rotor are studied separately based on real-time experiments of TRMS. The evidence from the graphs shows that in the case of the control voltage of the main rotor (input) – elevation (output), the static characteristics of elevation can be piece-wise linear regardless of the direction of input voltage change. It mean that the linearity for input voltage ranging from 0V to 2.5V differs from the linearity for input voltage ranging from 2.5V to 5V due to a sudden change in direction of main rotor movements. Furthermore, it is evident that the gain of the system is significantly influenced when the direction of propeller rotation changes, specifically when the direction of the control voltage changes. Higher voltages appear to result in higher gain and lower voltages appear to result in lower gain. Conversely, for the control voltage of the tail rotor (input) – azimuth (output), the static characteristics exhibit nonlinear behavior resembling a hysteresis curve which highly affect the control. Still in the Azimuth, higher voltages appear to result in higher gain and lower voltages appear to result in lower gain.

From presented graph, the static characteristic of the system appears to be piece-wise linear. It mean that the linearity for input voltage ranging from 0V to 2.5V differs from the linearity for input voltage ranging from 2.5V to 5V due to a sudden change in direction of main rotor movements.

Moreover, this thesis include black box identification method to investigate different TRMS identification methods and , namely AutoRegressive with eXogenous input (ARX), AutoRegressive Moving Average with eXogenous input (ARMAX), and fminsearch. A comprehensive comparison of these three approaches is conducted to evaluate their effectiveness in accurately modeling the TRMS. The primary objective is to de-

termine the most effective identification approach that yields precise models capable of accurately representing real-life TRMS scenarios. The results indicate that the linear plant model obtained from the "fminsearch identification" approach provides the best representation of the real laboratory model of TRMS. This finding highlights the significance of using appropriate identification techniques for improving the accuracy of the model and enhancing control strategies for the TRMS system. Thus, the linear plant identification obtained from the "fminsearch" approach is selected for further examination, serving as a reference point for testing the controller algorithm.

Furthermore, the basic system properties, such as State Controllability, Output Controllability, Observability, Stability, Step response, Hurtz Stability test, root locus, are studied separately for both elevation and azimuth of the linear plant model of a TRMS. This investigation aims to gain a deeper understanding of the system's behavior and characteristics, which in turn helps with controller design. From studied results, the system is controllable, observable and marginally stable system.

The core of the thesis centers around the design of both IOPID and FOPID controllers for the TRMS system. Various optimization algorithms, such as PSO, GA, and NM, are employed to optimize the controller parameters. The performance and effectiveness of each optimization technique are evaluated and compared for both linear plant and real labolatory model. The analysis and comparison provide valuable insights into the performance and suitability of the different controller designs for the TRMS system. Ultimately, real-time experiments demonstrate that the PSO-based FOPID controller utilizing the ITAE performance index for elevation yields superior outcomes compared to alternatives. This observation underscores the effectiveness of the FOPID controller algorithm in controlling the TRMS model. Similarly, practical testing reveals that the NM-based FOPID -ITAE controller for azimuth control likewise displays promising results in the control of the TRMS model.

During the entire laboratory experiment, two testing approaches are conducted. Firstly, the controller algorithm is tested on the linear plant model obtained from the "fminsearch" approach for both elevation and azimuth. This preliminary test, known as the Model in the Loop (MIL) test, aims to evaluate the controller's performance and effectiveness in stabilizing and controlling the TRMS system before deploying it on the actual plant. Conducting the MIL test provides valuable insights into the controller's behavior and its ability to achieve the desired control objectives under simulated conditions. This step ensures the controller's reliability and effectiveness prior to experimental testing on the physical TRMS system, allowing any limitations to be identified and addressed before implementing the controller in a live environment.

The second approach is the Hardware in the Loop (HIL) test. In this method, the controller is implemented in MATLAB and then validated and evaluated on the actual hardware (physical system). The HIL test allows for real-time assessment of the controller's behavior and control capabilities in a realistic environment. By running the controller on the physical system, this test provides a more accurate evaluation of its performance and its ability to interact with and control the TRMS system under real-world conditions.

Recommendations

This paper recommends a 2 DOF control design and implementation of TRMS, considering all nonlinearities and coupling effects. The aim of this approach is to enhance the performance of the controller and minimize both overshoot and settling time. By accounting for these complex factors, the proposed 2 DOF control design is expected to result in improved control performance and a more stable response in the Twin Rotor MIMO System.

This paper further suggests the identification of a fractional-order model for the TRMS system. This approach aims to enhance the fidelity of the plant's fractional-order model, leading to a more accurate representation of the real-time plant dynamics.

REFERENCES

[1] Ahmad, S.; Chipperfield, A.; Tokhi, O.: Dynamic modeling and optimal control of a twin rotor MIMO system. In *Proceedings of the IEEE 2000 National Aerospace and Electronics Conference. NAECON 2000. Engineering Tomorrow (Cat. No. 00CH37093)*, IEEE, 2000, pp. 391–398.

[2] Jadhav, T. S.; Gadgune, S. Y.: Controller and Observer Techniques for Twin Rotor MIMO System. *International Journal of Engineering and Advanced Technology (IJEAT) ISSN*: pp. 2249–8958.

[3] Mohammed Zinelaabidine, G.: Real time implementation of fuzzy gain-scheduled PID controller for twin rotor MIMO system (TRMS). 2018.

[4] Harshitha, S.; Shamanth, S.; Chari, A. K.: A Review of Various Controller Techniques Designed for the Operational Control of DC and Servo Motors. In *Journal of Physics: Conference Series*, volume 2273, IOP Publishing, 2022, p. 012001.

[5] Yasin, S. Y.: *Systematic methods for the design of a class of fuzzy logic controllers*. Western Michigan University, 2002.

[6] Kothari, K.; Mehta, U. V.; Prasad, R.: Fractional-order system modeling and its applications. *Journal of Engineering Science and Technology Review*, volume 12, no. 6, 2019: pp. 1–10.

[7] Abdulwahhab, O. W.; Abbas, N. H.: A new method to tune a fractional-order PID controller for a twin rotor aerodynamic system. *Arabian Journal for Science and Engineering*, volume 42, 2017: pp. 5179–5189.

[8] Azarmi, R.; Tavakoli-Kakhki, M.; Sedigh, A. K.; et al.: Analytical design of fractional order PID controllers based on the fractional set-point weighted structure: Case study in twin rotor helicopter. *Mechatronics*, volume 31, 2015: pp. 222–233.

[9] Coelho, J.; Neto, R. M.; Lebres, C.; et al.: Application of fractional algorithms in the control of a twin rotor multiple input-multiple output system. *ENOC 08*, 2008: pp. 1–8.

[10] DOĞRUER, T.; Nusret, T.: REAL TIME CONTROL OF TWIN ROTOR MIMO SYSTEM WITH PID AND FRACTIONAL ORDER PID CONTROLLER. *Mugla Journal of Science and Technology*, volume 6, 2020: pp. 1–9.

[11] Chalupa, P.; Přikryl, J.; Novák, J.: Modelling of Twin Rotor MIMO System. *Procedia Engineering*, volume 100, 2015: pp. 249–258, ISSN 1877-7058,

doi:https://doi.org/10.1016/j.proeng.2015.01.365, 25th DAAAM International Symposium on Intelligent Manufacturing and Automation, 2014.
URL https://www.sciencedirect.com/science/article/pii/S1877705815003926

[12] Ijaz, S.; Hamayun, M. T.; Yan, L.; et al.: Fractional order modeling and control of twin rotor aero dynamical system using nelder mead optimization. *Journal of Electrical Engineering and Technology*, volume 11, no. 6, 2016: pp. 1863–1871.

[13] Ramalakshmi, A.; Manoharan, P.: Non-linear modeling and PID control of twin rotor MIMO system. In *2012 IEEE International Conference on Advanced Communication Control and Computing Technologies (ICACCCT)*, IEEE, 2012, pp. 366–369.

[14] Hore, A.; Kumar, M. R.; Mishra, S. K.: Parameter Estimation for Fractional-Order with Delay Model of Twin Rotor MIMO System. In *2021 IEEE 4th International Conference on Computing, Power and Communication Technologies (GUCON)*, IEEE, 2021, pp. 1–5.

[15] Mishra, C.; Swain, S. K.; Mishra, S. K.; et al.: Fractional order sliding mode controller for the twin rotor MIMO system. In *2019 International Conference on Intelligent Computing and Control Systems (ICCS)*, IEEE, 2019, pp. 662–667.

[16] Alarfaj, Y. A.: *A Case Study of Fractional-order Control*. Lancaster University (United Kingdom), 2021.

[17] Abbas, N.; Pan, X.; Raheem, A.; et al.: Real-time robust generalized dynamic inversion based optimization control for coupled twin rotor MIMO system. *Scientific Reports*, volume 12, no. 1, 2022: p. 17852.

[18] Rotondo, D.; Nejjari, F.; Puig, V.: Quasi-LPV modeling, identification and control of a twin rotor MIMO system. *Control Engineering Practice*, volume 21, no. 6, 2013: pp. 829–846, ISSN 0967-0661, doi: https://doi.org/10.1016/j.conengprac.2013.02.004.
URL https://www.sciencedirect.com/science/article/pii/S0967066113000142

[19] Rahideh, A.; Shaheed, M.; Huijberts, H.: Dynamic modelling of a TRMS using analytical and empirical approaches. *Control Engineering Practice*, volume 16, no. 3, 2008: pp. 241–259, ISSN 0967-0661, doi: https://doi.org/10.1016/j.conengprac.2007.04.008.

URL https://www.sciencedirect.com/science/article/pii/S0967066107000962

[20] Pandey, S. K.; Laxmi, V.: Control of twin rotor MIMO system using PID controller with derivative filter coefficient. In *2014 IEEE Students' Conference on Electrical, Electronics and Computer Science*, 2014, pp. 1–6, doi:10.1109/SCEECS.2014.6804451.

[21] Kannad, H. V.: Control of Twin Rotor MIMO System (TRMS) Using PID Controller. 2015.

[22] Nguyen, H. N.: Modelling, simulation, and calibration of twin rotor mimo system. 2007.

[23] Benyettou, L.; Zeghlache, S.; Djerioui, A.; et al.: Real Time Implementation of Type-2 Fuzzy Backstepping Sliding Mode Controller for Twin Rotor MIMO System (TRMS). *Traitement du Signal*, volume 36, 2019: pp. 1–11.

[24] Twin Rotor, M.: System Advanced Teaching Manual 1 (33-007-4M5). *Feedback Instruments Ltd, Crowborough, UK*, 1998.

[25] Instruments, F.: Twin rotor mimo system control experiments. 33-949s. *Feedback Instruments Ltd., Park Road, Crowborough, East Sussex, TN6 2QR, UK*, volume 1, 2006: pp. 89–101.

[26] Arturo Urquizo: PID controller overview Wikipedia, The Free Encyclopedia. 2011, [Online; accessed 10 December 2011].
URL https://en.wikipedia.org/wiki/PID_controller

[27] Chew, J.; Lucas, P.; Webber, S.: Proceedings of the 2003 Particle Accelerator Conference. Volume 4 of 5. Technical report, INSTITUTE OF ELECTRICAL AND ELECTRONICSENGINEERS INC PISCATAWAY NJ, 2003.

[28] Vilanova, R.; Visioli, A.: *PID control in the third millennium*. Springer, 2012.

[29] unknown publisher: *Time Response Chapter Learning Outcomes*.
URL https://web.njit.edu/~mad29/refs/2ndorder_adfklhfw21.pdf

[30] MATLAB: *R2020a to R2023a*. The MathWorks Inc., 2020.
URL https://www.mathworks.com/help/control/ref/stepinfo.html

[31] Bingi, K.; Rajanarayan Prusty, B.; Pal Singh, A.: A Review on Fractional-Order Modelling and Control of Robotic Manipulators. *Fractal and Fractional*, volume 7, no. 1, 2023: p. 77.

[32] Normey-Rico, J. E.; Camacho, E. F.: *Control of dead-time processes*, volume 462. Springer, 2007.

[33] Melin, A. M.; Kisner, R. A.; Blaise, B.; et al.: Embedded Sensors and Controls to Improve Component Performance and Reliability-Final Report. Technical report, Oak Ridge National Lab.(ORNL), Oak Ridge, TN (United States), 2018.

[34] Phillips, A. E.: *A Study of Advanced Modern Control Techniques Applied to a Twin Rotor MIMO System*. Rochester Institute of Technology, 2014.

[35] Pay, M. L.: *Distributed learning for multi-agent control of a dynamic system*. Doctoral thesis, University of York, 2011.

[36] Strejc, P. V.: Lecture notes in Identification of dynamic system- Czech version.

[37] Tepljakov, A.; Petlenkov, E.; Belikov, J.: FOMCOM: a MATLAB toolbox for fractional-order system identification and control. *International Journal of Microelectronics and computer science*, volume 2, no. 2, 2011: pp. 51–62.

LIST OF ABBREVIATIONS

DC	Direct Current
TRMS	Twin Rotor MIMO System
PID	Proportional-Integral-Derivative
IOPID	Integral -Order Proportional-Integral-Derivative
FOPID	Fractional -Order Proportional-Integral-Derivative
MIMO	Multiple-Input Multiple-Output
SISO	Single-Input Single-Output
DOF	Degree of Freedom
MATLAB	Matrix Laboratory
ARX	AutoRegressive with eXogenous input
ARMAX	AutoRegressive Moving Average with eXogenous input
PSO	Particle Swarm Optimization PSO
GA	Genetic Algorithm
PSO	Particle Swarm Optimization
NM	Nelder-Mead
ITSE	Integral of time squared error
ITAE	Integral of time-weighted absolute error
IAE	Integral of the absolute error
ISE	Integral of the squared error
MIL	Model in the Loop
HIL	Hardware in the Loop
K_p	Proportional gain
K_i	Integral gain
K_d	Derivative gain
M_p	Overshoot
t_r	Rise Time
t_s	Settling Time
MU	MATLAB Unit
λ	Integral Order
μ	Differentiator Order

LIST OF FIGURES

LIST OF TABLES